



T.R.

EGE UNIVERSITY

Graduate School of Applied and Natural Science



**OPTIMAL CONTROL OF A REFRIGERATION  
CYCLE THAT USES SMART AND ARTIFICIAL  
INTELLIGENCE SYSTEMS**

**PhD Thesis**

Mert Sinan TURGUT

Mechanical Engineering Department

Izmir  
2019

T.R.  
EGE UNIVERSITY  
Graduate School of Applied and Natural Science

**OPTIMAL CONTROL OF A REFRIGERATION  
CYCLE THAT USES SMART AND ARTIFICIAL  
INTELLIGENCE SYSTEMS**

Mert Sinan TURGUT

Supervisor : Assoc. Prof. Dr. Mustafa Turhan ÇOBAN

Mechanical Engineering Department  
Mechanical Engineering Third Cycle Programme

Izmir  
2019

Mert Sinan TURGUT tarafından doktora tezi olarak sunulan “Optimal Control of a Refrigeration Cycle that Uses Smart and Artificial Intelligence Systems” başlıklı bu çalışma EÜ Lisansüstü Eğitim ve Öğretim Yönetmeliği ile EÜ Fen Bilimleri Enstitüsü Eğitim ve Öğretim Yönergesi'nin ilgili hükümleri uyarınca tarafımızdan değerlendirilerek savunmaya değer bulunmuş ve tarihinde yapılan tez savunma sınavında aday oybirliği/oyçokluğu ile başarılı bulunmuştur.

**Jüri Üyeleri:**

**İmza**

**Jüri Başkanı**

: .....

.....

**Raportör Üye**

: .....

.....

**Üye**

: .....

.....

**Üye**

: .....

.....

**Üye**

: .....

.....

# EGE ÜNİVERSİTESİ FEN BİLİMLERİ ENSTİTÜSÜ

## ETİK KURALLARA UYGUNLUK BEYANI

EÜ Lisansüstü Eğitim ve Öğretim Yönetmeliğinin ilgili hükümleri uyarınca Doktora Tezi olarak sunduğum “Optimal Control of a Refrigeration Cycle that Uses Smart and Artificial Intelligence Systems” başlıklı bu tezin kendi çalışmam olduğunu, sunduğum tüm sonuç, doküman, bilgi ve belgeleri bizzat ve bu tez çalışması kapsamında elde ettiğimi, bu tez çalışmasıyla elde edilmeyen bütün bilgi ve yorumlara atıf yaptığımı ve bunları kaynaklar listesinde usulüne uygun olarak verdiğimi, tez çalışması ve yazımı sırasında patent ve telif haklarını ihlal edici bir davranışımın olmadığını, bu tezin herhangi bir bölümünü bu üniversite veya diğer bir üniversitede başka bir tez çalışması içinde sunmadığımı, bu tezin planlanmasından yazımına kadar bütün safhalarda bilimsel etik kurallarına uygun olarak davrandığımı ve aksinin ortaya çıkması durumunda her türlü yasal sonucu kabul edeceğimi beyan ederim.

.... / .... / 20..

Mert Sinan TURGUT

## ÖZET

# BİR SOĞUTMA ÇEVİRİMİNİN AKILLI VE YAPAY ZEKA SİSTEMLERİ KULLANAN OPTİMAL KONTROLÜ

TURGUT, Mert Sinan

Doktora Tezi, Makine Mühendisliği Anabilim Dalı

Tez Danışmanı: Doç. Dr. Mustafa Turhan ÇOBAN

Mart 2019, 98? sayfa

Bu tezde, soğutma çevrimlerinin enerji verimliliğini artırıcı yöntemler incelenmiştir. İncelenen bu yöntemlerden birisi buhar sıkıştırırmalı soğutma çevriminin dinamik simülasyon analizi, diğeri ise yapay sinir ağları kullanarak bir buhar sıkıştırırmalı soğutma çevriminin optimal kontrolüdür.

Dinamik simülasyon analizinde, bir buhar sıkıştırırmalı soğutma çevrimi dinamik olarak modellenmiş, soğutucu akışkanlar olarak R134a ve R1234yf kullanılarak bu iki akışkanın soğutma performansları karşılaştırılmıştır.

Yapay sinir ağları destekli optimal kontrol çalışmasında ise, bir buhar sıkıştırırmalı soğutma çevriminin dinamik modellenmesi gerçekleştirilmiş, ardından simülasyon verileriyle bir yapay sinir ağı eğitilmiş ve bu yapay sinir ağını sistem modeli olarak kullanılıp sistemin optimal kontrolü gerçekleştirilmiştir.

**Anahtar sözcükler:** Buhar sıkıştırırmalı soğutma çevrimi, dinamik sistem simülasyonu, optimal kontrol, yapay sinir ağları.

## ABSTRACT

### OPTIMAL CONTROL OF A REFRIGERATION CYCLE THAT USES SMART AND ARTIFICIAL INTELLIGENCE SYSTEMS

TURGUT, Mert Sinan

PhD in Mechanical Eng.

Supervisor: Assoc. Prof. Dr. Mustafa Turhan ÇOBAN

March 2019, 98? pages

In this thesis, the methods that improve the energy efficiency of the refrigeration cycles have been analyzed. One of these methods is dynamic simulation analysis of a vapor compression refrigeration cycle, and the other is optimal control of a vapor compression refrigeration cycle with using the artificial neural networks.

In the dynamic simulation analysis, dynamic modeling of a vapor compression refrigeration cycle has been accomplished, thereafter, two refrigerants are employed in the cycle separately, R134a and R1234yf, and their cooling performances are compared with each other.

In the optimal control with using the artificial neural networks study, dynamic modeling of a vapor compression refrigeration cycle has been accomplished, afterwards, an artificial neural network has been trained with the simulation data and the optimal control of the system has been done by utilizing the artificial neural network as the main model of the system.

**Keywords:** Vapor compression refrigeration cycle, dynamic system simulation, optimal control, artificial neural networks.

## PREFACE

The basis of this thesis stems from my deep interest in control of different types of systems. I thought that applying the control theory to energy systems would be a good idea since energy efficiency is a popular topic in the energy research field currently. Also, my supervisor Assoc. Prof. Dr. Mustafa Turhan ÇOBAN encouraged me to prepare my thesis on this topic. I have spent lots of time on modeling the system, successfully training the artificial neural network and implementing the controller. I hope this thesis gives the reader an insight into non-linear control of the vapor compression cycles.

IZMIR

.../.../20..

Mert Sinan TURGUT

# TABLE OF CONTENTS

	<u>Page</u>
HALF-TITLE .....	ii
KABUL ONAY SAYFASI .....	vi
ETİK KURALLARA UYGUNLUK BEYANI.....	vii
ÖZET .....	x
ABSTRACT .....	xii
PREFACE .....	xiv
TABLE OF CONTENTS .....	xvi
LIST OF FIGURES .....	xviii
LIST OF TABLES .....	xx
LIST OF SYMBOLS AND ABBREVIATIONS .....	xxii
1.INTRODUCTION .....	
2.INTRODUCTION TO HEAT PUMPS AND DYNAMIC ANALYSIS OF A VAPOR COMPRESSION SYSTEM .....	
2.1 Introduction to Heat Pumps .....	
2.2 Dynamic Modeling of a Vapor Compression System .....	

## TABLE OF CONTENTS (continued)

	<u>Page</u>
3.OPTIMIZATION .....	
3.1 Optimization Problem .....	
3.2 Traditional Optimization Techniques .....	
3.2.1 Newton's Method .....	
3.2.2 Gradient Descent Algorithm.....	
3.2.3 Nelder-Mead Algorithm .....	
3.3 Modern Optimization Tehniques .....	
3.3.1 Genetic Algorithm .....	
3.3.2 Differential Evolution .....	
3.3.3 Particle Swarm Optimization .....	
3.3.4 Bat Algorithm .....	
3.3.5 Firefly Algorithm.....	
3.3.6 Cuckoo Search.....	
3.3.7 Artificial Bee Colony Algorithm.....	
3.3.8 Whale Optimization Algorithm .....	
4.ARTIFICIAL NEURAL NETWORKS .....	

## TABLE OF CONTENTS (continued)

	<u>Page</u>
4.1 Basics of the Artificial Neural Networks .....	
4.2 Training of an Artificial Neural Network.....	
4.3 Nonlinear Autoregressive Exogenous (NARX) Network .....	
5.MODEL PREDICTIVE CONTROL.....	
5.1 Introduction to Model Predictive Control .....	
5.2 Nonlinear Model Predictive Control .....	
5.3. Utilization of the Neural Networks in Model Predictive Control .....	
6.NEURAL NETWORK PREDICTIVE CONTROL OF A VAPOR COMPRESSION CYCLE .....	
6.1. Fundamentals of Vapor Compression Cycle Control.....	
6.2. Dynamic Modeling of the Heat Exchangers.....	
6.2.1. Multi-phase Flows in the Heat Exchangers .....	
6.2.2. Fixed Control Volume Approaches .....	
6.2.3. Moving Boundary Model .....	
6.3. Case Study of Designing a Neural Network Predictive Controller for a Vapor Compression Cycle.....	
7.CONCLUSION .....	

**TABLE OF CONTENTS (continued)**

	<u>Page</u>
LIST OF REFERENCES .....	
ACKNOWLEDGEMENTS .....	
CURRICULUM VITAE .....	

## LIST OF FIGURES

<u>Figure</u>	<u>Page</u>
1.1 Energy hierarchy (Renewable Energy World, 2018) .....	
2.1 Lord Kelvin's heat multiplier (Reay and Macmichael, 1988).....	
2.2 Diagram of the first constructed heat pump (Reay and Macmichael, 1988)....	
2.3 An absorption heat pump (Herold et al., 2016).....	
2.4 A vapor compression heat pump (Herold et al., 2016) .....	
2.5 Type of realizations of different kind of heat pumps (Dyakowski and Brodowicz, 1993) .....	
2.6 Thermodynamic representation of the heat pumps (Reay and Macmichael, 1988).....	
2.7 a) Graphical representation of an ideal cycle b)Temperature-entropy diagram of the ideal cycle (Hundy et al., 2016) .....	
2.8 Graphical representation of a vapor compression cycle operated with R134a (Hundy et al., 2016).....	
2.9 Pressure-enthalpy diagram of the vapor compression cycle (Hundy et al., 2016).....	
2.10 An absorption refrigeration cycle (Hundy et al., 2016).....	
2.11 Adsorption refrigeration cycle (Hundy et al., 2016).....	
2.12 Desiccant cooling system (Hundy et al., 2016).....	

## LIST OF FIGURES (continued)

<u>Figure</u>	<u>Page</u>
2.13 A typical demonstration of a vapor compression cycle (Rasmussen and Alleyne, 2006) .....	
2.14 Pressure-enthalpy diagram of a vapor compression cycle (Rasmussen and Alleyne, 2006) .....	
2.15 Discretized heat exchanger model (Korzen and Taler, 2015) .....	
2.16 A heat exchanger modeled with the MB method (Rasmussen and Alleyne, 2006) .....	
2.17 A discretized evaporator (Chowdhury et al., 2015) .....	
2.18 Internal structure of the compressor (McArthur, 1984) .....	
2.19 Inner structure of an expansion valve (Bright Hub Engineering, 2018) .....	
2.20 Initial and final shape of the temperature-entropy diagram for R134a .....	
2.21 Initial and final shape of the pressure-enthalpy diagram for R134a .....	
2.22 Temperature-entropy diagram for R1234yf at initial and final states .....	
2.23 Pressure-enthalpy diagram for R1234yf at initial and final states .....	
2.24 Change of the COP with time for the both refrigerants .....	
2.25 Change of the compressor work with time for the both refrigerants.....	
2.26 Change of the cooling load with time for the both refrigerants .....	
3.1 Traditional optimization technique (Vanderpaats, 2007).....	

## LIST OF FIGURES (continued)

<u>Figure</u>	<u>Page</u>
3.2 Effect of learning rate on the convergence (Towards Data Science, 2018) .....	
3.3 A sample simplex (Singer and Nelder, 2009) .....	
3.4 Reflection of the simplex (Singer and Nelder, 2009).....	
3.5 Expansion of the simplex (Singer and Nelder, 2009) .....	
3.6 Optimization algorithm procedure (Bozorg-Haddad, 2017) .....	
3.7 General structure of the GA (Venter, 2010).....	
3.8 Pseudo code of the BA (Yang, 2010).....	
3.9 Pseudo code of the FA (Yang, 2010) .....	
3.10 Pseudo code of the CS algorithm (Yang, 2010).....	
4.1 A biological and an artificial neural network (Aggrawal, 2018) .....	
4.2 Structure of a single neuron in an ANN (Haykin, 2009).....	
4.3 Activation Function (Aggarwal, 2018) .....	
4.4 Representation of a single-layer network (Silva et al., 2017) .....	
4.5 Representation of a multi-layer feedforward network (Silva et al., 2017).....	
4.6 A recurrent neural network (Silva et al., 2017).....	
4.7 A mesh network (Silva et al., 2017).....	

## LIST OF FIGURES (continued)

<u>Figure</u>	<u>Page</u>
4.8 Supervised learning procedure (Haykin, 2009).....	
4.9 Reinforcement learning (Haykin, 2009).....	
4.10 ADALINE network (Silva et al., 2017) .....	
4.11 The ADALINE training algorithm (Silva et al., 2017) .....	
4.12 Propogating the error (Rojas, 1996).....	
4.13 Backpropagation in a chain of nodes (Rojas, 1996).....	
4.14 Different architectures of the NARX network (Boussaada et al., 2018).....	
5.1 The NMPC algorithm (Nguyen and Szczerbicki, 2009) .....	
5.2 Block diagram of a NMPC algorithm (Yakub, 2013).....	
5.3 Block diagram of a NNPC (Vasickaninova et al., 2011) .....	
5.4 RBF neural network (Faris et al., 2017).....	
6.1 a) Schematic representation of a VCC b) Pressure-enthalpy diagram of the VCC (Wen and Mishra, 2018).....	
6.2 Different designs of heat exchangers (Wen and Mishra, 2018).....	
6.3 Different types of multi-phase flows in the heat exchangers (Wen and Mishra, 2018) .....	
6.4 Discretized heat exchanger (Wen and Mishra, 2018) .....	
6.5 MB depiction of a heat exchanger (Wen and Mishra, 2018) .....	

## LIST OF FIGURES (continued)

<u>Figure</u>	<u>Page</u>
6.6 Single-phase heat exchanger (Rasmussen and Alleyne, 2006) .....	
6.7 The Z coefficients (Rasmussen and Alleyne, 2006).....	
6.8 A demonstration of a VCC modeled with the MB method.....	
6.9 Photo of a compressor (Rasmussen and Alleyne, 2006) .....	
6.10 Photo of an EEV (Rasmussen and Alleyne, 2006).....	
6.11 The MB models of the evaporator and condenser.....	
6.12 Z matrix elements (Rasmussen and Alleyne, 2006) .....	
6.13 Z matrix elements (Rasmussen and Alleyne, 2006) .....	
6.14 Z matrix elements (Rasmussen and Alleyne, 2006) .....	
6.15 Perturbation signals to the systems .....	
6.16 Model verification results of the state variables.....	
6.17 Main structure of the Artificial Neural Network used as the model .....	
6.18 The training and validation losses of the ANN .....	
6.19 Condenser outlet enthalpy state variable validation.....	
6.20 Evaporator outlet enthalpy state variable validation .....	
6.21 Compressor outlet entropy state variable validation .....	
6.22 Desired cooling load trajectory .....	

## LIST OF FIGURES (continued)

<u>Figure</u>	<u>Page</u>
6.23	Pairwise trajectory tracking performance comparison of the controllers.....
6.24	Pairwise trajectory tracking performance comparison of the controllers.....
6.25	Variations of the control signals for the each controller .....
6.26	Variations of the control signals for the each controller .....
6.27	The exergy destruction rates of the components .....
6.28	The exergy destruction rates of the components .....
6.29	The compressor power consumption for the each controller .....
6.30	The COP and second law efficiency variations for the each controller .....

## LIST OF TABLES

<u>Table</u>	<u>Page</u>
6.1 Control signal boundaries.....	
6.2 Slew rate limits of the control signals .....	
6.3 Exergy destruction rates of the each component for the each controller .....	
6.4 Total energy consumption and exergy destruction rates for the controllers ....	

## LIST OF SYMBOLS AND ABBREVIATIONS

<u>Symbol</u>	<u>Description</u>
$A$	Area (m <sup>2</sup> )
$b$	Bias
$C_p$	Specific heat (J/kgK)
$d$	Diameter (m)
$e$	Error signal
$f$	Friction factor
$h$	Entalpy (J/kg)
$k$	Thermal conductivity (W/mK)
$L$	Length (m)
$M, m$	Mass (kg)
$\dot{m}$	Mass flow rate (kg/m <sup>3</sup> )
$Nu$	Nusselt number
$P$	Pressure (Pa)
$Pr$	Prandtl number
$\dot{Q}$	Amount of heat transfer (W)
$q$	Heat transfer (J)
$T$	Temperature (K)

## LIST OF SYMBOLS AND ABBREVIATIONS (continued)

<u>Symbol</u>	<u>Description</u>
<i>Re</i>	Reynolds number
<i>s</i>	Entropy (kJ/kgK)
<i>u</i>	Input
<i>V</i>	Velocity (kg/s)
<i>Vol</i>	Volume (m <sup>3</sup> )
<i>w</i>	<i>Weight</i>
<i>X</i>	Exergy destruction rate (W)
<i>x</i>	Quality, expansion valve openness, design variable
<i>y</i>	Output
<i>α</i>	Heat convection coefficient (W/m <sup>2</sup> K)
<i>γ</i>	Ratio of specific heats, learning rate, mean void fraction
<i>μ</i>	Viscosity (kg/ms)
<i>η</i>	Efficiency
<i>ρ</i>	Density (kg/m <sup>3</sup> )
<i>ω</i>	Compressor motor speed (rpm)
<u>Subscript</u>	
<i>abs</i>	Absorber

## LIST OF SYMBOLS AND ABBREVIATIONS (continued)

<u>Subscript</u>	<u>Description</u>
<i>comp</i>	Compressor
<i>cond</i>	Condenser
<i>evap</i>	Evaporator
<i>gen</i>	Generator
<i>H</i>	High
<i>i</i>	Inlet
<i>L</i>	Low
<i>l,liq</i>	Liquid phase
<i>o</i>	Outlet
<i>shell</i>	Compressor shell
<i>cyl</i>	Compressor cylinder
<i>v,vap</i>	Vapor phase
<i>valv</i>	Expansion valve
<i>w</i>	Heat exchanger wall
<u>Abbreviation</u>	
<i>ANN</i>	Artificial neural network
<i>COP</i>	Coefficient of performance

## LIST OF SYMBOLS AND ABBREVIATIONS (continued)

<u>Abbreviation</u>	<u>Description</u>
<i>EEV</i>	Electronic expansion valve
<i>FCV</i>	Finite control volume
<i>HVAC</i>	Heating ventilation and air conditioning
<i>MB</i>	Moving boundary
<i>MPC</i>	Model predictive control
<i>NNPC</i>	Neural network predictive control
<i>VCC</i>	Vapor compression cycle
<i>WOA</i>	Whale optimization algorithm

## 1. INTRODUCTION

Nowadays HVAC systems have widespread household and industrial applications and play a leading role in the energy consumption of the countries. According to the US Department of Energy (DOE), HVAC systems constituted 30% of the yearly total energy consumption of commercial buildings in 2017, which is 5.35 quadrillion btu/year (Goetzler et al., 2017). Some of the prominent goals of the researchers have been reducing the energy consumption the HVAC systems with providing the similar amount of performance and minimizing the environmental impacts of the consumed energy. Therefore, the researchers have proposed the sustainable energy policies to turn the energy consuming systems such as HVAC systems into more managable, efficient and clean systems. The energy hierarchy is proposed by the researchers to emphasize the priorities to move towards a more sustainable energy policy. The energy hierarchy is depicted in the figure below.

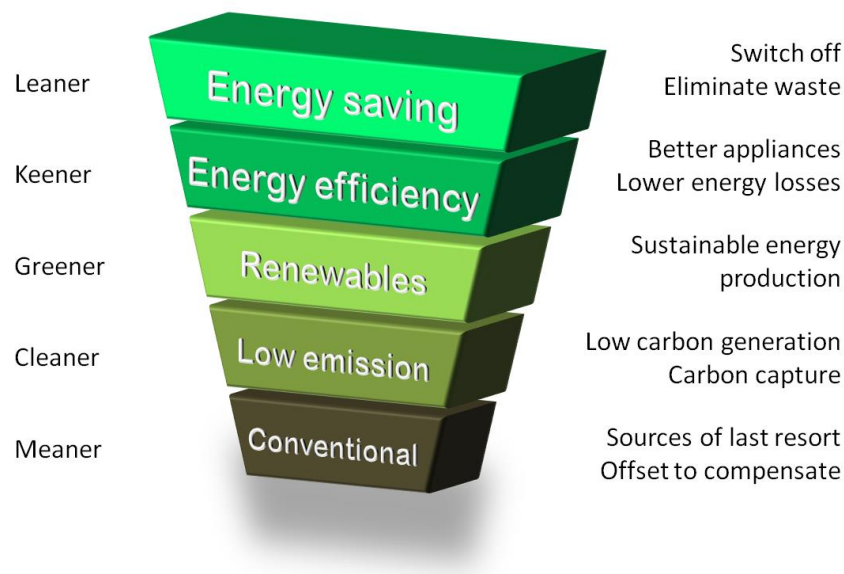


Figure 1.1. Energy hierarchy (Renewable Energy World, 2018)

As can be seen from the Figure 1, energy saving, energy efficiency and renewable energy systems are the top priorities of the sustainable energy policy. Energy saving is switching off the unnecessary devices or finding solutions to decrease the extra energy consumption and lowering the electricity bills. More and more countries are encouraging their

citizens to save more energy to cut back extra energy consumption. For example, covering around the windows with an insulation material may be a sensible solution for reducing the heat losses from the buildings. Therefore, people can use less HVAC systems to condition the building and energy can be saved.

Energy efficiency and renewable energy are put forward as the two pillars of the sustainable energy policy by the researchers (Prindle et al., 2007). Energy efficiency may cause serious cost-effective energy savings and emission reductions. However, renewable energy draws the attention of the policymakers and public more compared to energy efficiency. Energy efficiency is a key term for slowing the energy supply and carbon emission to make clean sources catch up with the ever-growing energy demand. Also, unless the renewable energy sources are utilized in large measures, the carbon emission levels are not expected to reach favorable levels. Therefore, it can be said that energy efficiency and renewable energy are the two pillars of the sustainable energy policy that requires effective teamwork together to carry the humanity to a more clean and sustainable environment.

This thesis deals with the energy efficient analysis, optimization and control of the HVAC systems. For this reason, the emphasis will be on energy efficiency of the energy systems, especially HVAC systems, from this point forward. The researchers have mainly studied on the thermodynamic analysis, optimization and control of the HVAC systems to develop more energy-efficient and environmentally-friendly HVAC systems. Analyzing the steady-state and dynamical behavior of these systems is an key factor in design and control of such systems (Turgut and Coban, 2018). For this reason, the first studies that have found their place in the literature were mainly about the steady-state and dynamical behavior of the HVAC systems.

American National Standards Bureau carried out one of the pioneer studies regarding the dynamical behavior of the HVAC systems, particularly refrigeration cycles. In these studies the researcher have investigated the steady-state and dynamical behavior of the chiller (Chi, 1979) and boiler (Chi, 1976). As a follow-up study, Chi and Didion (1982) developed a software model that can dynamically simulate a heat pump called TRPUMP. The researchers included the models of the all components to the software in lumped parameter form and compared the results of the model with the experiments. Bonne et al. (1980) investigated the

dynamic simulation of a heat pump that is driven by a electrical motor powered compressor and analyzed the system performance with on-off control of the compressor. MacArthur (1984) developed the dynamic model of a vapor-compression refrigeration cycle for the accomplishment of a closed-loop control task. The author has modeled the evaporator and the condenser by utilizing the finite-difference method and compressor and expansion valve by using static relationships. As a result of this study, the author has achieved the dynamic simulation, investigated the system stability and compared the results of the model and experimental setup. Chen and Lin (1991) analyzed the optimal component design combination that minimizes the energy consumption of a small-scaled refrigeration cycle. The authors have achieved to reduce the energy consumption of the system by 5.1% with various dynamic simulation studies. Fu et al. (2003) studied the dynamic modelling of a dual-mode air-to-water heat transfer based heat pump. Studies in dynamic modelling of the refrigeration cycles are continuing and more and more papers, such as (Zhu et al., 2013), are finding their place in the literature.

Steady-state analysis of the HVAC systems have also been long studied by the researchers. Hepbasli (2005) studied the thermodynamic analysis of a ground-source heat pump utilized for district heating. The authors have studied energetic and exergetic analysis of a ground-source heat pump that is available in their institute. Bayrakci and Ozgur (2009) investigated the energetic and exergetic performance of a vapor compression refrigeration system which employs pure hydrocarbon refrigerants. Four unique hydrocarbons and two non-hydrocarbons are analyzed in the refrigeration cycle, the hydrocarbons are R290, R600, R600a and R1270, and the non-hydrocarbons are R22 and R134a. Steady-state thermodynamic analysis have been performed for the each refrigerant in the cycle and the authors have found out that R1270 resulted in the best performance in terms of COP and second law efficiency. Ahamed et al. (2010) studied the steady-state thermodynamic investigation of a vapor compression refrigeration cycle that employs R600 and R600a refrigerants. As a result of this study, the authors have concluded that exergetic efficiency of the cycle operated with R600a is 50% higher than that of R134a. The authors have also found out that the cycle showed similar performances with R134a, R600 and R600a refrigerants. Arora and Kaushik (2008) investigated the theoretical steady-state thermodynamic analysis of a vapor compression refrigeration cycle that employs R502, R404a and R507a refrigerants. The authors have studied the operation condition ranges of the evaporator and the condenser respectively from -

50°C to 0°C and 40°C to 55°C. As a result of the study, the authors have concluded that the cycle gives more favorable performance results when it employs R507, instead of R502 and R404a refrigerants.

Thermodynamic design optimization of the HVAC systems is another significant field of study for the energy-efficiency of the HVAC systems and have been studied extensively by the researchers. HVAC thermodynamic design optimization problems are naturally nonlinear, highly constrained and mixed continuous-discrete. The emerging metaheuristic techniques is regarded as a useful alternative to the traditional methods by the researchers. By studying exclusively on this topic, the authors have concluded that Evolutionary Algorithm is a more effective tool compared to traditional methods, such as direct search methods (Wright and Hanby, 1987), and heuristic methods, especially Genetic Algorithm (GA) while tackling with HVAC design optimization problems (Wright, 1996; Fong et al., 2009). Fong et al. (2009) investigated a centralized HVAC system and studied on minimizing the total energy consumption of the system with respect to hourly cooling load profile of a day. The authors have modeled the optimization problem with one objective, seven design variables and nine design constraints. The Robust Evolutionary Algorithm (REA) has been used to solve the optimization problem. The results found by the REA is compared with that of the GA and it is found out that REA gives more favorable properties that results in lower total daily energy consumption rates.

Sayyaadi and Nejatolahi (2011) studied the multi-objective optimization of a cooling tower assisted vapor compression refrigeration system. The authors have modeled the optimization problem in a multi-objective manner. The two objectives are the total cost and total irreversibility of the cycle. The authors have utilized the multi-objective Genetic Algorithm to solve the problem. The problem is modeled with eight design variables and it has been found out that multi-objective optimization results are more favorable thermodynamic and economic properties than two single-objective optimization cases. Jain et al. (2016) accomplished the multi-objective design optimization of a cascaded absorption-vapor compression refrigeration cycle. The considered cycle employs R410a on the vapor compression side and LiBr-H<sub>2</sub>O fluid pair on the absorption side. The authors have modeled the optimization problem with seven design variables and the two objective functions are total irreversibility and total cost of the cycle. The Non-dominated Sorting Genetic Algorithm II

(NSGA-II) is utilized for the solution of the multi-objective optimization problem. As a result of this study, it has been found out that multi-objective case resulted in more favorable cycle thermodynamic and economic properties than that of single-objective cases.

Control of the HVAC systems is an emerging field and new studies are incorporated into the literature. Advancement of the new technologies such as microchips, data storage and communication devices have made possible the advanced control methods to become applicable to the HVAC systems (Afram and Janabi-Shafiri, 2014). However, traditional control methods such as PID and on/off are still applied to the HVAC systems due to their simplicity and ease of operation and formulation. A major downfall of the traditional control algorithms have been giving inconsistent performances among HVAC systems. Jain and Alleyne (2015) accomplished the formulation an exergy-based dynamic model of a vapor compression cycle. The authors realized the linearization of the non-linear model around a working point and applied the linear model predictive control (MPC) method to the system. Comparison of the two different cases have been investigated in this study, namely minimization of the total exergy destruction and minimizing the compressor work, thus the maximization of the COP of the cycle over time. The authors have concluded by analyzing the simulation results that exergy destruction minimization case resulted in 40% more favorable exergetic efficiency than the compressor work minimization case.

Yin et al. (2016) presented a unique cascade control strategy for the vapor compression cycles in their study. The presented cascade control strategy is made up of two different loops, namely inner and outer loops. The pressure difference between the evaporator and the condenser and the superheat temperature are controlled by applying the MPC algorithm to the system in the inner loop and a PI controlled is utilized to determine the set point of the superheat by considering a non-linear relationship between the cooling demand and superheat temperature. By investigating the results, the authors have found out that the presented control strategy results in 5.8% improvements of the first law efficiency of the system compared to contestant control methods.

This thesis is about energy-efficient analysis and control of HVAC systems, particularly refrigeration cycles. As discussed above, dynamic analysis of the thermodynamic systems is a key factor in energy-efficient design and control of such systems. The energy demand of the

humanity is increasing day by day as the technology advances and world's population increases. For this reason, necessity of more energy-efficient and environmentally-friendly HVAC systems are increasing. Control and energy-efficient design of such systems may be a solution for the problems described above. The thesis starts with the dynamic analysis of a vapor compression refrigeration cycle. All of the components in the cycle is modeled with methods used in dynamic analysis. The methods used in dynamic analysis of the heat exchangers, such as the evaporator and the condenser, are described and then a case study is presented, which includes performance comparison of the refrigeration cycle that employs R134a and R1234yf refrigerants. The refrigerant R1234yf is put forward by the researchers as an alternative to R134a. R1234yf has more favorable Ozone Depletion Potential (ODP) and Global Warming Potential (GWP) values compared to that of R134a. Then the thesis continues with the control study of a vapor compression refrigeration cycle. The non-linear model of the cycle is developed by utilizing the Moving-Boundary (MB) method and static relations. An artificial neural network is trained to predict the behavior of the cycle. And Non-linear Model Predictive Control (NMPC) algorithm is implemented to control the system. Each optimization problem in the NMPC is solved by applying the Whale Optimization Algorithm (WOA) (Mirjalili and Lewis, 2016). The WOA is swarm-based nature-inspired metaheuristic algorithm that mimics the hunting behavior of the whales in the environment. The WOA have favorable exploration and exploitation capabilities and can effectively search large solution spaces.

Some of the novel aspects of this thesis are:

- The dynamic characteristics of the two contending refrigerants, R134a and R1234yf, are investigated.
- The dynamic modeling of the refrigeration cycles is studied.
- Neural network-based NMPC is applied to control a vapor compression refrigeration cycle.
- A metaheuristic optimization algorithm, the WOA, is utilized to solve the problems arise in the each time step in NMPC.

## 2. INTRODUCTION TO HEAT PUMPS AND DYNAMIC ANALYSIS OF A VAPOR COMPRESSION SYSTEM

### 2.1. Introduction to Heat Pumps

Heat pumps have been in interest of the researchers and scientists for decades. Theoretically, the first vapor compression heat pump is proposed in the works and thesis of Carnot in the early 19th century (Reay and Macmichael, 1988). This first proposed cycle is named after Carnot and is called as the Carnot cycle. Later, William Thomson (Lord Kelvin) proposed the first application of the Carnot cycle and called it as 'heat multiplier'. The heat multiplier is the first application that a refrigeration machine that can also heat the environment if needed. During that time, conventional furnaces did not permit continuous combustion of the fuel for heating. Lord Kelvin claimed that his heat pump can contuously condition the environment with consuming less fuel compared to conventional furnaces. The diagram representation of the heat multiplier is given in Figure 2.1.

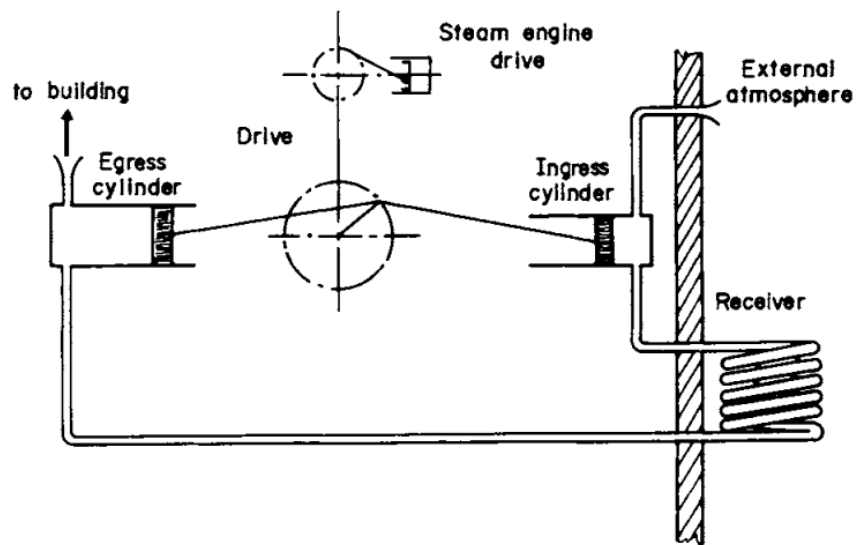


Figure 2.1. Lord Kelvin's heat multiplier (Reay and Macmichael, 1988)

The heat multiplier employed air as the working fluid and mainly consisted of two water tanks (Dyakowski and Brodowicz, 1993). The two water tanks took the roles of the high- and low-temperature heat sources. The air was processed in the cycle and then released to the environment. Later, it is claimed that Lord Kelvin's heat multiplier is successfully produced in Switzerland. The refrigeration system that is built in Switzerland is depicted in Figure 2.2.

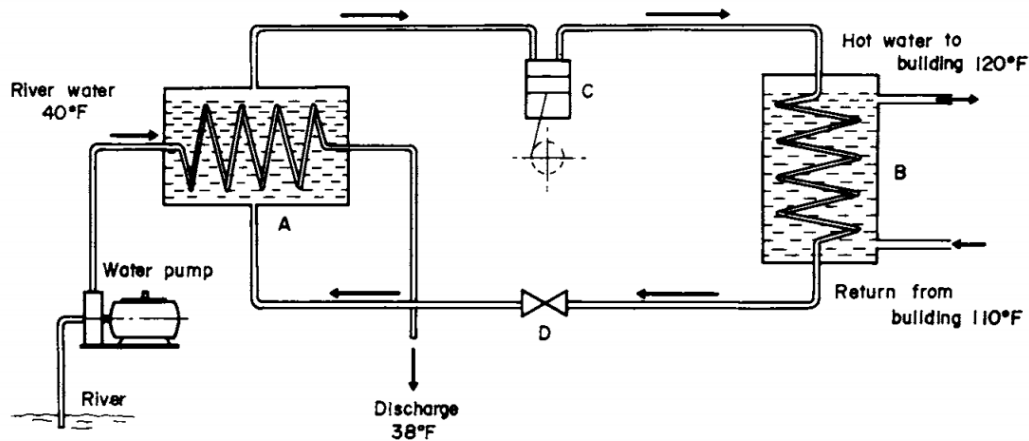


Figure 2.2. Diagram of the first constructed heat pump (Reay and Macmichael, 1988)

Twentieth century witnessed rapid development of the heat pumps. One of the first conventional vapor compression refrigeration cycle is installed by Southern California Edison Co. in Los Angeles in 1930. The cycle had the power of 1050 kW and the Coefficient of Performance (COP) of the cycle was 2.5. Likewise, the Zurich Technical University ETH installed a heat pump that had 7MW power and 3 COP value in 1942. The use of organic fluids as the working fluid of the heat pumps are popularized in 1940s and first household commercial heat pump products began to appear at the stores. United States was quick to adopt this new technology due to having more suitable climatic conditions and installed many modern heat pump products to the buildings. In the first full year production, around 1000 commercial heat pumps are manufactured. This number is doubled by 1954 and increased tenfold by 1957. The majority of the products are installed in southern parts of the United States. By the 1980s, 30% of the all newly constructed houses in the United States had a heat pump. Afterwards, other countries that have different climatic conditions than the United States such as France, Sweden, Norway also adopted the heat pump technology and began to install heat pumps to the buildings. Nowadays, the heat pump technology is still widely used in many countries and constitutes a large amount of energy consumption of the countries.

The vapor compression heat pumps convert electrical energy into heat energy. The smaller vapor compression heat pumps do not consume much electrical energy and their installation are easy. Therefore, they do not constitute much problem. However, larger heat pumps requires more electrical energy to operate. And larger electrical-to-heat energy conversion results in lower exergetic efficiency. The sorption heat pumps are a great alternative to vapor compression heat pumps. The sorption heat pumps do not have a

compressor that consumes large electrical energy. Instead, they utilize a pump that operates with much lower electrical energy. Their capital cost is much lower than their vapor compression counterparts in advantageous conditions. They are hazardous to the environment. For these reasons, more and more countries are installing sorption heat pumps into factories and houses. One of the common types of sorption heat pumps are the absorption heat pumps. As discussed before, the absorption requires very little work input to transfer the heat between the high- and low-temperature environments and can be operated with renewable energy technologies such as solar panels (Herold et al., 2016). Schematic representation of an absorption heat pump and a vapor compression heat pump are depicted in Figure 2.3 and Figure 2.4, respectively.

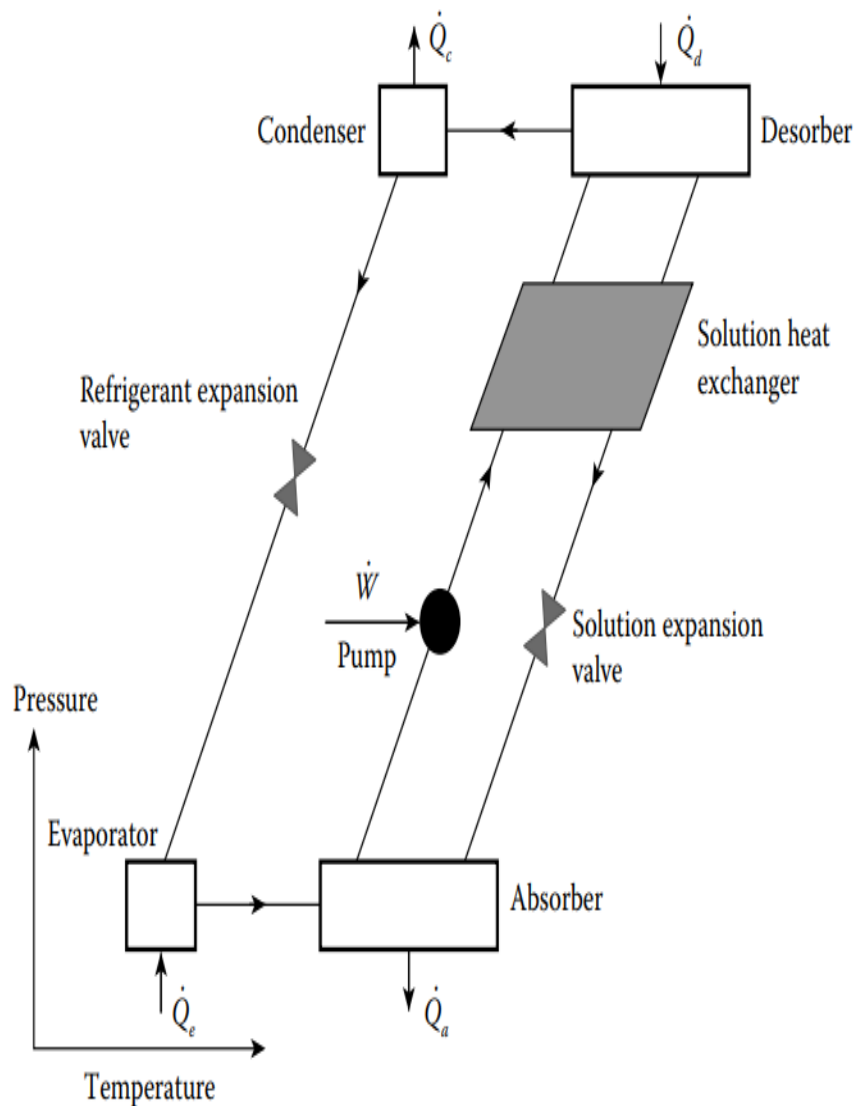


Figure 2.3. An absorption heat pump (Herold et al., 2016)

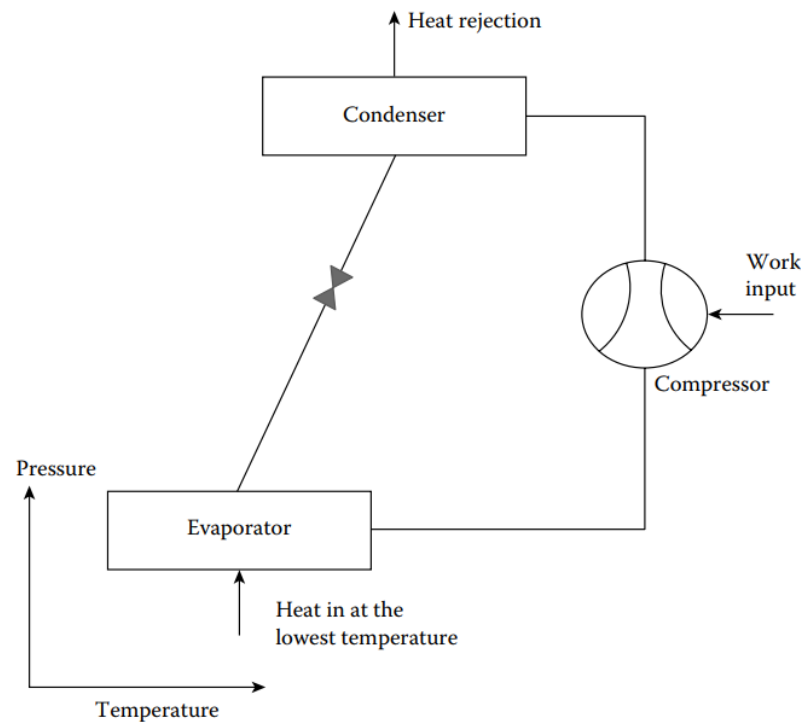


Figure 2.4. A vapor compression heat pump (Herold et al., 2016)

Using a heat pump can be advantageous in some applications. These are,

- If there is a place to be heated and the temperature of the place is too low compared to the environment.
- If the place to be conditioned needs both heating and cooling depending on the season.
- If there is a large energy flow in an industrial factory that can be reversed.
- If the industrial factory that the heat pump will be installed already has a heat regeneration system.
- If the energy is conveyed to a far away distance. So that the capital cost can be decreased by utilizing a heat pump.

There has been arguments among the politicians and the researchers over the years about whether the development of the heat pump technology is necessary or not. People that defend the usage of the heat pumps assert the following points.

- The heat pumps can help humanity to reduce its energy consumption. The economy can not expand much further without the reducing of energy consumption.
- By integrating the heat pump into a energy system, we can modernize and reduce the

capital investment cost of the system.

- A heat pump works for both ways. It can be utilized as either for cooling or heating. It is a perfect technology for a space to be conditioned depending on the season.

- A vapor compression heat pump is not hazardous to environment. It can be used in houses where there is low environmental pollution and factories where there are high environmental pollution.

The arguments against the usage of heat pumps are as follows.

- The US and the northern European countries have different climates. Thus, for example in countries like Poland, one can not only rely on using only the heat pumps over a year.

- Same as above, district heating systems in northern European countries are more preferable to heat pump systems in terms of energy consumption.

- Coal-fired heating systems is more preferable to heat pump systems in terms of economic cost.

- Large vapor compression heat pumps that consume megawatts of energy is more appropriate for usage in sizable energy districts.

- Larger heat pumps should be manufactured and designed separately. These heat pumps are less traditional and more complex than their smaller counterparts. Thus, more qualified workforce and more economic sufficiency are required to employ such systems.

- Current working fluids that are employed in the heat pumps do not achieve favorable performance.

As discussed above, heat pumps can be of different kinds. Also, each type of cycle can be realized differently. A brief summary of this fact is depicted in Figure 2.5.

The most basic type of cycle is the ideal cycle, in other words the Carnot cycle. The ideal cycle can be thought as the reverse type of heat engine. The heat engine extracts heat from the high-temperature environment and releases heat to the low-temperature environment. By doing so, it outputs work. On the other hand, the heat pump requires work input to operate. By supplying the work input to the system, the cycle extracts heat from the high-temperature environment and releases the heat to the low-temperature environment. If the circuit direction of the working fluid is reversed, the cycle operates reversely. It extracts heat from the low-temperature environment and releases to the high-temperature environment. Thermodynamically, this process can be depicted as in Figure 2.6.

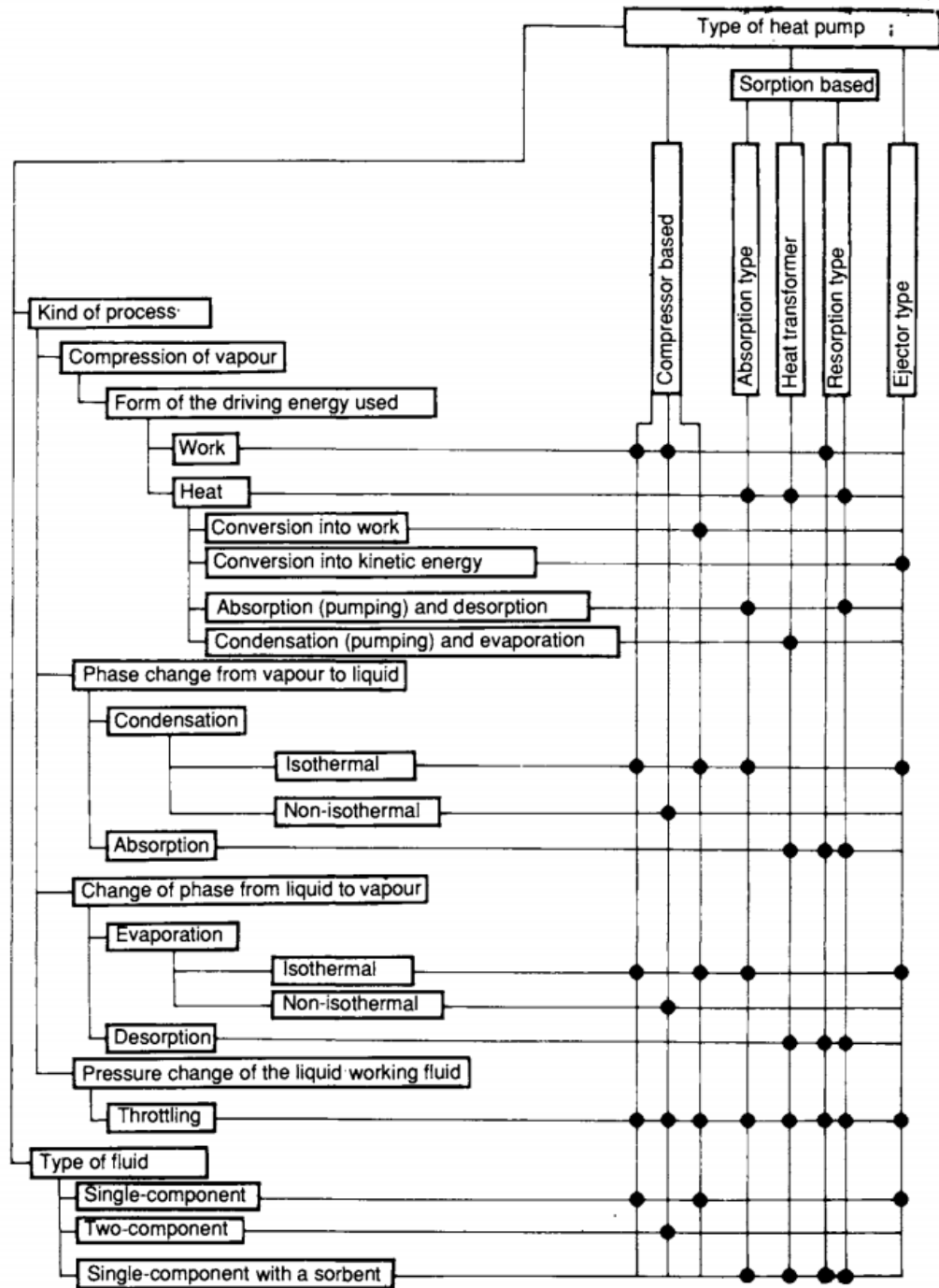


Figure 2.5. Type of realizations of different kind of heat pumps (Dyakowski and Brodowicz, 1993)

The ideal cycle consists of four different processes (Hundy et al., 2016). These four processes are expansion, compression, evaporation and condensation. The working fluid goes through these processes and returns to its original state after completing the cycle. In the expansion and compression processes, entropy of the working fluid remains constant, thus these processes are isentropic. Work is supplied to the system during the compression process

and extracted from the system during the expansion process. And the heat is transferred to the system during the evaporation process and extracted from the system during the condensation process. By considering these idealizations, the process is accomplished with maximum amount of heat transfer and minimum amount of work. Therefore, the maximum efficiency, the Carnot cycle efficiency is accomplished. A graphical representation of a ideal cycle and its corresponding temperature-entropy diagram is given in Figure 2.7.

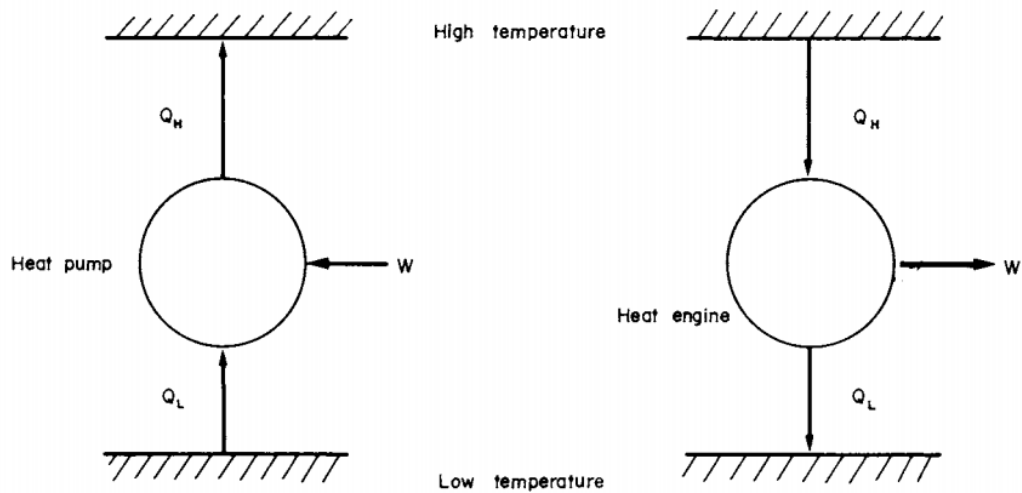


Figure 2.6. Thermodynamic representation of the heat pumps (Reay and Macmichael, 1988)

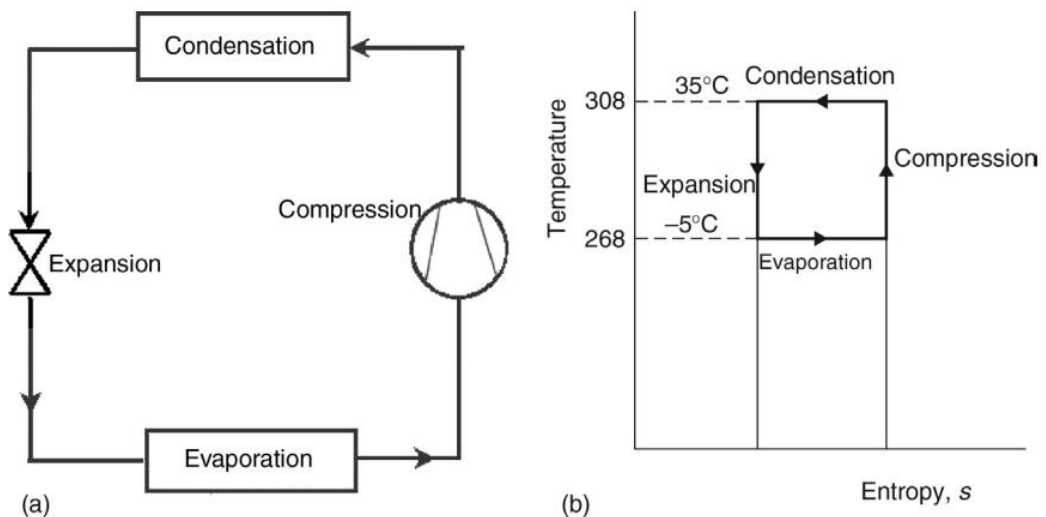


Figure 2.7. a) Graphical representation of an ideal cycle b) Temperature-entropy diagram of the ideal cycle (Hundy et al., 2016)

The Carnot cycle efficiency can be calculated with the following formula,

$$COP = \frac{T_L}{T_H - T_L} + 1 \quad (2.1)$$

The vapor compression refrigeration cycle can be thought as application of the ideal Carnot cycle to the real world. The vapor compression cycle is mainly used for refrigeration and it has the same components with the ideal Carnot cycle. The working fluid is compressed at the compressor and its pressure and enthalpy goes up. Then the fluid releases its heat energy to the environment and condensates at the condenser. Afterwards, the working fluid that is in the liquid phase is expanded and transforms into liquid-vapor phase at the expansion valve. Finally, the liquid-vapor fluid absorbs the heat energy from the secondary fluid and evaporates at the evaporator. The graphical representation and the pressure-enthalpy diagram of the corresponding cycle are given in Figure 2.8 and Figure 2.9, respectively.

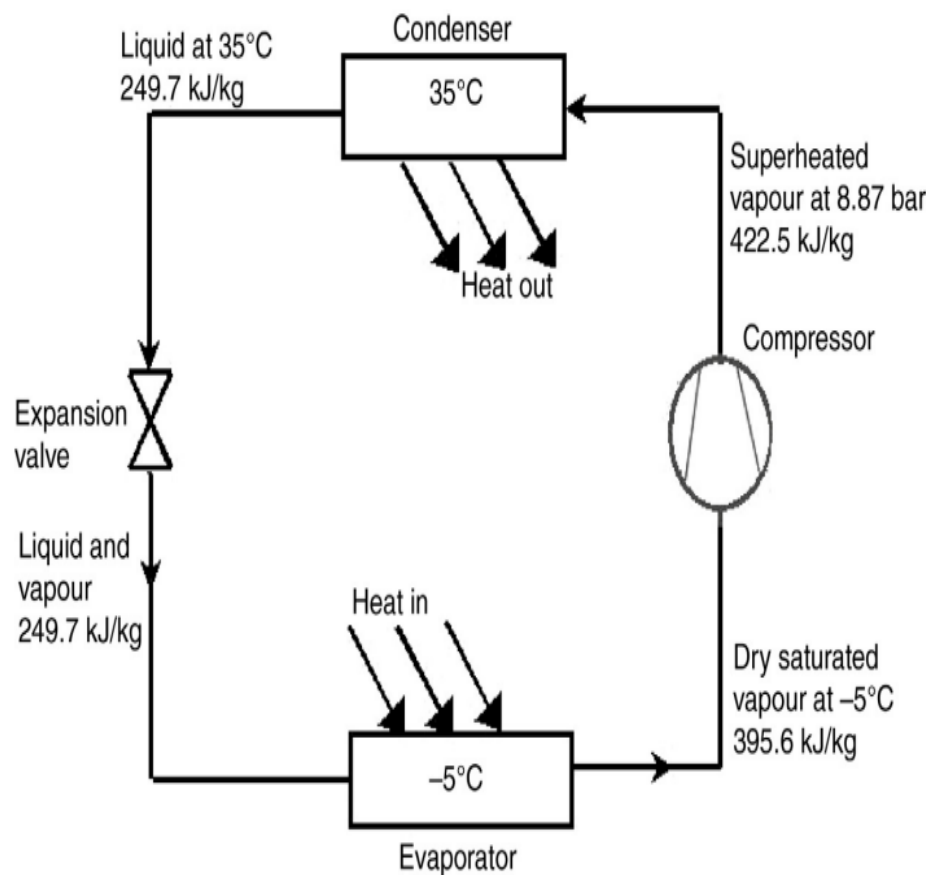


Figure 2.8. Graphical representation of a vapor compression cycle operated with R134a (Hundy et al., 2016)

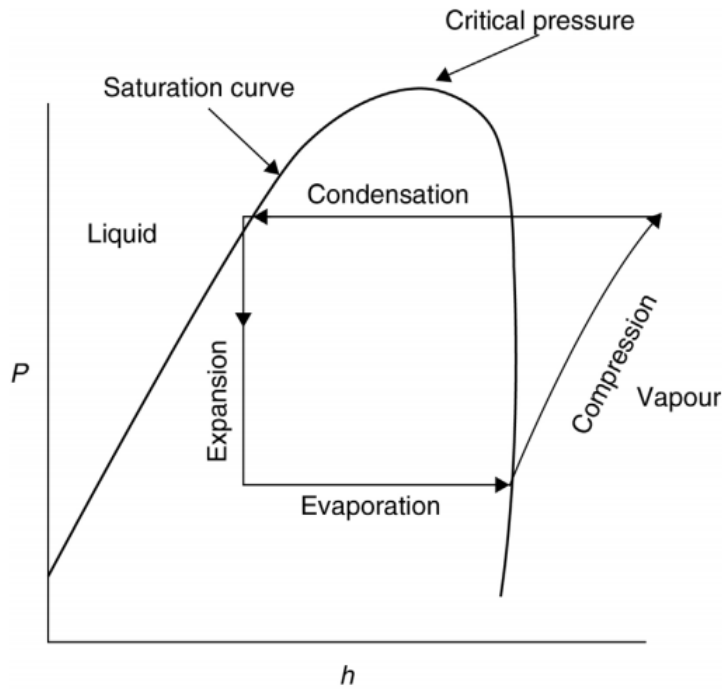


Figure 2.9. Pressure-enthalpy diagram of the vapor compression cycle (Hundy et al., 2016)

Another type of heat pump is called the absorption refrigeration cycle. A schematic representation of an absorption refrigeration cycle is shown in Figure 2.10.

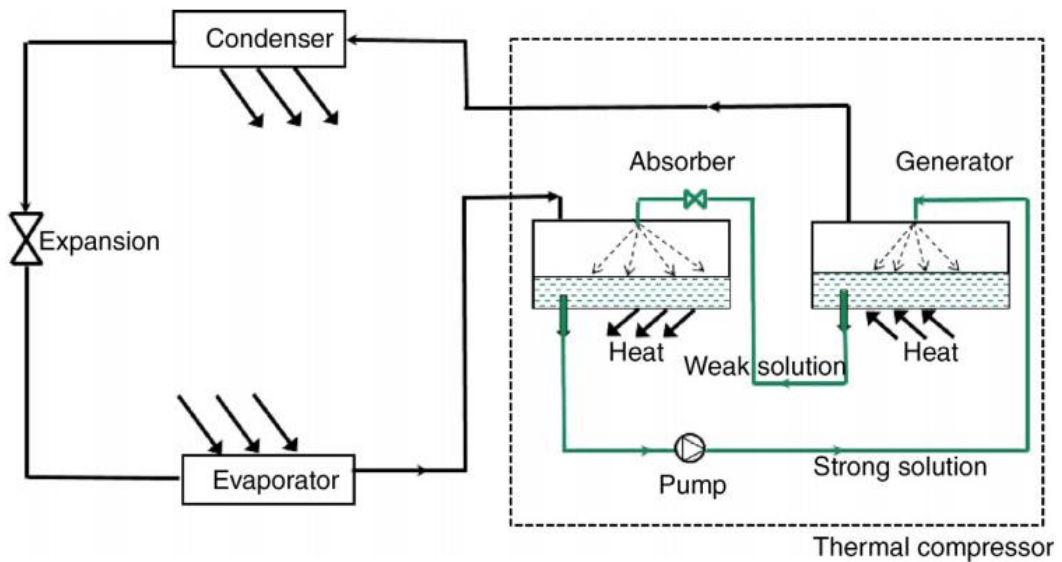


Figure 2.10. An absorption refrigeration cycle (Hundy et al., 2016)

As can be seen in Figure 2.10, difference between the vapor compression cycle and the absorption cycle is that the compressor is replaced with a absorber-generator system. The

refrigerant leaves the evaporator in vapor form and absorbed by an absorbent. The concentration of the absorption fluid increases as the fluid passes through the absorber. Then the temperature of the fluid increases at the generator and is pumped back to the condenser. The solution with low concentration that is left at the generator is expanded and is pumped back to the absorber.

Mainly two different working fluids are used in the absorption cycles. These are the ammonia-water and lithium bromide-water solutions. The lithium bromide-water solution is appropriate for general chilling applications. However, the ammonia-water solution is appropriate for chilling applications that have evaporation temperature below 0°C. The absorption refrigeration cycles take much more energy input than the vapor compression cycles, however, they do not require much work input. Therefore, they are suitable for renewable energy systems. The COP of an absorption cycle can be calculated as follows,

$$COP = \frac{\frac{1}{T_{abs}} - \frac{1}{T_{gen}}}{\frac{1}{T_{evap}} - \frac{1}{T_{cond}}} \quad (2.2)$$

where  $T_{abs}$ ,  $T_{gen}$ ,  $T_{evap}$ ,  $T_{cond}$  are the absorber, generator, evaporator and condenser temperatures, respectively.

Adsorption refrigeration cycle is another type of heat pump. Adsorption refrigeration cycle utilizes materials such as silica gels and zeolites which can adsorb refrigerants up to %30 of their weight. Choice of the adsorbent and refrigerant combination changes with the application. However the most widely used ones are carbon with ammonia and silica gel with water. The amount of refrigerant adsorbed depends on system temperature and pressure. A schematic representation of an adsorption refrigeration cycle is depicted in Figure 2.11. The processes shown in Figure 2.11 can be described as follows. Initially, the system is at low pressure and low temperature state (state a). Thereafter, in b, the adsorbent is heated and the adsorbed refrigerant is released and moves on the next vessel. This release process increases the pressure and the temperature of the system. Then, in c, the system is cooled back to the environment temperature and re-adsorption of the refrigerant and drop in system temperature and pressure begin. Finally, in d, the reduced pressure of the system causes the refrigerant in the second vessel to absorb heat energy from the environment and refrigeration phenomenon happens.

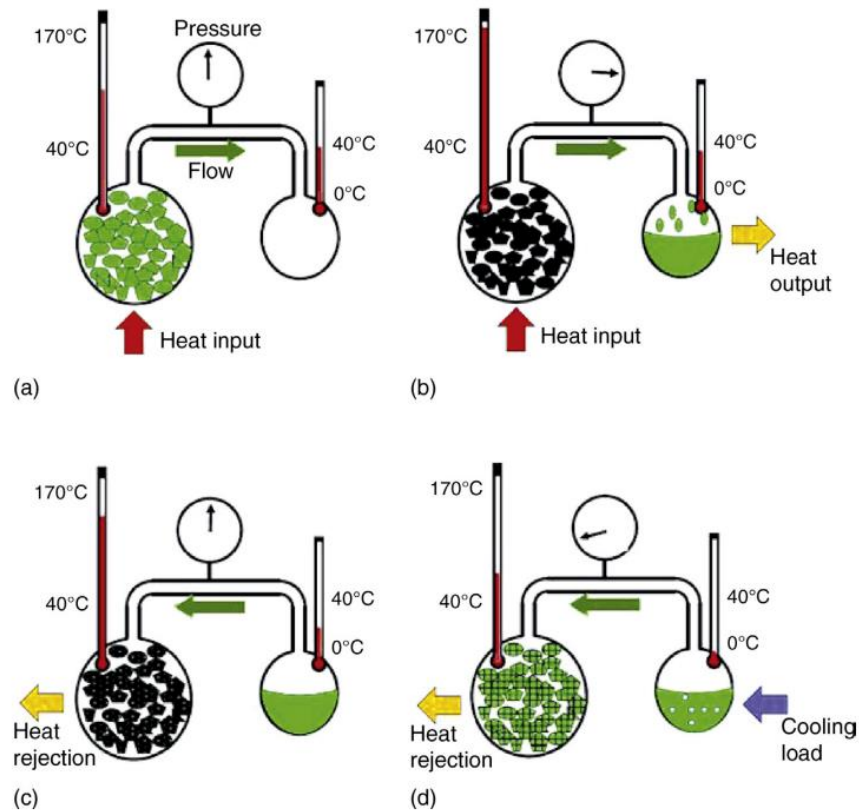


Figure 2.11. Adsorption refrigeration cycle (Hundy et al., 2016)

Desiccant cooling systems is the last type of heat pump technology that will be described in this thesis. A basic desiccant cooling system is shown in Figure 2.12. Desiccant cooling system is an open cycle. It consists of two separate wheels, namely temperature and humidity wheels. The desiccant can be re-activated by utilizing solar or waste heat energy. Thus, desiccant cooling is an environmentally-friendly technology. The thermal is wheel is generally selected as a rotary heat exchanger and recovers the heat energy between the supply air and exhaust air. The desiccant wheel works the same way except it also re-activates the desiccant.

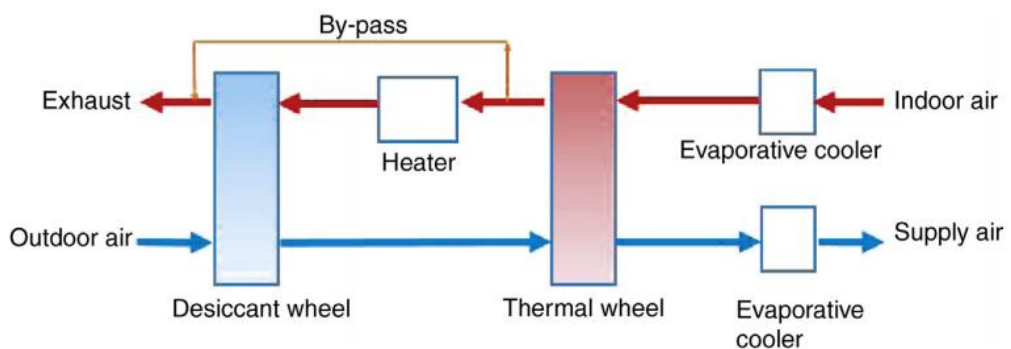


Figure 2.12. Desiccant cooling system (Hundy et al., 2016)

## 2.2. Dynamic Modeling of a Vapor Compression System

As described above, there are four basic components in a standard vapor compression cycle. These components are compressor, expansion valve, evaporator and condenser. A general demonstration and pressure-enthalpy diagram of a vapor compression cycle that is analyzed in this study are given below in Figure 2.13 and Figure 2.14 respectively.

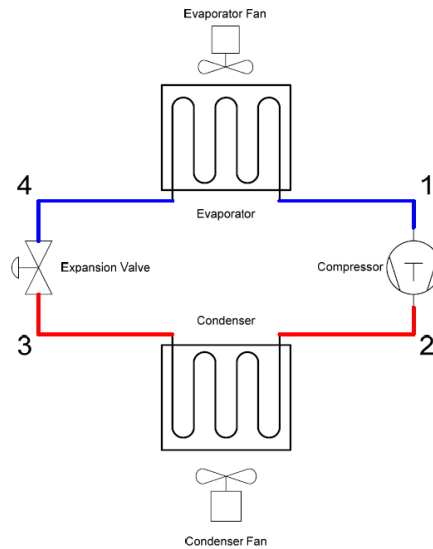


Figure 2.13. A typical demonstration of a vapor compression cycle (Rasmussen and Alleyne, 2006)

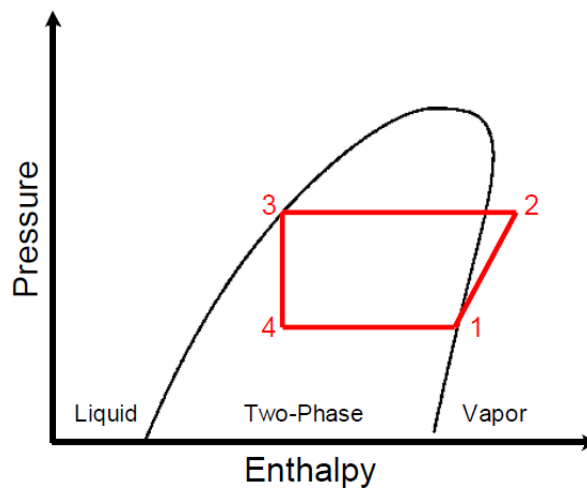


Figure 2.14. Pressure-enthalpy diagram of a vapor compression cycle (Rasmussen and Alleyne, 2006)

Bendapudi and Braun (2002) and Lebrun and Bourdouxhe (1998) included a large literature review on this topic in their studies. As Bendapudi noted in his study, modeling of the heat exchangers takes up the bigger work in dynamic simulation of a vapor compression cycle. Modeling of the heat exchangers are generally accomplished by utilizing three different

group of approaches. These are lumped parameter approach, discretization approach and moving-boundary approach. Modeling of the compressor and expansion valve are generally done with nonlinear static relationships due to their higher evolving dynamics compared to that of the heat exchangers. Brief descriptions of the each heat exchanger modeling approaches are given in the paragraphs below.

Lumped parameter models are perhaps the most primitive and simplified of the three modeling approaches. Due to its simplicity, most of the time the focus is on a different point that heat exchanger dynamics in the papers that utilizes the lumped parameter models. Work of the Chi and Didion (1982) may be a good example of lumped parameter modeling of the heat exchangers.

Discretized models are highly-reliable approaches for the modeling of the heat exchangers. Nowadays, most commercial software packages use different types of discretization approaches for the modeling of the heat exchangers. The most widely-used discretization approaches for the modeling of the heat exchangers are finite-difference (FDM) and finite-control volume (FCV) methods. In the discretization methods, the heat exchangers are divided into homogenous finite-sized control areas or volumes. High-level of discretization generally results in more accurate outcomes, however, it requires more computation power to calculate the results. Some of the studies in the literature that utilizes the discretization approach are MacArthur (1984), Chen and Lin (1991) and Fu et al. (2003). Demonstration of a discretized heat exchanger is given in Figure 2.15.

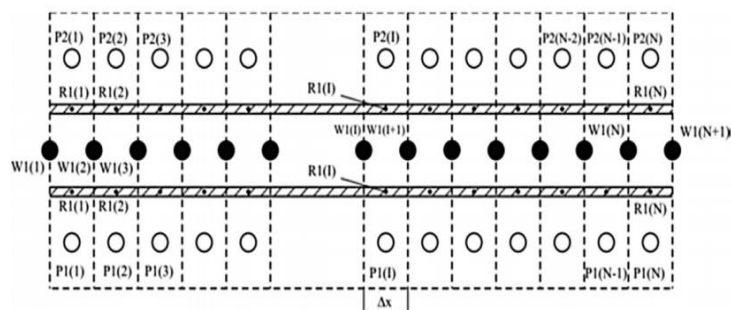


Figure 2.15. Discretized heat exchanger model (Korzen and Taler, 2015)

The MB method attempts to capture the multi-phase dynamics in a heat exchanger at the same time benefiting from the simplicity of the lumped parameter method. In the MB method, each fluid phase in the heat exchanger is evaluated as a separate control volume and the boundaries that separate the each control volume represents the phase transitions of the fluid. Physical and thermal properties of the fluid are evaluated as lumped averages inside each region. Many studies in the literature utilized the MB method for the modeling of the heat exchanger dynamics (Rasmussen, 2015; Rasmussen and Shenoy, 2008; McKinley and Alleyne, 2008; Li and Alleyne, 2010). The studies in the literature proved that MB is a preferable alternative to discretized models with less accuracy and less computational load. A sample demonstration of a heat exchanger modeled with the MB method is depicted in Figure 2.16.

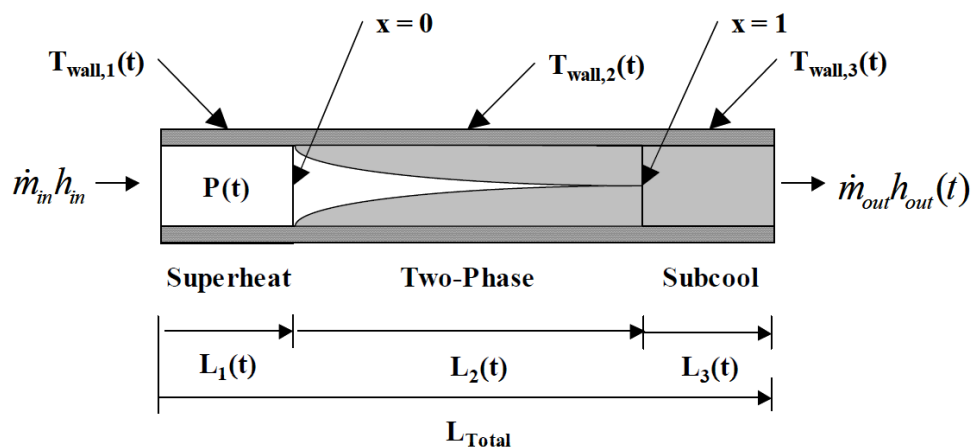


Figure 2.16. A heat exchanger modeled with the MB method (Rasmussen and Aleyne, 2006)

From this point forward, the dynamic modeling of a vapor compression cycle will be presented. R134a and R1234yf refrigerants are employed in the cycle and their performances in the cycle will be compared with each other. The evaporator and condenser are modeled with the FDM. Following assumptions are made for the modeling of the heat exchangers:

- The heat exchangers are double pipe heat exchangers with long and horizontal tubes.
- Axial conduction that occurs in the heat exchangers are neglected.
- Refrigerant flow in the heat exchangers is considered as one-dimensional flow.
- Pressure drops, kinetic and potential energy variations and viscous flow frictions that occur in the heat exchangers are neglected.

The evaporator is considered as a cross-flow double pipe heat exchanger. The

evaporation process that happens in the evaporator is modeled with the Gungor and Winterton (1985) correlation. The following equations describe the Gungor and Winterton correlation.

$$Bo = \frac{q}{\rho v h_{liq}} \quad (2.1)$$

$$X_{tt} = \left(\frac{1-x}{x}\right)^{0.9} \left(\frac{\rho_v}{\rho_{liq}}\right)^{0.5} \left(\frac{\mu_{liq}}{\mu_v}\right)^{0.1} \quad (2.2)$$

$$E = 1 + 24000Bo^{1.16} + 1.37(1/X_{tt})^{0.86} \quad (2.3)$$

$$S = \frac{1}{1+1.15 \times 10^{-6} E^2 Re^{1.17}} \quad (2.4)$$

$$h_1 = 0.023 Re^{0.8} Pr^{0.4} k/d \quad (2.5)$$

$$h_{pool} = 55 Pr^{0.12} (\log_{10} Pr)^{-0.55} M^{-0.5} q^{0.67} \quad (2.6)$$

$$h_{tp} = E h_1 + S h_{pool} \quad (2.7)$$

Gnielinski (1976) is utilized for the modeling of the determination of the Nusselt number in single phase turbulent flows,

$$Nu = \frac{\left(\frac{f}{2}\right)(Re-1000)Pr}{1+12.7(Pr^{2/3})\sqrt{f/2}} \quad (2.8)$$

The friction factor for the determination of the Nusselt number is calculated as follows,

$$Re = \frac{\rho V D}{\mu} \quad (2.9)$$

$$f = \frac{64}{Re} \quad \text{Laminar} \quad (2.10)$$

$$f = (0.79 \ln Re - 1.64)^{-2} \quad \text{Turbulence}$$

A sample demonstration of a discretized evaporator is depicted in Figure 2.17 below.

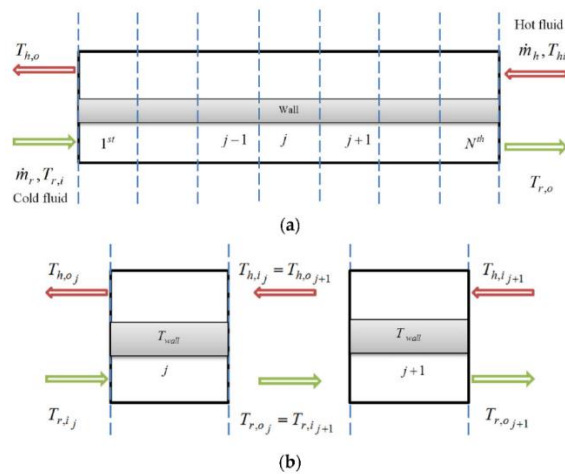


Figure 2.17. A discretized evaporator (Chowdhury et al., 2015)

Behavior of the primary fluid in the evaporator is calculated by solving following set of

differential equations,

$$\frac{\partial \dot{m}_v h_v}{\partial t} = \dot{m}_{ev} h_{liq} - \frac{\partial \dot{m}_v h_v}{\partial x} dx \quad (2.11)$$

$$\frac{\partial \dot{m}_{liq} h_{liq}}{\partial t} = h_{in} p_{in} dx (T_w - T_{ref}) - \frac{\partial \dot{m}_{liq} h_{liq}}{\partial x} dx - \dot{m}_{ev} h_{liq} \quad (2.12)$$

Behavior of the secondary fluid is modeled with the following equation,

$$\rho \frac{\partial h}{\partial t} - \rho V \frac{\partial h}{\partial x} - \frac{h_{out} p_{out}}{A} (T_w - T_{liq}) = 0 \quad (2.13)$$

Finally wall temperature of the evaporator is calculated with the following equation,

$$C \rho V ol \frac{\partial T_w}{\partial t} - h_{in} p_{in} (T_{ref} - T_w) + h_{out} p_{out} (T_w - T_{liq}) \quad (2.14)$$

The condenser is also considered as cross-flow double pipe heat exchanger. The condensation process is modeled with the Travis (1971) correlation. The correlation consists of following equations,

$$\begin{aligned} Re_{liq} < 50 & \quad F_2 = 0.707 Pr_{liq} Re_{liq}^{0.5} \\ 50 < Re_{liq} < 1125 & \quad F_2 = 5 Pr_{liq} + 5 \ln[1 + Pr_{liq} (0.0963 Re_{liq}^{0.585} - 1)] \\ Re_{liq} > 1125 & \quad F_2 = 5 Pr_{liq} + 5 \ln(1 + Pr_{liq}) + 2.5 \ln(0.00313 Re_{liq}^{0.812}) \end{aligned} \quad (2.15)$$

$$F(X_{tt}) = 0.15(X_{tt}^{-1} + 2.85X_{tt}^{-0.476}) \quad (2.16)$$

$$\frac{Nu_{F_2}}{Pr_{liq} Re_{liq}} = F(X_{tt})^{1.15} \quad (2.17)$$

Primary fluid behavior in the condenser is modeled with the following set of equations,

$$\frac{\partial \dot{m}_{liq} h_{liq}}{\partial t} = \dot{m}_{co} h_{liq} - \frac{\partial \dot{m}_{liq} h_{liq}}{\partial x} dx \quad (2.18)$$

$$\frac{\partial \dot{m}_v h_v}{\partial t} = h_{out} p_{out} dx (T_{ref} - T_w) - \frac{\partial \dot{m}_v h_v}{\partial x} dx - \dot{m}_{co} h_{liq} \quad (2.19)$$

Following equation represents the behavior of the secondary fluid,

$$\rho \frac{\partial h}{\partial t} - \rho V \frac{\partial h}{\partial x} - \frac{h_{out} p_{out}}{A} (T_w - T_{liq}) = 0 \quad (2.20)$$

And the wall temperature of the condenser is calculated with,

$$C \rho V ol \frac{\partial T_w}{\partial t} - h_{in} p_{in} (T_{ref} - T_w) + h_{out} p_{out} (T_w - T_{liq}) \quad (2.21)$$

Heat transfer phenomena that occurs in the compressor is made up of two different processes. First, the fluid coming from the evaporator interacts with the environment until it reaches the compression room, then the polytropic compression process takes place in the compression room. Design of the compressor is depicted in Figure 2.18.

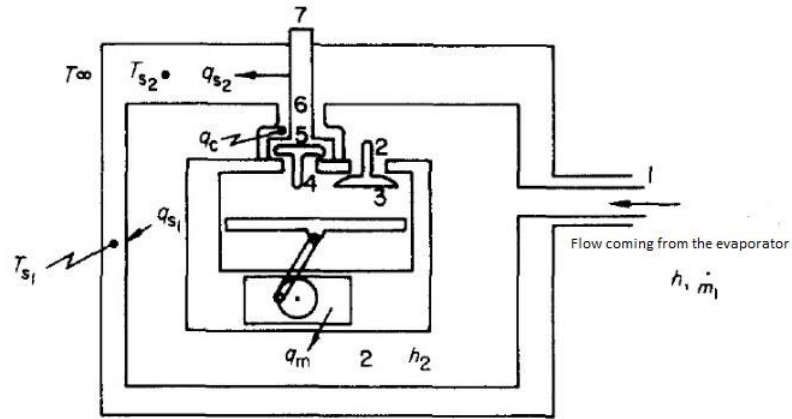


Figure 2.18. Internal structure of the compressor (McArthur, 1984)

First phase of the heat transfer, fluid interacting with the environment, is modeled with the following set of equations,

$$\rho_{ref} V_{ref} (T_3 - T_1) = h_{cout} (T_{cy} - T_1) - h_{s1} (T_1 - T_{s1}) \quad (2.22)$$

$$(C_{cy} \rho_{cy} V_{cy}) \frac{dT_{cy}}{dt} = h_{cin} (T_5 - T_{cy}) - h_{cout} (T_{cy} - T_1) \quad (2.23)$$

$$(C_{shell} \rho_{shell} V_{shell}) \frac{dT_{s1}}{dt} = h_{s1} (T_2 - T_{s1}) - h_{s10} (T_{s1} - T_{\infty}) \quad (2.24)$$

The polytropic compression process is modeled as follows,

$$\left(\frac{T_4}{T_3}\right) = \left(\frac{P_{co}}{P_{ev}}\right)^{\frac{\gamma-1}{\gamma}} \quad (2.25)$$

The orifice equation given in James and James (1987) is utilized to model the expansion valve. It is assumed that the refrigerant enthalpy does not change between the expansion valve inlet and outlet.

$$\dot{m} = 0.0683x\sqrt{(P_{co} - P_{ev})} \quad (2.26)$$

Inner structure of an expansion valve is given in Figure 2.19.

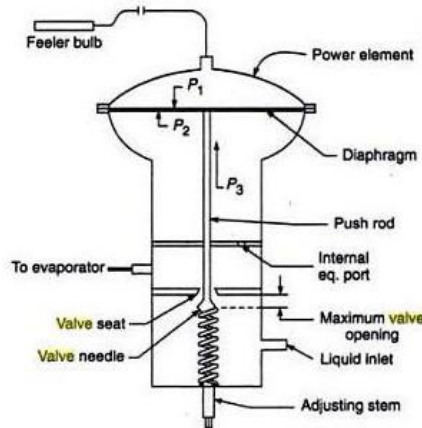


Figure 2.19. Inner structure of an expansion valve (Bright Hub Engineering, 2018)

Thermodynamic and thermophysical properties of the refrigerants R134a and R1234yf are acquired from the CoolProp library (Bell et al., 2014). Mass flow rate of the refrigerants are considered as 0.2kg/sec. The mass flow rate is applied to the system as step input and beginning from the entrance to the evaporator and returning back to the evaporator entrance is considered as a time step. Water is employed in the cycle as the secondary fluid and thermodynamic and thermophysical properties of the water is acquired from the CoolProp library. Isentropic compression rates of the R1234yf and R134a are respectively taken as 1.1 and 1.2. Heat exchanger walls and the compressor shell are assumed to be made of steel. Internal pressures of the evaporator and condenser are calculated as respectively 200kPa and 796.6kPa given 1.1mm openness of the expansion valve needle.

Boiling and condensing temperatures of the R134a and R1234yf refrigerants under the given pressures are -10°C and 31°C and -13°C and 30.5°C respectively. Refrigerant flow inside the heat exchangers are taken as 0.7m/sec which indicates that the flow is turbulent. Design properties of the evaporator and condenser are considered as follows, inner and outer tube diameters are 0.01m and 0.018m, respectively and tube lengths are 14m. Initial temperature of the compressor cylinder, shell and environment are assumed as 25°C. And initial temperatures of the refrigerant, water and wall of the evaporator are taken as -11°C, 0°C and 0°C, respectively, and the water and wall temperatures for the condenser as 23°C and 23°C, respectively. Time steps are considered as 3 sec. and length steps in the heat exchangers are taken as 0.1m. The simulations have been done in the Java programming environment and the performance results of the cycles that operates R134a and R1234yf are compared. Following figures, Figure 2.20, Figure 2.21, Figure 2.22 and Figure 2.23, depict the initial and final temperature-entropy and pressure-enthalpy diagrams of the refrigerants R134a and R1234yf.

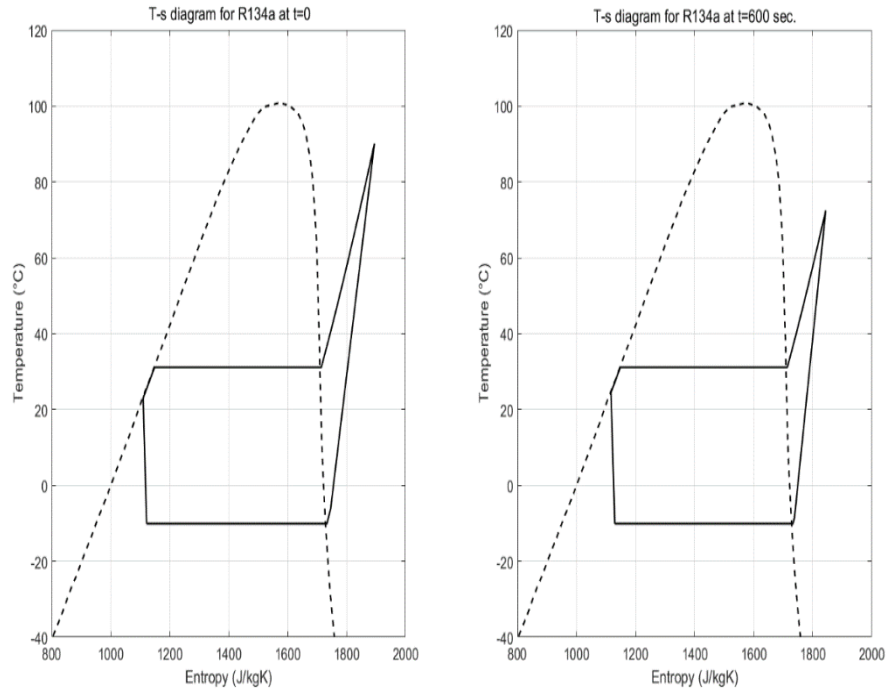


Figure 2.20. Initial and final shape of the temperature-entropy diagram for R134a

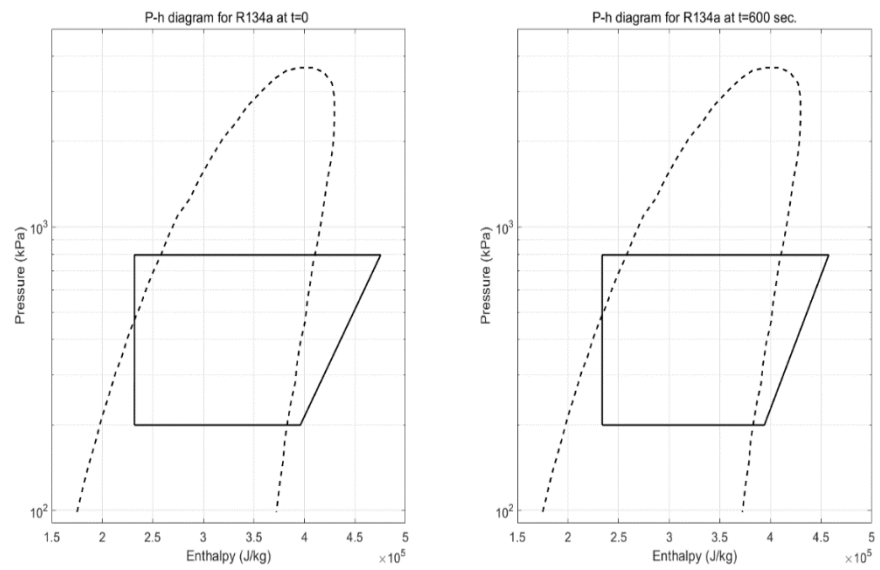


Figure 2.21. Initial and final shape of the pressure-enthalpy diagram for R134a

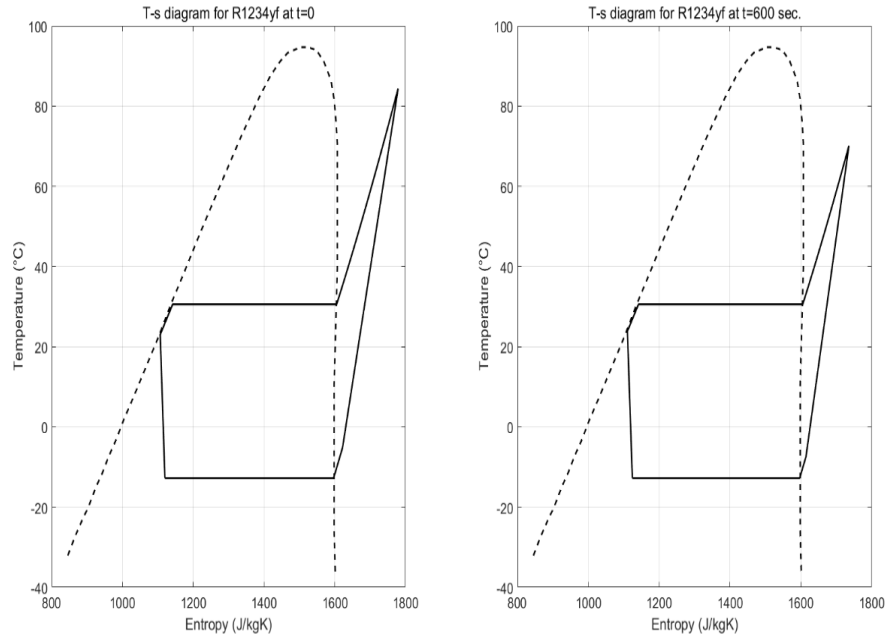


Figure 2.22. Temperature-entropy diagram for R1234yf at initial and final states

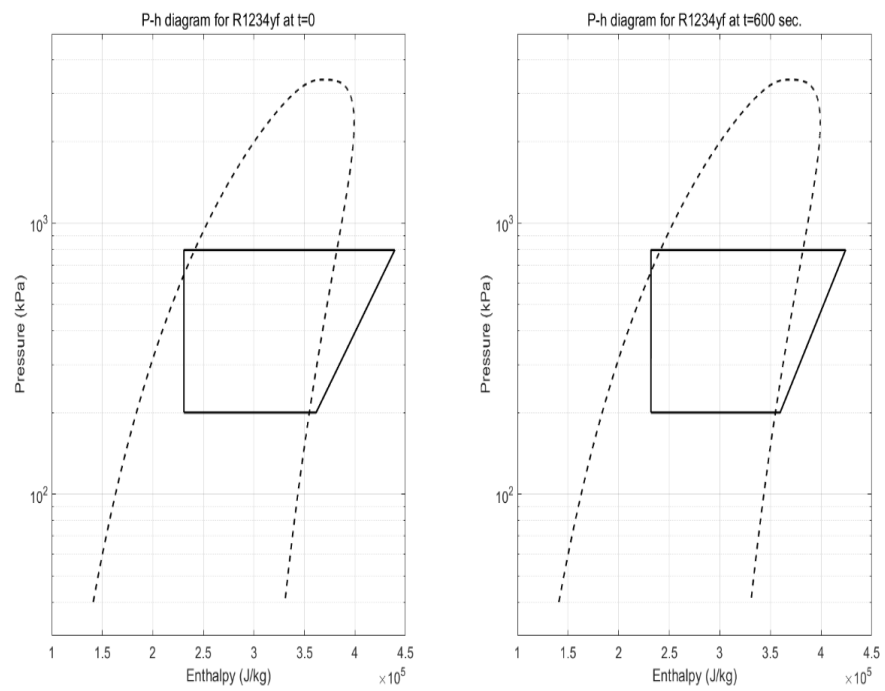


Figure 2.23. Pressure-enthalpy diagram for R1234yf at initial and final states

It can be seen from the Figure 2.20 that initial evaporator, condenser and compressor outlet

temperatures are respectively  $-6.17^{\circ}\text{C}$ ,  $23^{\circ}\text{C}$  and  $90.07^{\circ}\text{C}$  and in the final state they become  $-8.51^{\circ}\text{C}$ ,  $24.47^{\circ}\text{C}$  and  $71.85^{\circ}\text{C}$ , respectively. Likewise it can be seen from the Figure 2.22 that initial evaporator, condenser and compressor outlet temperatures are respectively  $5.15^{\circ}\text{C}$ ,  $23.01^{\circ}\text{C}$  and  $84.37^{\circ}\text{C}$  and in the final state they become  $-7.45^{\circ}\text{C}$ ,  $23.86^{\circ}\text{C}$  and  $70.08^{\circ}\text{C}$ , respectively. The condenser and evaporator wall temperatures varies with time, therefore, superheat and subcool temperatures of the refrigerant decreases and increases with time, respectively. For this reason, the superheat and subcool temperatures get inside to the saturation dome after some time. The system loses its stability and the COP drops to zero after these temperatures get inside to saturation dome. Change of the COP, compressor work and the cooling load with time for the both refrigerants are depicted in Figure 2.24, Figure 2.25 and Figure 2.26, respectively.

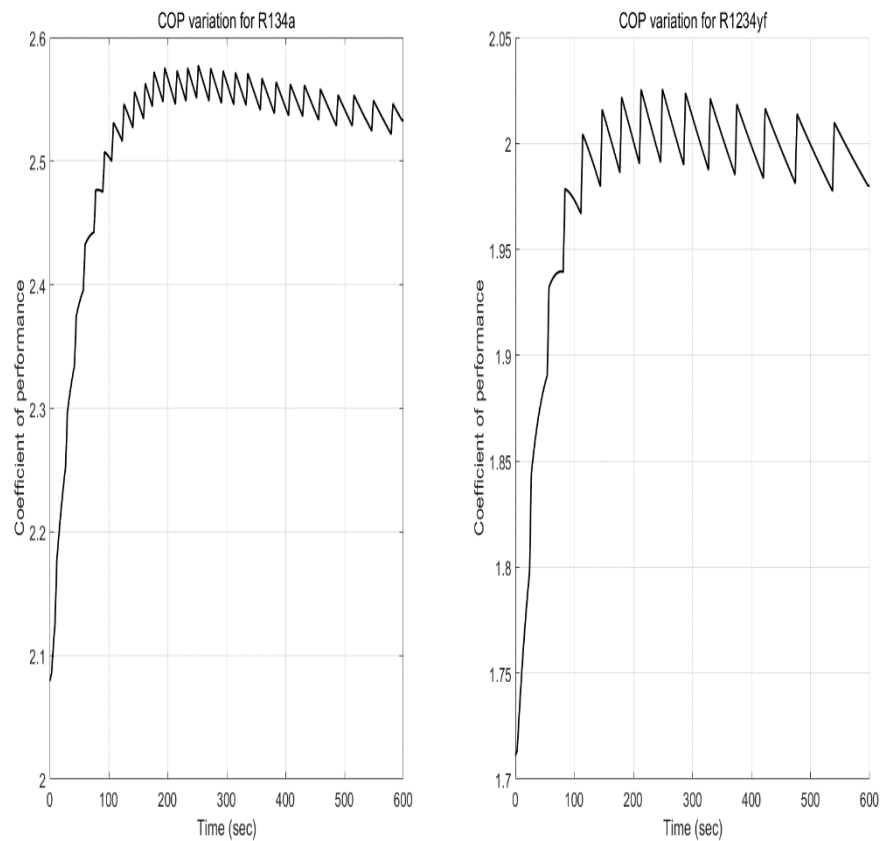


Figure 2.24. Change of the COP with time for the both refrigerants

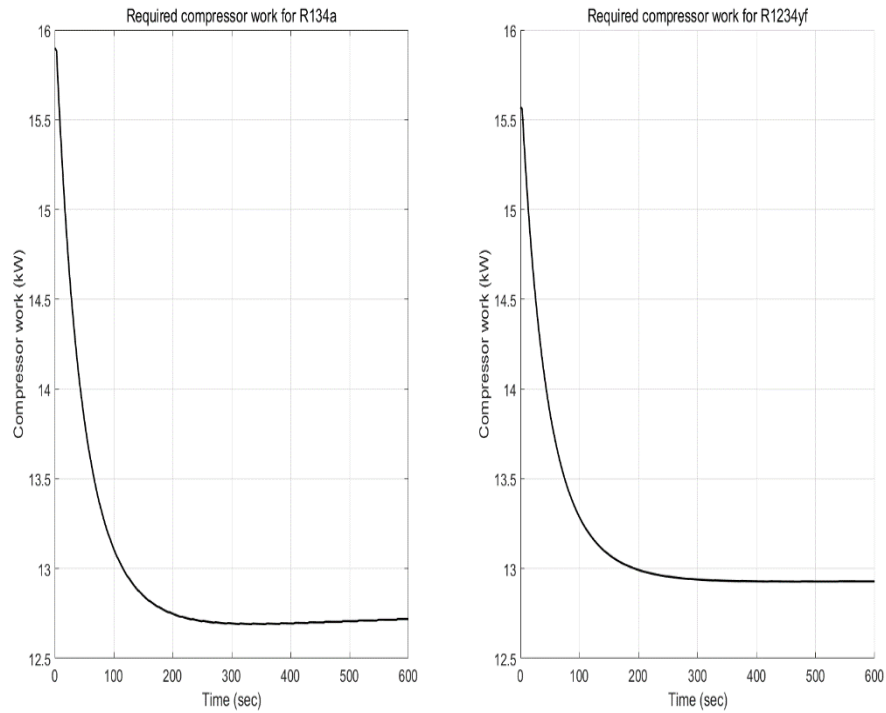


Figure 2.25. Change of the compressor work with time for the both refrigerants

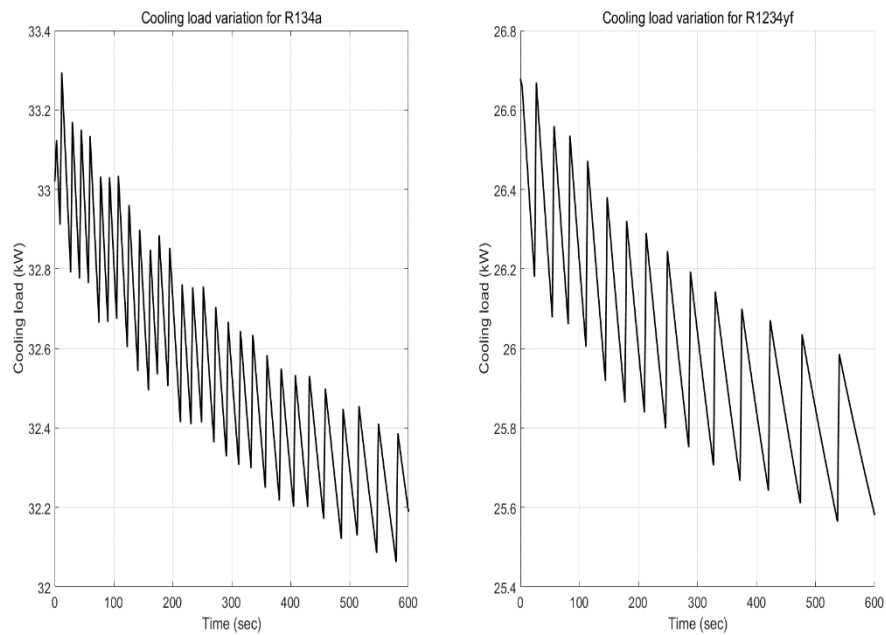


Figure 2.26. Change of the cooling load with time for the both refrigerants

It can be seen that there are zig-zags in the cooling load trajectory changing with time. These zig-zags happens because of the instabilities in the evaporation correlation. Moreover, it can be

noticed that as the superheat temperature drops, compressor work also drops with time. R134a absorbs more heat from the secondary fluid in the evaporator, however, required compressor works for the both refrigerants are similar. For this reason, it can be said that performance of the cycle that employs R134a is greater than that of employs R1234yf. The reason for this phenomena occurs because of the more favorable thermodynamic and thermophysical characteristics of the R134a compared to R1234yf.

### 3. OPTIMIZATION

#### 3.1. Optimization Problem

Engineers generally come across with various type of optimization problems. A common task to accomplish in optimization problems is finding a set of design variables which is subject to a set of constraints that minimizes or maximizes an objective function. A non-linear, single-objective and constrained optimization problem can be mathematically formulated as follows (Bozorg-Haddad et al., 2017),

$$\begin{aligned} \text{Min:} & \quad f(x) \\ \text{Subject to:} & \quad g_j(x) \leq 0 \quad j = 1, p \\ & \quad h_k(x) = 0 \quad k = 1, r \\ & \quad x_{iL} \leq x_i \leq x_{iU} \quad i = 1, s \end{aligned} \quad (3.1)$$

where  $g_j(x)$ ,  $h_k(x)$  are respectively the inequality and equality constraints,  $f(x)$  is the objective function and  $x$  is the decision variables vector.

#### 3.2. Traditional Optimization Techniques

There are different types of optimization techniques such as linear programming, quadratic programming, trust-region methods, etc. (Yang, 2018). Traditional optimization algorithms have some drawbacks compared to modern optimization algorithms. These are,

- Traditional algorithms are mostly local search algorithms. Therefore they do not guarantee to find the global optimum since they only rely on derivative information to find the optimum point especially for non-linear problems.

- Traditional algorithms are generally problem-specific. Since the search space landscape changes from problem to problem, it is possible that with changing derivative information, the algorithm may not converge to global minimum.

- Traditional algorithms can not deal with highly non-linear and multimodal problems. They also can not deal with discontinuity in the problems.

- For most of the traditional algorithms, the final solution is tied to the initial point. If a traditional algorithm is utilized with the same initial points, it is expected for the algorithm to converge to a similar point.

As discussed above, the traditional algorithms mostly work on derivative knowledge of the search space. For this reason, they can be called as local optimization techniques. These algorithms generally have less computational load compared to their modern counterparts and they mostly require little parameter-tuning (Venter, 2010). Following figure can be a good way to explain how a traditional gradient-based algorithm works.

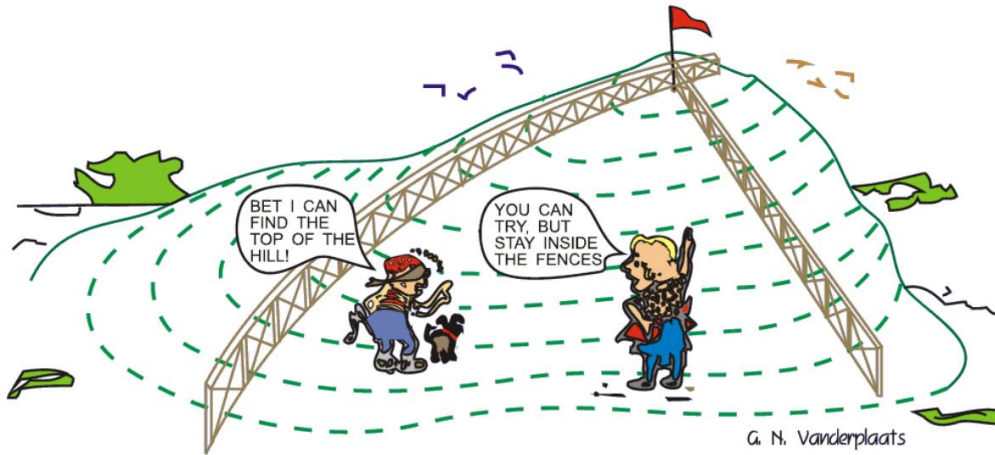


Figure 3.1. Traditional optimization technique (Vanderpaats, 2007)

In Figure 3.1, the blindfolded boy represents the searching agent, the flag on top of the hill represents the maximum point, or the objective, and the fences are the constraints of the problem. A primary objective would be making sure that the boy start from inside of the fences since he can not get over the fences blindfoldedly. This situation shows the first design problem of the traditional optimization techniques. Then the boy takes some steps in the  $x$  and  $y$  directions to approach to top of the hill. By using the information he got from his previous steps, he can predict where he can go next until he realizes that he makes no progress. This may be reaching a fence or getting a steeper place. If he reaches a fence, this means that the algorithm has reached the limits of the workspace, so the boy should go back. If he comes to a steeper place, where he would not have any information about where he can go next, this means that he reached the top of the hill, optimum point, or he arrived to a small tip, local minimum.

There are many different local optimization techniques in the literature. Some of the most famous local optimization techniques are described in the following sub-sections.

### 3.2.1. Newton's Method

Newton's method is one of the most classic and used traditional optimization technique. Newton's method is based on the Taylor expansion formula defined below,

$$f(x) \approx f(x^0) + \nabla f(x^0)^T (x - x^0) + \frac{1}{2} (x - x^0)^T H(x^0) (x - x^0) \quad (3.2)$$

where  $H(x)$  is the hessian matrix. Next step is updating the candidate design vector according to the following rule,

$$x = x^0 - H(x^0)^{-1}\nabla f(x^0) \quad (3.3)$$

The step size is assumed to be one in the above equations. One of the major drawbacks of the Newton's method is second derivative term in the Hessian matrix. The second derivative term makes the method impractical and hard to calculate for many situations.

### 3.2.2. Gradient Descent Algorithm

Gradient Descent (GD) algorithm is also one of the oldest and still widely used traditional optimization algorithms (Towards Data Science, 2018). In the GD algorithm, the first step is defining the initial point. The candidate decision variable vector is iteratively updated by calculating the gradients towards a steeper position in the search space. The GD algorithm can be mathematically represented as follows,

$$x^{i+1} = x^i - \gamma \nabla f(x^i) \quad (3.4)$$

where  $\gamma$  is the learning rate. A higher learning rate means higher step sizes. However, in higher step sizes, the algorithm jumps over and may not converge to the optimum point. This phenomenon is depicted in the figure below.

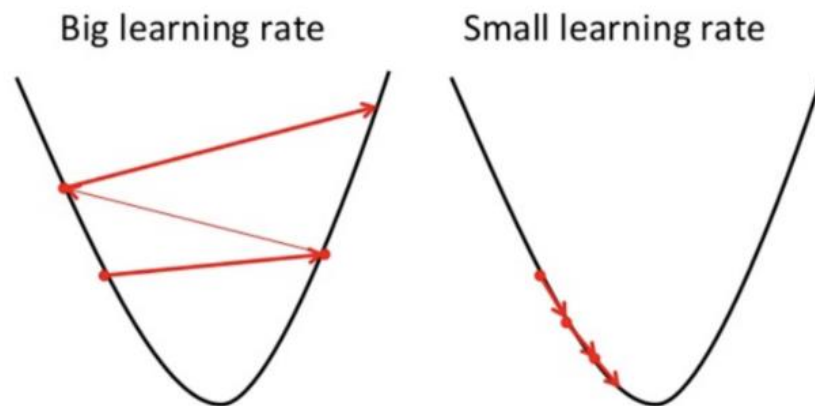


Figure 3.2. Effect of learning rate on the convergence (Towards Data Science, 2018)

### 3.2.3. Nelder-Mead Algorithm

The Nelder-Mead (NM) algorithm is also a well-known and widely used traditional optimization algorithm. The NM algorithm is simplex-based (Singer and Nelder, 2009). A simplex is a convex hull that consists of  $n+1$  vertices where  $n$  is the dimension of the optimization problem. A sample simplex representation is depicted in the figure below,

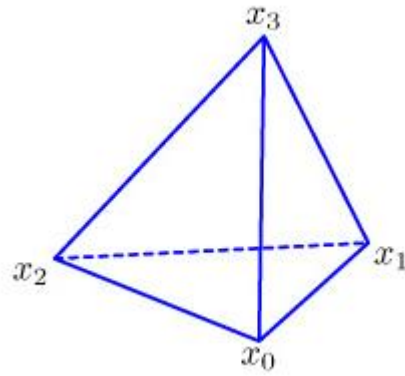


Figure 3.3. A sample simplex (Singer and Nelder, 2009)

The simplex is placed on the search space and moves like a ameba until the termination criterion is met. Generally NM algorithm consists of the following steps,

- Initialize the simplex
- Repeat the following steps until the termination criterion is met
  - Calculate the fitness value of the simplex vertices
  - If the fitness value does not satisfy the termination criterion transform the simplex
  - Return the fitness value of the best vertex.

In the NM algorithm, the simplex have four different transformations. The first one is the reflection. Reflection of a simplex is depicted in the following figure with red line represents the new form and blue line represents the initial form,

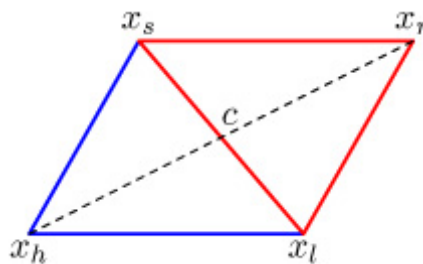


Figure 3.4. Reflection of the simplex (Singer and Nelder, 2009)

Reflection process is mathematically described as follows,

$$x_r = c + \beta(c - x_h) \tag{3.5}$$

Second type of transformation is expansion. The expansion process shown in the following figure,

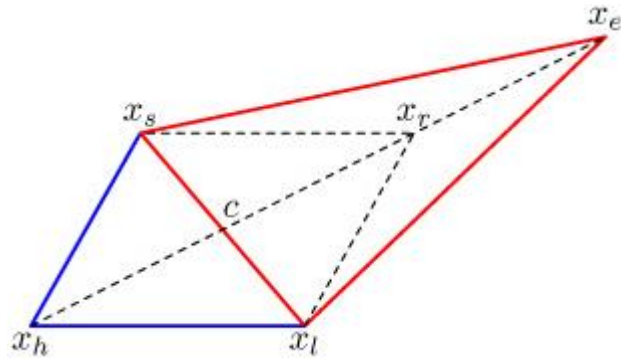


Figure 3.5. Expansion of the simplex (Singer and Nelder, 2009)

Expansion is mathematically described as follows,

$$x_r = a + \beta(a - x_n) \quad (3.6)$$

The other type of transformation is contraction which is the opposite of extraction and mathematically shown as the following equation,

$$x_m = a + \beta(x_n - a) \quad (3.7)$$

And the last type of transformation is shrink. As the name suggests, the simplex shrinks from one side.

### 3.3. Modern Optimization Techniques

Modern optimization techniques have been proposed by the researchers to overcome the drawbacks of the traditional algorithms discussed above. Modern optimization techniques can be grouped into three classes, heuristics, metaheuristics and evolutionary algorithms. Heuristic techniques are mostly based on trial-and-error and random walks. On the other hand, metaheuristic and evolutionary techniques utilize memory, learning methods and solution history. Advantages of the metaheuristics compared to traditional techniques can be summarized as follows,

- They treat the optimization as black box problems. Thus, they are problem independent.
- They are gradient-free. Therefore, they are more likely to find the global minimum in highly non-linear search spaces.
- They are mostly designed as global optimizers.
- They contain stochastic components. Therefore, by utilizing random walks and other stochastic techniques, they can explore the search space more effectively.

Mainly, an optimization algorithm works as follows. First, a set of decision variables are generated by the algorithm. Then, the decision variables are applied to the optimization problem and outputs, or state variables, are obtained. Then, the objective function, constraints and fitness values are determined in order. Finally, the obtained fitness value is checked if it is

optimal or not. This procedure is presented Figure 3.6 below.

The main difference between the metaheuristic and evolutionary algorithms is their approach to storing old best values and artificial intelligence techniques that they use.

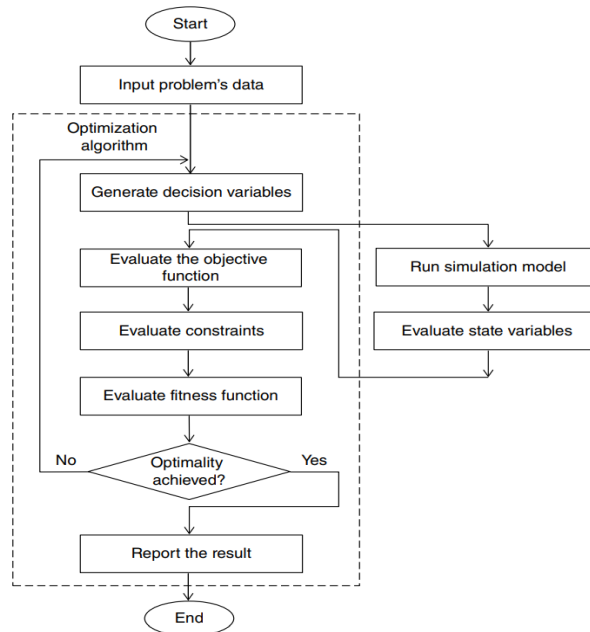


Figure 3.6. Optimization algorithm procedure (Bozorg-Haddad, 2017)

Metaheuristic and evolutionary algorithms can be divided into several sub-categories. These are nature-inspired and non-nature-inspired algorithms, population-based and non-population-based algorithms and memory-based and memory-less algorithms. Algorithms such as Genetic Algorithm (GA) (Goldberg, 2008), Artificial Bee Colony (ABC) (Karaboga, 2005) and Simulated Annealing (SA) (Van Laarhoven and Aarts, 1987) are classified as nature-inspired algorithms. The GA is derived from the Darwin's law of evolution while the ABC utilizes the food finding behavior of the bees in the nature. On the other hand the algorithms like Tabu Search (TS) (Glover, 1989) have no inspiration from nature and their origins are unclear.

Some modern algorithms are based on populations. Each member of the population scatter around the search space to find the global minimum. GA and ABC are good examples to population-based algorithms. On the other hand, algorithms like SA relies on a single searching agent to explore the search space. Finally, there are algorithms that do not use the best solution from the previous iteration. They can be classified as memoryless algorithms.

Any modern optimization technique can be modified as a memoryless or memory-based algorithm. Some modern optimization techniques will be presented in the following subsections.

### 3.3.1. Genetic Algorithm

The GA is inspired from the behavior of the genetic structures of the living creatures and Darwin's law of evolution. In the nature, fittest member of a society survives and passes its own genetic information to the next generation. This phenomenon consists the main idea of the GA algorithm.

The GA is made up of three different processes: crossover, mutation and selection. First, an initial set of chromosomes that represents the candidate solutions are created for the implementation of the algorithm. Each chromosome consists of genes that represent each decision variable. Then, a number of child solutions are generated by exchanging a serie of genes with each other and a new solution chromosome is generated. This process is called the crossover. Thereafter, the place of the genes in the chromosome can be swapped with each other to create a new set of solution chromosome. This process is called the mutation. And finally, fitness values of the each chromosome is evaluated. The chromosome with the most desirable fitness value is selected and it is stored for the next generation, or iteration, of candidate solutions. Generally, the algorithm have two unique parameters to be tuned. The crossover operator, the first one, decides how frequent the crossover operation to be carried out in a generation. Higher crossover operator values increases the exploration intensification. However, a very high crossover operator value may drive away the algorithm from the global optimum. The mutation operator, the second one, decides how frequent the mutation operation to be carried out in a generation. A high mutation operator value increases the explotation intensification. Overview of the GA algorithm is depicted in the following figure,

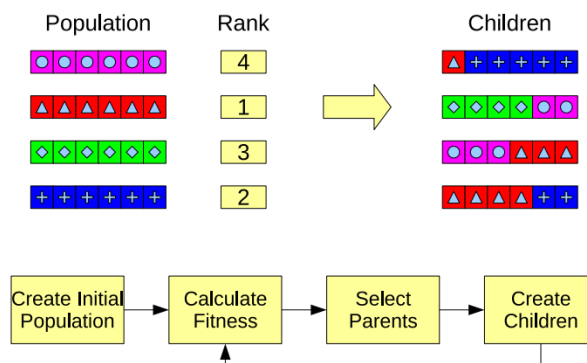


Figure 3.7. General structure of the GA (Venter, 2010)

### 3.3.2. Differential Evolution

Differential Evolution (DE) is parallel direct search method proposed by Storn and Price (1997). DE algorithm utilizes the same three processes that GA has, crossover, mutation and selection. The DE algorithm employs chromosomes just like the GA to find the global optimum. The mutation process is accomplished by the following procedure,

$$v_{i,gen+1} = x_{a_1,gen} + F(x_{a_2,gen} - x_{a_3,gen}) \quad (3.8)$$

where  $a_1$ ,  $a_2$  and  $a_3$  are the random numbers,  $x$  is the solution vector,  $F$  is the mutation factor and  $v$  is the differential vector. Then the crossover process is applied depending on the value of the crossover factor. The crossover operation is mathematically shown as follows,

$$u_{ji,gen+1} = \begin{cases} v_{ji,gen+1} & \text{if } rand \leq CRO \\ x_{ji,gen+1} & \text{if } rand > CRO \end{cases} \quad (3.9)$$

In the last step of the algorithm, the chromosome with the best fitness value is selected and its values are stored for the next generation of solutions.

### 3.3.3. Particle Swarm Optimization

The Particle Swarm Optimization (PSO) is a swarm-based nature-inspired metaheuristic algorithm proposed by the Kennedy and Eberhart (1995). PSO algorithm is one of the well-known and widely used modern optimization techniques. The algorithm has low computational load and shares many similarities with the GA such as perturbation at each generation and memorization of the best member for the current generation. However, it also has some differences. It does not rely on procedures in the GA such as crossover, mutation and selection. The algorithm mimics the social life of the animal swarms, such as bird and fish flocks. The animals gather together and form swarms and flocks to defend themselves from the predators, to hunt preys or to migrate a more fruitful feeding zones in the nature. The PSO mathematically models this phenomenon to find the global optimum in the search space.

There are different types of best locations that are stored for the next generations in the PSO. One is the personal best. Each member of the swarm remembers the best location it has achieved so far and stores it for the later generations. The other best value is the group best. The swarm also watches for the best fitness value it has achieved so far and stores that value for later generations. And the last best location is the global best. After all generations has been completed, the algorithm compares the last generation swarm best with the global best

and decides the best solution it has found. The algorithm mathematically described with the following formulas,

$$v_i^{g+1} = v_i^g + \gamma r_1 (gbest - x_i^g) + \delta r_2 (pbest_i - x_i^g) \quad (3.10)$$

$$x_i^{g+1} = x_i^g + v_i^{g+1} \quad (3.11)$$

where  $r_1$  and  $r_2$  are the randomly generated numbers between 0 and 1,  $\gamma$  and  $\delta$  are the learning parameters usually selected between 0 and 2,  $x$  is the solution vector and  $v$  is the velocity vector that determines the destination of the member. The  $\delta$  parameter can be perceived as how much a member of the swarm trusts itself, on the other hand, the  $\gamma$  parameter can be perceived as how much the particle trusts the group. Literature suggests that the both learning parameters should be taken as 2. First, the velocity vector is calculated by the algorithm, then each particle's corresponding velocity vector is added to itself. Thereafter, for the selection of the best solution, the global best,  $gbest$ , is compared with the personal or swarm best,  $pbest$ , and the solution with more favorable fitness value is selected for the each iteration. The position of the each particle plays an important role for the exploration of the global optimum.

#### 3.3.4. Bat Algorithm

The Bat Algorithm (BA) is a nature-inspired swarm-based metaheuristic algorithm proposed by Yang (2010). BA is inspired from the echolocation behavior of the microbats in the nature. In the BA algorithm, it is assumed that each bat in the swarm knows its exact position and there are no barriers that blocks their communication with each other. BA also employs the wave characteristics of the bats such as amplitude, loudness and frequency. Movement of a bat in the algorithm is modeled with the following equations,

$$f_a = f_{min} (f_{max} - f_{min}) \delta \quad (3.12)$$

$$v_a^g = v_a^{g-1} + (x_a^g - x_*) f_a \quad (3.13)$$

$$x_a^g = x_a^{g-1} + v_a^g \quad (3.14)$$

where  $f$  is the frequency of the wavelength,  $\delta$  is a vector consists of randomly generated numbers between 0 and 1,  $x$  is the location of the bats,  $v$  is the velocity of the bats and  $x_*$  is the best global solution of the swarm so far. And the balance between the exploration and exploitation is provided with the loudness and pulse emission of the wave that bats use to communicate. These parameters are calculated as follows,

$$A_a^{g+1} = \rho A_a^g, r_a^{g+1} = r_a^0 [1 - \exp(-\tau t)] \quad (3.15)$$

where  $A$  is the loudness,  $r$  is the pulse emission and  $\rho$  and  $\tau$  are the constants. Pseudo code of the bat algorithm is defined in the following figure.

### Bat Algorithm

---

Objective function  $f(\mathbf{x})$ ,  $\mathbf{x} = (x_1, \dots, x_d)^T$   
Initialize the bat population  $\mathbf{x}_i$  ( $i = 1, 2, \dots, n$ ) and  $\mathbf{v}_i$   
Define pulse frequency  $f_i$  at  $\mathbf{x}_i$   
Initialize pulse rates  $r_i$  and the loudness  $A_i$   
**while** ( $t < \text{Max number of iterations}$ )  
Generate new solutions by adjusting frequency,  
and updating velocities and locations/solutions  
  **if** ( $\text{rand} > r_i$ )  
    Select a solution among the best solutions  
    Generate a local solution around the selected best solution  
  **end if**  
  Generate a new solution by flying randomly  
  **if** ( $\text{rand} < A_i$  &  $f(\mathbf{x}_i) < f(\mathbf{x}_*)$ )  
    Accept the new solutions  
    Increase  $r_i$  and reduce  $A_i$   
  **end if**  
Rank the bats and find the current best  $\mathbf{x}_*$   
**end while**  
Postprocess results and visualization

---

Figure 3.8. Pseudo code of the BA (Yang, 2010)

### 3.3.5. Firefly Algorithm

The Firefly Algorithm (FA) is another swarm-based nature-inspired metaheuristic algorithm proposed by Yang (2010). The algorithm is based on flashing characteristics of the fireflies in the nature. Following idealizations have been made to make the algorithm feasible for implementation in a computer program,

- All fireflies are assumed to be unisex. Therefore, each member of the swarm can attract each other.

- Attractiveness of a firefly is proportional to its brightness. Therefore, among two fireflies, the brighter one will attract the other one.

- The brightness of the butterfly is determined by the position of the firefly in the search space.

The light intensity of the fireflies is calculated as follows,

$$I = I_0 e^{-\sigma r} \quad (3.16)$$

where  $\sigma$  is the light absorption parameter and  $r$  is the distance between the fireflies. Afterwards, attractiveness of a firefly,  $\alpha$ , can be determined depending on the light intensity,

$$\alpha = \alpha_0 e^{-\sigma r^2} \quad (3.17)$$

where  $\alpha_0$  is the attractiveness where the two fireflies are at the same location. Finally, movements of the fireflies is formulated as follows,

$$x_a = x_a + \alpha_0 e^{-\sigma r_{ab}^2} (x_b - x_a) + \tau \epsilon_a \quad (3.18)$$

where  $x$  is the position of the each firefly,  $\sigma$  and  $\tau$  are the tuning parameters and  $\epsilon_a$  is the vector of randomly generated numbers. Pseudo code of the algorithm is given in the figure

below,

---

```

Firefly Algorithm
Objective function  $f(\mathbf{x})$ ,  $\mathbf{x} = (x_1, \dots, x_d)^T$ 
Initialize a population of fireflies  $\mathbf{x}_i$  ( $i = 1, 2, \dots, n$ )
Define light absorption coefficient  $\gamma$ 
while ( $t < \text{MaxGeneration}$ )
for  $i = 1 : n$  all  $n$  fireflies
for  $j = 1 : i$  all  $n$  fireflies
Light intensity  $I_i$  at  $\mathbf{x}_i$  is determined by  $f(\mathbf{x}_i)$ 
if ( $I_j > I_i$ )
Move firefly  $i$  towards  $j$  in all  $d$  dimensions
end if
Attractiveness varies with distance  $r$  via  $\exp[-\gamma r]$ 
Evaluate new solutions and update light intensity
end for  $j$ 
end for  $i$ 
Rank the fireflies and find the current best
end while
Postprocess results and visualization

```

---

Figure 3.9. Pseudo code of the FA (Yang, 2010)

### 3.3.6. Cuckoo Search

The Cuckoo Search (CS) algorithm is a nature-inspired swarm-based metaheuristic algorithm proposed by Yang and Deb (2010). CS algorithm is inspired from the nesting behavior of the cuckoos. Some idealizations have been made to make the algorithm feasible for implementation. These are,

- Each cuckoo in the swarm lays one egg at a time and discards it in a randomly chosen nest.
- The egg with the best quality (solution) is carried over to the next generation.
- The number of host nests are constant.

Flight behavior of many animals and insects depict the characteristics of Levy flights. Therefore, Levy flights is utilized in the CS. New solutions in the CS algorithm is generated with the following equation,

$$x_a^{g+1} = x_a^g + \beta \oplus Levy(\alpha) \quad (3.19)$$

where  $\beta$  is the step size. Levy flights are essentially a random walk method which can be calculated as,

$$Levy \sim u = t^{-\alpha} \quad (3.20)$$

Pseudo code of the CS algorithm is given in the following figure.

---

```

Objective function  $f(\mathbf{x})$ ,  $\mathbf{x} = (x_1, \dots, x_d)^T$ ;
Initial a population of  $n$  host nests  $\mathbf{x}_i$  ( $i = 1, 2, \dots, n$ );
while ( $t < \text{MaxGeneration}$ ) or (stop criterion);
    Get a cuckoo (say  $i$ ) randomly by Lévy flights;
    Evaluate its quality/fitness  $F_i$ ;
    Choose a nest among  $n$  (say  $j$ ) randomly;
    if ( $F_i > F_j$ ),
        Replace  $j$  by the new solution;
    end
    Abandon a fraction ( $p_a$ ) of worse nests
        [and build new ones at new locations via Lévy flights];
    Keep the best solutions (or nests with quality solutions);
    Rank the solutions and find the current best;
end while
Postprocess results and visualisation;

```

---

Figure 3.10. Pseudo code of the CS algorithm (Yang, 2010)

### 3.3.7. Artificial Bee Colony Algorithm

Artificial Bee Colony (ABC) algorithm is another widely-used nature-inspired swarm-based metaheuristic algorithm proposed by Karaboga (2005). The algorithm mimics the food source searching behavior of a bee swarm in the nature. There are three different types of bees in the swarm in the ABC algorithm. They are, the employed bees which are associated with the food sources, the onlooker bees which observes the dance of the employed bees and choose a food source and the scout bees which search for food sources randomly (Karaboga, 2010). In the initial phase of the algorithm, scout bees randomly searches around to locate food sources. Then the onlooker and employed bees draws food from these sources until they become exhausted. Thereafter, the exhausted employed bees becomes scout bees and search for new potential food sources. Initialization of the ABC is accomplished with the following formula,

$$x_a = lower_a + \alpha(upper_a - lower_a) \quad (3.21)$$

where *lower* and *upper* are respectively the minimum and maximum values that the decision variables can take and  $\alpha$  is a random variable between 0 and 1. Thereafter, the employed bees start to search for new food sources. This phenomenon is modeled with the following equation,

$$v_a = x_a + \beta_a(x_a - x_b) \quad (3.22)$$

where  $x_b$  is a randomly selected food source and  $\beta_a$  is a randomly generated random that is drawn from a Gaussian distribution. Then, probability value of an onlooker bee selecting of a food source is calculated as follows,

$$p_m = \frac{fit(x)}{\sum_{a=1}^m fit(x)} \quad (3.23)$$

where  $fit$  is the fitness value of the each member of the bee swarm. Finally, scout bee phase starts and scout bees search for new food sources in substitution for the abandoned sources. General order of the execution phases of the ABC algorithm can be listed as follows,

- Initialization phase
- Repeat the following states until the termination criterion is met
- Execute the employed bees phase
- Execute the onlooker bees phase
- Execute the scout bees phase

### 3.3.8. Whale Optimization Algorithm

The Whale Optimization Algorithm (WOA) is a new nature-inspired swarm-based metaheuristic algorithm proposed by Mirjalili and Lewis (2016). The WOA is inspired from hunting and foraging behavior of the humpback whales in the nature. It has been observed that humpback whales group up and form a spiral of bubbles through the surface of the water before to communicate before hunting. This behavior of the humpback whales is modeled in the WOA with following steps, encircling prey, spiral bubble-net feeding maneuver and search prey.

In the encircling prey step, the whales do not know the position of the prey initially. The algorithm initially assumes that the optimum solution is the target prey. However, the candidate optimum solution is later updated with the whale, member, with the best solution and all other whales move towards to the best solution. This behavior is mathematically modeled as follows,

$$\vec{G} = |\vec{F}\vec{X}_*(b) - \vec{X}(b)| \quad (3.24)$$

$$\vec{X}(b+1) = \vec{X}_*(b) - \vec{E}\vec{G} \quad (3.25)$$

where  $b$  is the iteration number,  $\vec{X}$  is the position vector of the swarm,  $\vec{X}_*$  is the position vector of the best solution and  $\vec{E}$  and  $\vec{F}$  are the coefficient vectors.  $\vec{E}$  and  $\vec{F}$  are calculated as follows,

$$\vec{E} = 2\vec{m}\vec{n} - \vec{m} \quad (3.26)$$

$$\vec{F} = 2\vec{n} \quad (3.27)$$

where  $\vec{m}$  is a vector that its value drops from 2 to 0 over the course of iterations, and  $\vec{n}$  is a random vector between 0 and 1.

The spiral bubble-net feeding maneuver consists of two phases. First is the shrinking encircling mechanism. This behavior represents the value of  $\vec{E}$  decreasing over the iterations. As the value of the  $\vec{E}$  decreases, the circle becomes smaller and smaller, thus, the algorithm converges to a optimal point. The second one is the spiral position updating. The whales update their position according to the position of the prey with the following equation,

$$\vec{X}(b+1) = \vec{G}'e^{hk} \cos(2\pi k) + \vec{X}^*(b+1) \quad (3.28)$$

where  $\vec{G}'$  is the distance between the member and the best solution achieved so far and  $h$  is a constant parameter that decides the shape of the spiral and  $k$  is a randomly gerated number between 0 and 1. It is assumed in the algorithm that whales approach to the prey with 0.5 probability by utilizing the Eq. (3.25) and 0.5 by utilizing the Eq. (3.28).

The last phase, searching the prey, models the looking for new food sources behavior of the whales. The mathematical model of this phase is as follows,

$$\vec{G} = |\vec{F}\vec{X}_{rand} - \vec{X}| \quad (3.29)$$

$$\vec{X}(b+1) = \vec{X}_{rand} - \vec{E}\vec{G} \quad (3.30)$$

where  $\vec{X}_{rand}$  is a vector of randomly generated numbers. More details about the WOA can be found in Mirjalili and Lewis (2016).

## 4. ARTIFICIAL NEURAL NETWORKS

### 4.1. Basics of the Artificial Neural Networks

Artificial Neural Networks (ANN) is a graph-based artificial intelligence algorithm that takes the inspiration from the neural networks in the brains of the living beings (Aggrawal, 2018). All living beings in the world have cells in their brains which are called neurons. Each neuron in the brain is connected with each other axons and dendrites. The connecting region between the dendrites are called synapses. A stronger synaptic connection means better the new information is learned. This phenomenon constitutes the core of the artificial neural network algorithm. A demonstration of a brain cell and an artificial neural network graph is presented in the following figure.

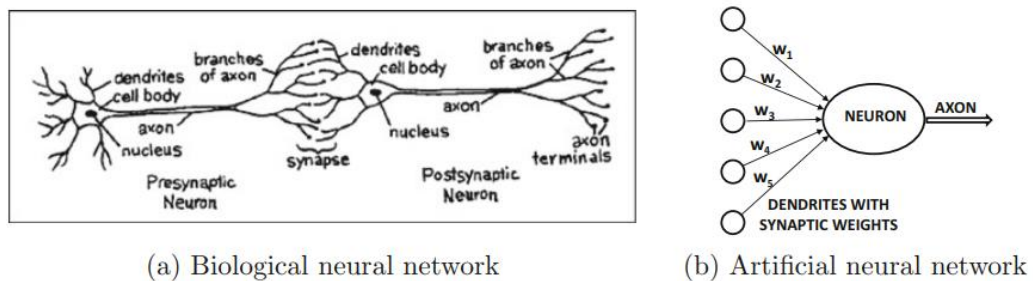


Figure 4.1. A biological and an artificial neural network (Aggrawal, 2018)

As can be seen in the Figure 4.1., the synaptic connection between the neurons are symbolized with the arrows with each of them having weight values that represent their connection strength. And the neuron is symbolized with an elliptic circle. In the ANNs, an information is fed to the network with the input neurons, then the information passes through the synapses and processed in the neurons. At last, the processed information is gathered from the output neurons. Weights of the synapses during the information processing are updated at the each iteration. This process provides the learning mechanism in the network. Accuracy of the output prediction can be improved by feeding more and more information to the network with large amount of iterations.

Graph-based representation of a single neuron in an ANN is depicted in the following figure.

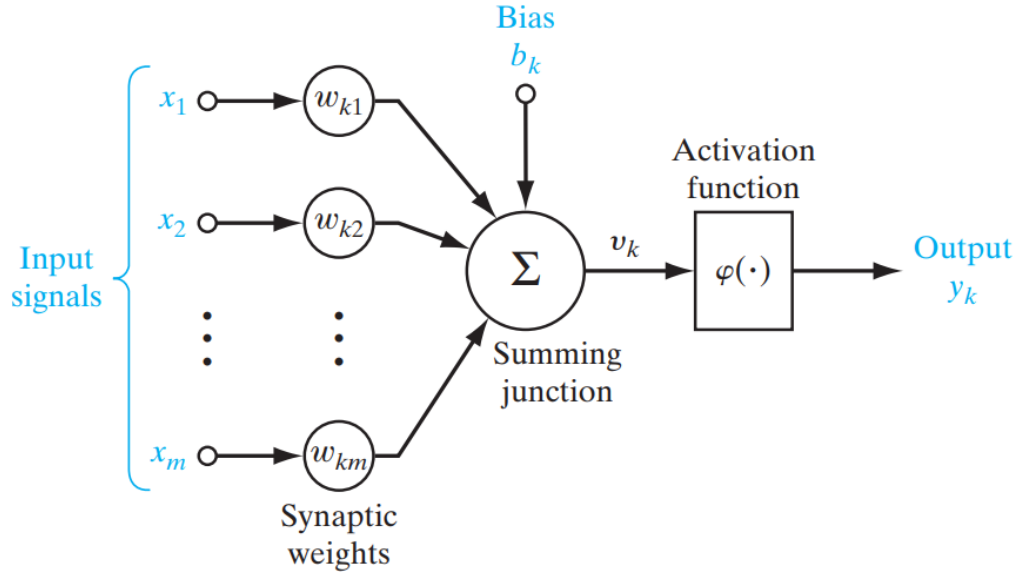


Figure 4.2. Structure of a single neuron in an ANN (Haykin, 2009)

An ANN is made up of three different components. The first one is synapses. Each synapse has its own weight. A signal,  $x_j$ , arrives to a synapse through an input neuron. Then the signal is multiplied with the weight,  $w_{kj}$ , and goes through the neuron. Thereafter, the second component comes into play, that is the adder. Each multiplied weight and signal combination and the bias of the neuron is added in the adder component of the neuron. And finally, the third component, the activation function, takes the added value and limits for a finite range. This processes summarize the mathematical behavior of a neuron in an ANN. Mathematically the above mentioned processes can be shown with the following equations,

$$u_k = \sum_{a=1}^m w_{ka} x_a \quad (4.1)$$

$$y_k = \varphi(u_k + b_k) \quad (4.2)$$

where  $x$  is the input signal,  $w$  is the synaptic weight and  $\varphi(\cdot)$  is the activation function. Formulas and graphical demonstration of the some of the most used activation functions are given below.

- Identity:  $f(x) = x$

- Sign:  $f(x) = \begin{cases} 0 & x < 0 \\ 1 & x \geq 0 \end{cases}$

- Sigmoid:  $f(x) = \frac{1}{1+e^{-x}}$

- Tanh:  $f(x) = \frac{(e^x - e^{-x})}{(e^x + e^{-x})}$

- ReLU:  $f(x) = \begin{cases} 0 & x < 0 \\ x & x \geq 0 \end{cases}$

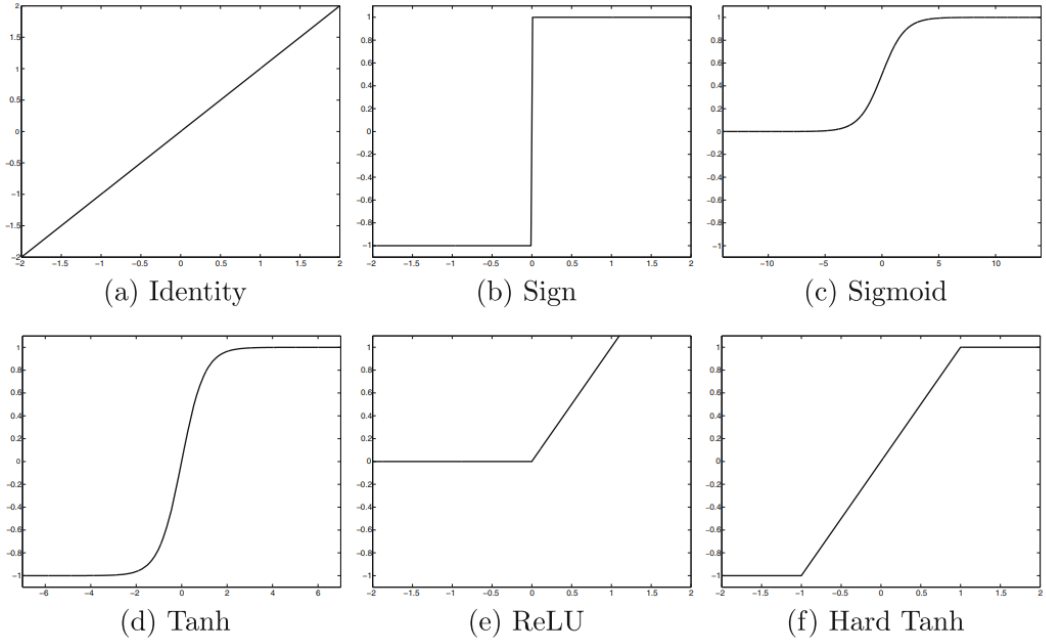


Figure 4.3. Activation Function (Aggarwal, 2018)

Recently ReLU and tanh activation functions are taking place of sigmoid activation function due to ease of training of the ANN. Loss function is another fundamental aspect of an ANN. Different loss functions can come up with different results depending on the type of learning. For example, log-loss function is used for mostly classification purposes and mean square error loss function is mostly used for numerical regression problems. Some of the mostly used loss functions in the literature are given with mathematical formulations below.

- Mean squared error:  $L = \frac{1}{n} \sum_{i=1}^n (y_i - \hat{y}_i)^2$
- Mean absolute error:  $L = \frac{1}{n} \sum_{i=1}^n |y_i - \hat{y}_i|$
- Mean absolute percentage error:  $L = \frac{1}{n} \sum_{i=1}^n \left| \frac{y_i - \hat{y}_i}{y_i} \right| 100$
- L2:  $L = \sum_{i=1}^n (y_i - \hat{y}_i)^2$
- L1:  $L = \sum_{i=1}^n |y_i - \hat{y}_i|$
- Mean squared logarithmic error:  $L = \frac{1}{n} \sum_{i=1}^n |\log(y_i + 1) - \log(\hat{y}_i + 1)|$
- Negative logarithmic likelihood:  $L = -\frac{1}{n} \sum_{i=1}^n \log(\hat{y}_i)$

A group of neuron that are at the same level of processing forms a layer. The layers constitute the backbone of an ANN (Silva et al., 2017). There are three different types of layers in ANN. Those are the input layer, the hidden layer and the output layer. The input layer receives the external data from the environment and propagates the data through the entire

network. Generally the data is fed to the input layer with normalized form. Normalization makes the regression easier if there are huge variations among the input data. The second class of layers is the hidden layer. The hidden layer neurons do the largest amount of work in the network. They extract the patterns from the data and analyze it. The third type of layer is the output layer. The neurons in the output layer are responsible for final processing of the data and presenting the results.

Based on the types of neuron interconnectedness and order of the layers, the ANNs are classified into four main groups. These are single-layer feedforward networks, multiple-layer feedforward networks, recurrent networks and mesh networks. Single-layer feedforward network consists of only an output layer. The output layer is the input layer at the same time. This type of neural networks are mainly used in linear regression and classification problems. A sample presentation of a single-layer network is given in the figure below.

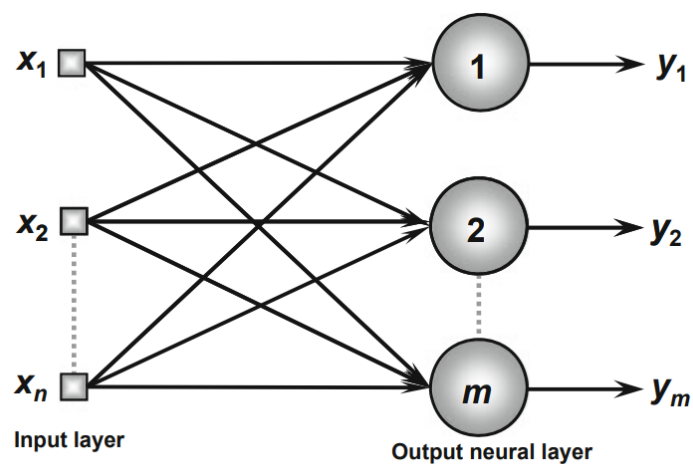


Figure 4.4. Representation of a single-layer network (Silva et al., 2017)

The multi-layer feedforward networks are more popular and useful type of networks. They consist of an input layer, one or more hidden layers and an output layer. These type of networks have gained popularity in robotics, pattern recognition, system identification, control and non-linear regression research fields. The most used type of multi-layer feedforward networks are Multi-Layer Perceptron (MLP) and Radial Basis Function (RBF) networks. As mentioned above, the number of hidden layers can be more than one. However, this variation can affect the learning capability and convergence of the network. This issue will be described in more detail in the upcoming sub-sections. Representation of a multi-layer feedforward

network is depicted in the following figure.

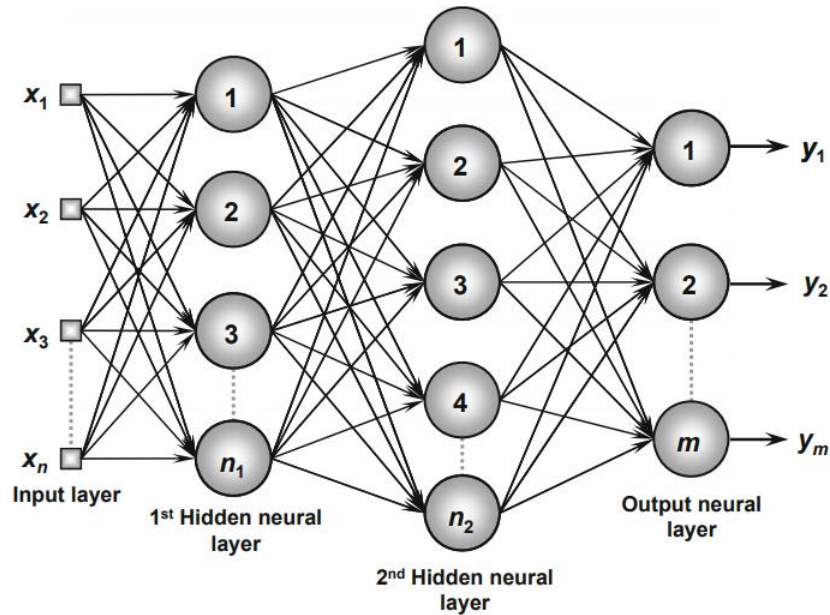


Figure 4.5. Representation of a multi-layer feedforward network (Silva et al., 2017)

The recurrent networks are widely-used in areas that utilize time-variant systems such as dynamic system identification, process control and robotics. In the recurrent networks, the output neurons are connected to the input neurons with a feedback connection. Jordan, Elman and Hopfield networks are popular type of recurrent neural network architectures. Also, a type of recurrent neural network called NARX network is utilized for the system identification part of this paper. More details about the NARX network architecture and training procedure will be given in the following sub-sections. The following figure demonstrates a recurrent neural network.

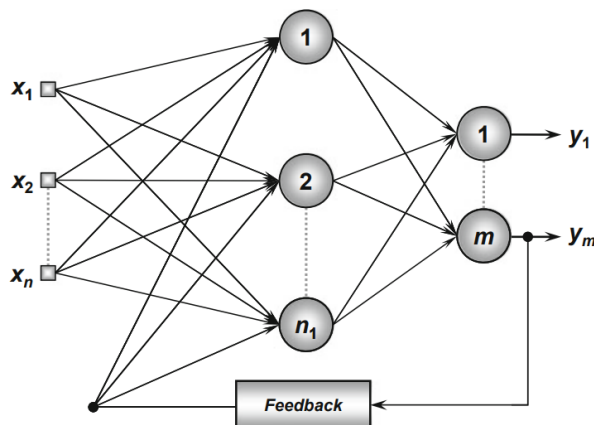


Figure 4.6. A recurrent neural network (Silva et al., 2017)

The mesh networks are generally designed by spatially placing neurons to extract patterns from the data. These type of networks are used in pattern recognition, optimization and graphs. The Kohonen network is one of the most popular mesh network architecture. Graphical representation of a mesh network is given in the following figure.

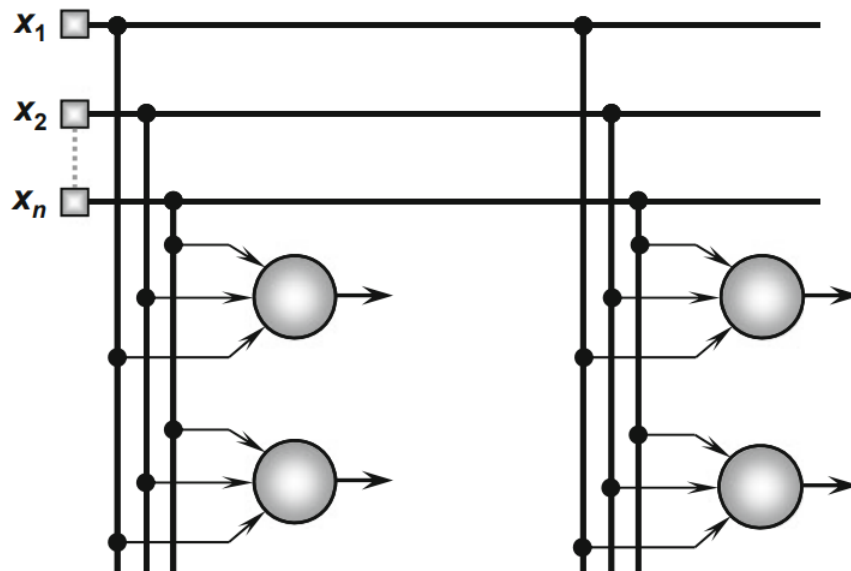


Figure 4.7. A mesh network (Silva et al., 2017)

The neural networks can be trained in different manners. They can either be trained online or off-line. The off-line training is also called the batch training. In the off-line training, all of the dataset are provided to the neural network at once. The numerical adjustments of the weights are made after all the data is provided to the network. For this reason, at least one iteration is needed to accomplish the learning procedure in off-line training tasks. In the online training, update of the weights are made after each piece of training data is provided. Each training sample can be disregarded after they are presented to the network. Training of the ANN in an online manner should be made more carefully. Because the new training data can disrupt the behavior of the network and make the previous data redundant.

A neural network can be trained with three different learning algorithms. These are supervised learning, unsupervised learning and reinforcement learning. The supervised learning procedure can be thought as learning with a teacher. The neural network has no information about the environment initially and the teacher has knowledge about the

environment. The environment information of the teacher can be thought as optimum input and output data combinations. The following sums up the supervised learning procedure.

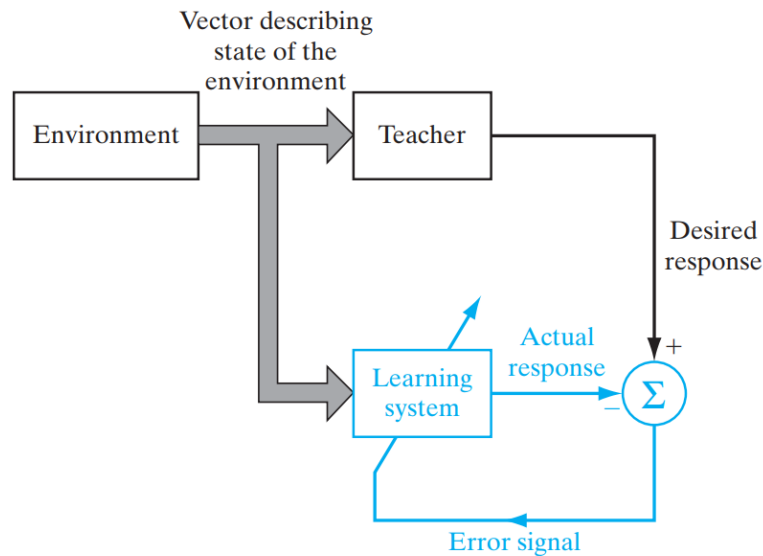


Figure 4.8. Supervised learning procedure (Haykin, 2009)

It can be seen from the Figure 4.8 that the environment provides data to both the teacher and the system. The teacher completely knows the environment and provides the corresponding data for the input to the system. The difference between the desired response and the actual response is fed back to the system as the error signal. And the weight adjustments have been performed with the error signal. In other words, the learning process can be interpreted as the system ‘emulates’ the teacher.

The other two methods do not contain a teacher to assist the learning process. In the supervised learning, the environmental data is directly presented to the system without the help of a teacher. Therefore, the network needs to figure out the patterns in the data. This method may sound not practical, however, by presenting the network the number of clusters or any other properties, learning can be accomplished. The reinforcement learning presents an additional critic component compared to the supervised learning. In the reinforcement learning, the system ‘learns’ the environment by continually interacting with it. The proper input-output combination is produced through minimizing a performance index. The reinforcement learning procedure is depicted in the following figure.

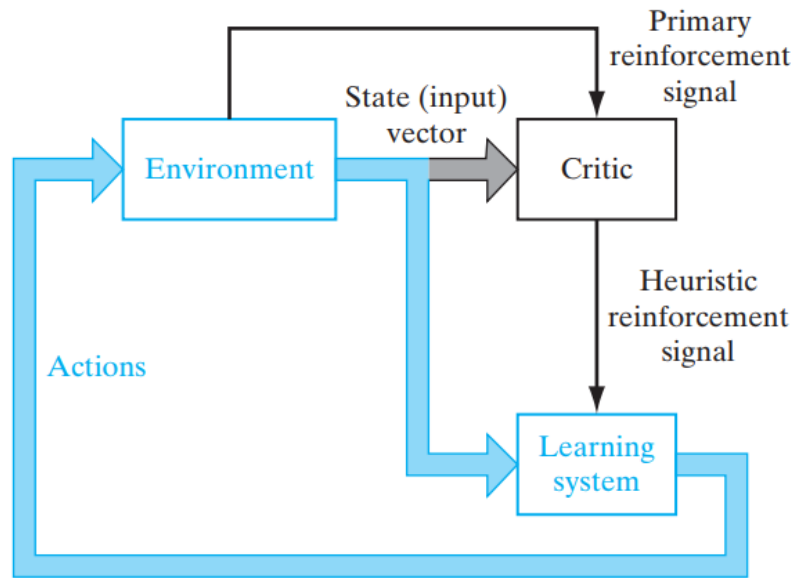


Figure 4.9 Reinforcement learning (Haykin, 2009)

As can be seen from Figure 4.9, the critic converts the primary reinforcement signal into heuristic reinforcement signal and provides the information to the learning system. The main object of the reinforcement learning is minimizing the cost-to-go function. The minimized cost-to-go function results in optimal actions combination to reach the objective.

#### 4.2 Training of an Artificial Neural Network

A basic part of an ANN is the perceptron. Each neuron that consists of an adder and the activation function is called a perceptron. The most basic type of ANN is called the ADALINE network. ADALINE network consists of only one perceptron in one layer and mostly used in pattern recognition applications. Practicing with an ADALINE network is a good way to start to understand the fundamentals of training an ANN. Presentation of an ADALINE network is depicted in the following figure.

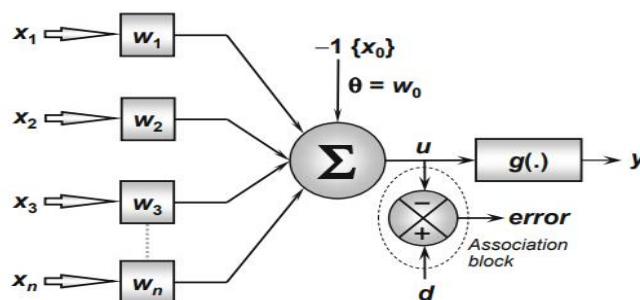


Figure 4.10 ADALINE network (Silva et al., 2017)

The ADALINE perceptron adds all the weight-input multiplications and adds the bias. Then, the result is passed through an activation function and the output of the network is produced. This process is mathematically expressed as follows,

$$u = \sum_{a=1}^n x_a w_a - \theta \quad (4.3)$$

$$y = g(u) \quad (4.4)$$

where  $x$  is the input data,  $w$  is the weight,  $\theta$  is the bias and  $g(\cdot)$  is the activation function. Knowledge of the error signal is needed for training the network and adjusting the weights. The error signal can be mathematically formulated in a supervised learning manner as follows,

$$e = d - y \quad (4.5)$$

where  $e$  is the error signal and  $d$  is the desired output.  $d$  can be thought as the output knowledge that the teacher provides in the supervised learning problems. Since the ADALINE network is generally used for linear regression problems, the activation function is generally selected as step or bipolar step function. Furthermore, the weights and biases can be updated by applying the following equations,

$$w_a^c = w_a^p + \delta(d - y)x_a \quad (4.6)$$

$$\theta_a^c = \theta_a^p + \delta(d - y)(-1) \quad (4.7)$$

where the  $c$  superscript means the current value,  $p$  superscript means the previous value and  $\delta$  is the learning rate. The learning rate must be chosen very carefully. For higher values of the learning rate, the algorithm may jump over the global optimum and converge to a local minimum. On the other hand, for lower values of the learning rate, the algorithm may converge to global optimum very slowly, thus may require too many iterations to converge. At each iteration, the weights and the bias must be updated in order to make the error signal equal to zero. The ADALINE network or perceptron training algorithm can be summarized as the following figure.

**Begin {PERCEPTRON Algorithm – Training Phase}**

- <1> Obtain the set of training samples  $\{\mathbf{x}^{(k)}\}$ ;
- <2> Associate each desired output  $\{d^{(k)}\}$  to each sample;
- <3> Initialize vector  $\mathbf{w}$  with small random values;
- <4> Specify the learning rate  $\{\eta\}$ ;
- <5> Initialize the epoch counter  $\{epoch \leftarrow 0\}$ ;
- <6> Repeat the following instructions:
  - <6.1>  $error \leftarrow$  "none";
  - <6.2> For all training samples  $\{\mathbf{x}^{(k)}, d^{(k)}\}$ , do:
    - <6.2.1>  $u \leftarrow \mathbf{w}^T \cdot \mathbf{x}^{(k)}$ ;
    - <6.2.2>  $y \leftarrow \text{signal}(u)$ ;
    - <6.2.3> If  $y \neq d^{(k)}$ 
      - <6.2.3.1> then  $\begin{cases} \mathbf{w} \leftarrow \mathbf{w} + \eta \cdot (d^{(k)} - y) \cdot \mathbf{x}^{(k)} \\ error \leftarrow \text{"existent"} \end{cases}$
  - <6.3>  $epoch \leftarrow epoch + 1$ ;
- Until:  $error \leftarrow$  "none"

**End {PERCEPTRON Algorithm – Training Phase}**

Figure 4.11 The ADALINE training algorithm (Silva et al., 2017)

The next step of the learning phenomenon of an ANN is the backpropagation algorithm. The backpropagation algorithm is used mainly for teaching a dataset to a multi-layer ANN. The process of backpropagation algorithm starts with initializing the values of the weight and biases (Rojas, 1996). Suppose that there is a training set  $\{(x_1, t_1), \dots, (x_m, t_m)\}$  which consists of specific patterns of inputs and outputs. And the activation functions of the neurons are differentiable and continuous. Assume that the output of the ANN is  $o_i$ . Then, the main function to be minimized can be formulated in least mean squares terms as,

$$E = \frac{1}{2} \sum_{i=1}^m \|o_i - t_i\|^2 \quad (4.8)$$

The minimized form of the above function is propagated back to the network and the weights and biases are adjusted accordingly to minimize the error for a given dataset. The network should distinguish a new data from the learned dataset.

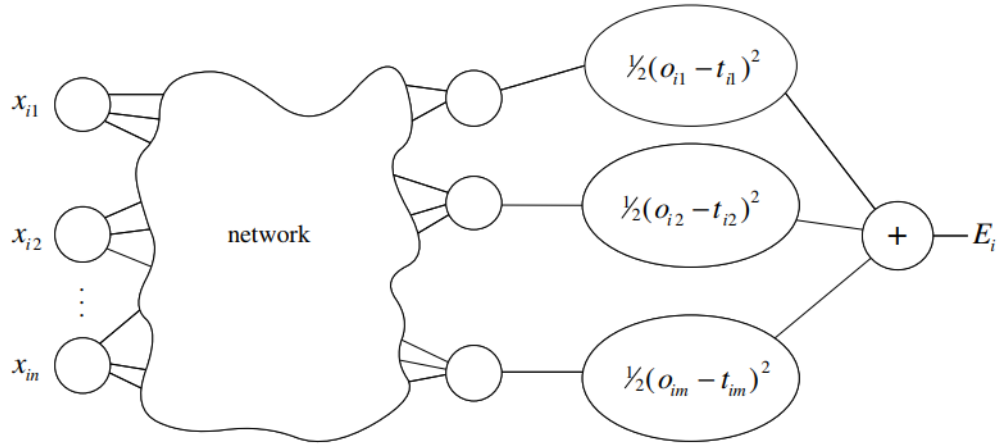


Figure 4.12 Propogating the error (Rojas, 1996)

For each  $t_i$ , there is an  $E_i$  is calculated. Each of the objective function is added up and a total error  $E$  is formed. The error is mathematically formulated as follows,

$$E = E_1 + E_2 + \dots + E_m \quad (4.9)$$

Main objective in training an ANN is adjusting the weights and biases to make the  $E$  as low as possible. The only way to adjust the weights in the network is calculating the gradients of  $E$  for each weight and backpropogating the derivatives. Mathematical representation of the gradients is as follows,

$$\nabla E = \left( \frac{\delta E}{\delta w_1}, \frac{\delta E}{\delta w_2}, \frac{\delta E}{\delta w_3}, \dots, \frac{\delta E}{\delta w_m} \right) \quad (4.10)$$

Adjustment of the each weight and bias at each iteration is calculated with the following equations,

$$\Delta w_m = -\mu \frac{\delta E}{\delta w_m} \quad (4.11)$$

$$\Delta \theta_m = -\mu \frac{\delta E}{\delta \theta_m} \quad (4.12)$$

where  $\mu$  is the learning rate and the reason it is negative because the optimum point is always in the negative direction of the gradient. Once the numerical values of the gradients are calculated, the weight and bias value combinations that make the error gradient zero can be obtainable.

The backpropagation algorithm consists of two basic steps. These are the feed-forward and the backpropagation phases. In the feedforward case, the input is fed to the network and propagated through the output. The derivatives of the functions are also computed in this phase. In the backpropagation step, the network is employed through backwards. The error in

the output node is propagated through the input nodes by taking into account of the derivatives of the activation functions. For example, if we focus on one of the weights, assume that  $w_{ab}$ . And let's assume that the result of one of the output nodes is  $o_a$ . The first derivative at the output node is computed as follows,

$$\frac{\delta E}{\delta w_{ab}} = o_a \frac{\delta E}{\delta o_a w_{ab}} \quad (4.13)$$

If we consider the backpropagated error at the b-th node as  $\delta_b$  then the derivative to be backpropagated in that node is,

$$\frac{\delta E}{\delta w_{ab}} = o_a \delta_b \quad (4.14)$$

And the weight update values can be calculated as follows,

$$\Delta w_{ab} = -\mu o_a \delta_b \quad (4.15)$$

At each iteration the weights and biases will adjust themselves and lead to better predictions. The above mentioned mathematical case of backpropagation can be summarized as the following figure where the left side of the  $j$ -th output unit is the derivative of the activation function.

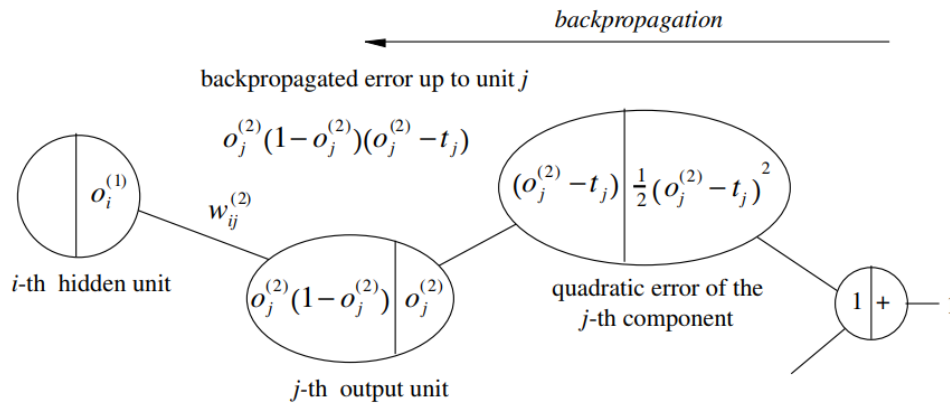


Figure 4.13 Backpropagation in a chain of nodes (Rojas, 1996)

### 4.3. Nonlinear Autoregressive Exogenous (NARX) Network

NARX is a type of recurrent neural network. It is a generalization of autoregressive equations (Boussaada et al., 2018). NARX is an effective tool for non-linear time-series identification, particularly dynamic systems. NARX network is also used in this thesis for the identification of the non-linear system. In order to correctly predict the next time output, the current time input and output is fed to the network with the previous time input and output. The following figure summarizes the two different architectures of the NARX network.

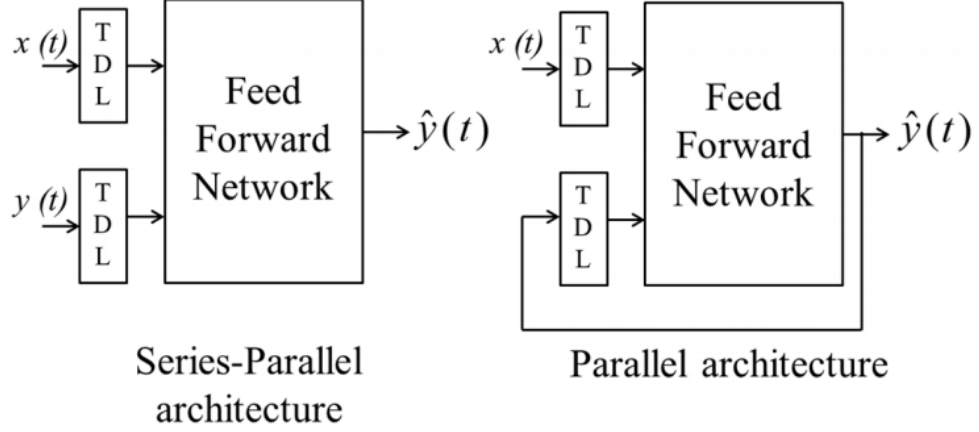


Figure 4.14 Different architectures of the NARX network (Boussaada et al., 2018)

In the parallel architecture, the next time output is calculated from the current time input and previous time output predictions. In the series-parallel architecture, the next time output is predicted by the current time and previous time input and outputs. The series-parallel architecture is more favorable compared to the parallel architecture because of its ability to converge much faster and it can be trained by in feedforward backpropagation manner. For this reason, the series-parallel architecture is used in this thesis for the identification of the system. Finally the mathematical representations of the series-parallel and parallel architectures are respectively given in the following equations,

$$\hat{y}(t+1) = f \left( \begin{array}{c} y(t), y(t-1), \dots, y(t-n_b), \\ x(t+1), x(t), x(t-1), \dots, x(t-n_a) \end{array} \right) \quad (4.16)$$

$$\hat{y}(t+1) = f \left( \begin{array}{c} \hat{y}(t), \hat{y}(t-1), \dots, \hat{y}(t-n_b), \\ x(t+1), x(t), x(t-1), \dots, x(t-n_a) \end{array} \right) \quad (4.17)$$

where  $\hat{y}$  is the predicted output,  $y$  is the output,  $x$  is the input,  $f(\cdot)$  is the neural network function and  $n_b$  and  $n_a$  are the output and input delays, respectively.

## **5. MODEL PREDICTIVE CONTROL**

### **5.1. Introduction to Model Predictive Control**

Model Predictive Control (MPC) algorithms were improved from the optimal control theory first developed in 1950s. By the end of 1970s first MPC algorithms began to find their place in the literature (Findelsen et al., 2007). The chemical industry quickly adopted the MPC due to its simplicity, effectivity and requirement of only a step input identification of the system which leads to easier models of the system.

MPC is assumed as a developed method for controlling the systems that are linear and have slow dynamics. Other systems, such that the ones have nonlinear, fast evolving dynamics are considered to be beyond the realm of the MPC. However, recent studies in the literature showed that the MPC algorithm is applicable to nonlinear, hybrid, fast evolving dynamics systems. In the industries, many processes are nonlinear. However, MPC algorithms are mainly applied to linear or linearized processes. There are two reasons for this preference: the first one is, identification of a linear system is easy and the second reason is, if the plant operates around the linearized working point, the linearized system gives precisely true results. Furthermore, if the system is linearized, it creates a convex objective function that is easier to optimize for each time step and these kind of objective functions are well established and studied over time for the commercial products. If the system is not linearized around a working point and constraints are assumed as nonlinear, then a Nonlinear Model Predictive Controller (NMPC) is utilized to control the system.

For most of the processes in the industry, the system is nonlinear and the working point of the system changes much often. NMPC are not frequently used in the market, however, it has applications on some products that has high nonlinearities and change of operating points. Today, NMPC applications are growing due to advances in technology and computing power and seems to have a promising future for future products. However, NMPC algorithms has also some drawbacks compared to their linear counterparts. Solution of a nonlinear objective function is much harder compared to a convex objective function. Also, finding the global optimum of a nonlinear problem is not always guaranteed.

As described above, different kind of system models can be used for the identification of

the system. Nonlinear models are generally difficult to construct since there are no knowledge about how to cover all the nonlinearities in the system. Another problem is, it is not generally known which parameter to include to the model. Nonlinear models overall can be divided into mainly two categories. These are input-output models and the state-space models.

Input-output models can be perceived as mapping between the state input and corresponding output at the following time step. This kind of models are generally discrete-time. A general representation of this kind of models are nonlinear auto-regressive moving average model with exogenous input (NARMAX). Mathematical description of a NARMAX model is given in the following equation,

$$y(k) = f[y(k-1), \dots, y(k-n), u(k-1), \dots, u(k-n), e(k-1), \dots, e(k-n)] \quad (5.1)$$

where  $y$  is the output,  $k$  is the discrete time,  $u$  is the input,  $e$  is the error and  $f$  is the mapping function.

Volterra models are the first class are the first type of nonlinear model templates which became highly successful in linear MPC field. They generally resemble the Taylor series expansion of a model. The mathematical representation of the Volterra models are as follows,

$$y(k) = y_0 + \sum_{l=0}^N h_1(l)u(k-l) + \sum_{l=0}^M \sum_{m=0}^M h_2(l,m)u(k-l)u(k-m) \quad (5.2)$$

The first term after  $y_0$  is the linear term and the remaining term adds the nonlinearity into equation. The other type of nonlinear model is the local models. The main idea of the local models is dividing the curve into local linearities. The advantageous part of the local models compared to neural networks are they are not black-box and relationships between the parameters can be seen clearly. The nonlinear model is divided into submodels and each submodel can be thought as a linearized system. Mathematical representation of the local models can be depicted as follows,

$$y(k+1) = f(\mu(k), \pi(k)) = \sum_{l=0}^M f_l(\mu(k), \sigma_l(\pi(k))) \quad (5.3)$$

There are  $M$  submodels in the nonlinear model and  $\sigma$  is the basis function. The basis functions decide to include the submodel approximation into the nonlinear model.

The ANNs are one of the most utilized nonlinear models in the MPC algorithms. They are able to seize the nonlinear dynamics of the system and model it in a black-box fashion. Since ANNs are universal approximators, they can model any nonlinear system with ease. Large scale success of the ANNs in the MPC applications have paved the way for utilization

of ANNs in many appliances in the industry and consumer products. The applications of ANNs to MPC algorithms will be widely covered in the upcoming subsections since the case study in the following chapter will utilize an ANN for the identification of the nonlinear system.

The linear state-space models can be modified to cover nonlinear dynamics of the system. A nonlinear system can be represented in the state-space form with the following equations,

$$x(k+1) = F(x(k), u(k)) \quad (5.4)$$

$$y(k) = G(x(k)) \quad (5.5)$$

Where  $x$  is the state vector and  $F$  and  $G$  are the nonlinear mappings. It should be noticed that if the differential equations that represent the dynamic behavior of the system is known, then the differential equations can be converted to the above-described equation form. The most used form of state-space representation is Piece Wise Affine models. They divide the nonlinear model into local linear models and process them separately. Mathematically, the Piece Wise Affine models can be shown as follows,

$$x(k+1) = A_i x(k) + B_i u(k) + f_i \quad (5.6)$$

## 5.2. Nonlinear Model Predictive Control

The basic idea of the NMPC algorithms are, at an sampling time  $k$ , the behavior of the system is optimized over a time horizon  $m=1,2,3,\dots,M$  (Grüne and Pannek, 2011). The optimal sequence of the inputs over time is calculated to make the system follow the reference trajectory stably. The basic idea and block diagram of the NMPC algorithm are depicted in Figure 5.1 and Figure 5.2, respectively.

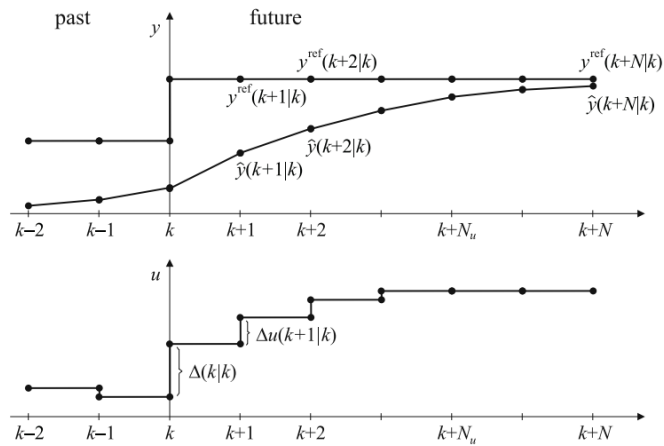


Figure 5.1. The NMPC algorithm (Nguyen and Szczerbicki, 2009)

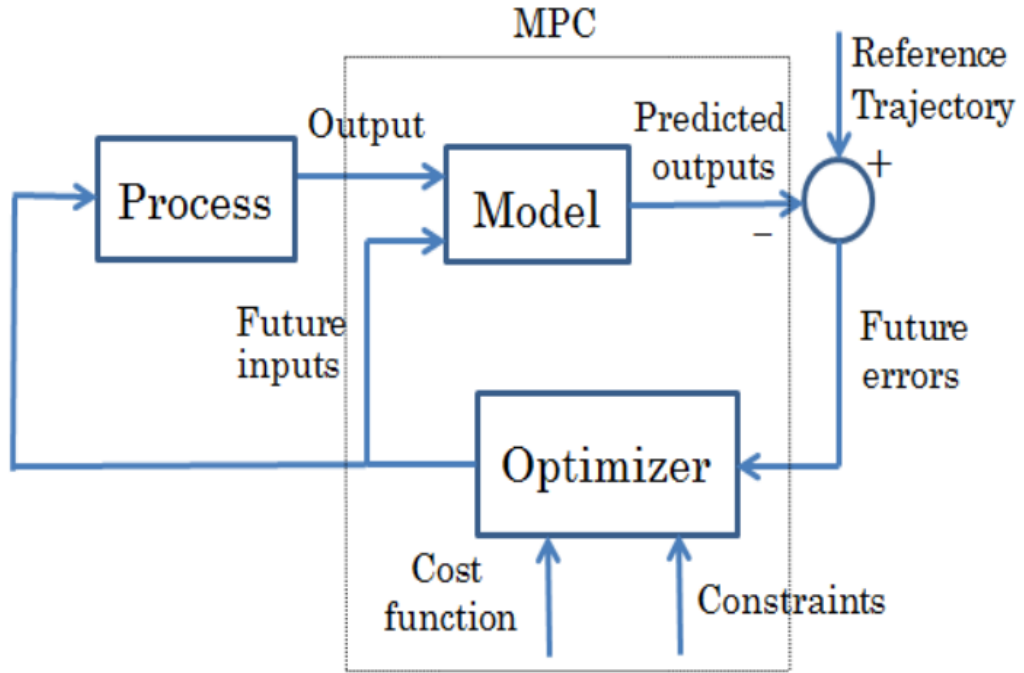


Figure 5.2. Block diagram of a NMPC algorithm (Yakub, 2013)

Assume that the plant is formalized as follows,

$$x^* = F(x^*, u^*) \quad (5.7)$$

The states and the inputs are generally limited with constraints. Limiting the states with constraints makes the control problem more sensible. For example, a mass can not move 100 metres in around 0.1 seconds. Also, most of the time the inputs and the change of inputs are limited with constraints. For example, a force acting on a mass can not change from 2 Newton to 5000 Newton in a small time step. These constraints are depicted as follows,

$$u^{min} < u(k + m) < u^{max}, m=1,2,3,\dots,n_u-1 \quad (5.8)$$

$$\Delta u^{min} < \Delta u(k + m) < \Delta u^{max}, m=1,2,3,\dots,n_u-1 \quad (5.9)$$

$$x^{min} < x(k + m) < x^{max}, m=1,2,3,\dots,n-1 \quad (5.10)$$

Where *min* and *max* superscripts show the minimum and maximum notations, respectively. Thereafter, the objective function of the NMPC algorithm can be formalized as follows,

$$J = \sum_{m=1}^n \left( y_{ref}(k + m|k) - y_{pred}(k + m|k) \right)^2 + \sum_{m=0}^{n-1} \mu (\Delta u(k + m|k))^2 \quad (5.11)$$

Where  $\mu$  is the weighting factor and  $\Delta u$  is the input increment. The input increment can be formalized as follows,

$$\Delta u(k + 1) = u(k + 1) - u(k) \quad (5.12)$$

The input sequence can be predicted by optimizing the objective function consequently for the each time step. With the above mentioned definitions, the basic NMPC algorithm for the constant state reference trajectory can be algorithmically represented as follows,

1. Obtain the states of the system.
2. Minimize the objective function given in Eq. (5.11) subject to constraints given in Eqs. (5.8) – (5.10).
3. Calculate the optimum input and apply it to the system.
4. Jump to the next time step and return to the first step of the algorithm until the last time step has been reached.

The algorithm must be feasible for implementation. That means, for each time step, there must be an optimal input available. For the each time step, newly calculated inputs must be supplied back to the system as the state feedback law.

### **5.3. Utilization of the Neural Networks in Model Predictive Control**

The ANNs are widely-used for the modeling of the system to be utilized in MPC (Nguyen and Szczerbicki, 2009). General representation of a Nonlinear Auto Regressive with External Input (NARX) model can be depicted as follows,

$$y(k) = f[u(k - 1), \dots, u(k - n), \dots, y(k - 1), \dots, y(k - n)] \quad (5.13)$$

Where  $n$  is the previous time values of the inputs and the states and  $f$  is a nonlinear function that can be thought as combination of activation functions. Generally, Multi Layer Perceptron (MLP) and Radial Basis Function (RBF) architectures are utilized for the modeling of the nonlinear systems since both of them are considered as universal approximators. Furthermore, they both have less parameters to be tuned and both have simple structures. Block diagram representation of a Neural Network Predictive Controller (NNPC) is shown in Figure 5.3.

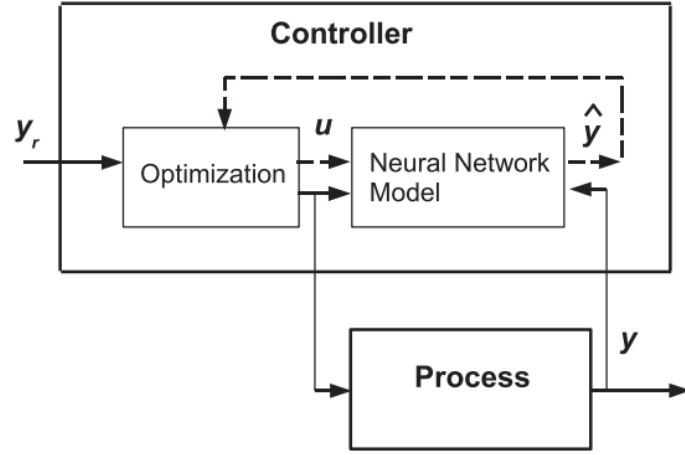


Figure 5.3. Block diagram of a NNPC (Vasickaninova et al., 2011)

As can be seen from the Figure 5.3, at first, the neural network model is trained with the input-output data of the plant. Thereafter, the objective function that is given in Eq. (5.11) is formed with the outputs of the neural network model and the objective function is optimized at each time step.

The output of the MLP model can be mathematically depicted as follows,

$$y(k) = w_0^2 + \sum_{a=1}^M w_a^2 \alpha(z_a(k)) \quad (5.14)$$

Where  $\alpha$  is the nonlinear activation function,  $a$  is the number of neurons in the hidden layer and  $z$  is the sum of the inputs of the neural network. Value of  $z$  can be calculated as,

$$z(k) = w_0^1 + \sum_{j=1}^{\alpha} w_{i,j}^1 u(k - \mu + 1 - j) + \sum_{j=1}^n w_{i,\alpha+j}^1 y(k - j) \quad (5.15)$$

Where  $\mu$  is the time delay. RBF method utilizes Gaussian activation function in the hidden layer neurons. Mathematical formulation of the output of a RBF is given below,

$$y(k) = w_0^2 + \sum_{a=1}^M w_a \exp(-||x(k) - c_a||) \quad (5.15)$$

Graphical demonstration of a RBF is given in Figure 5.4.

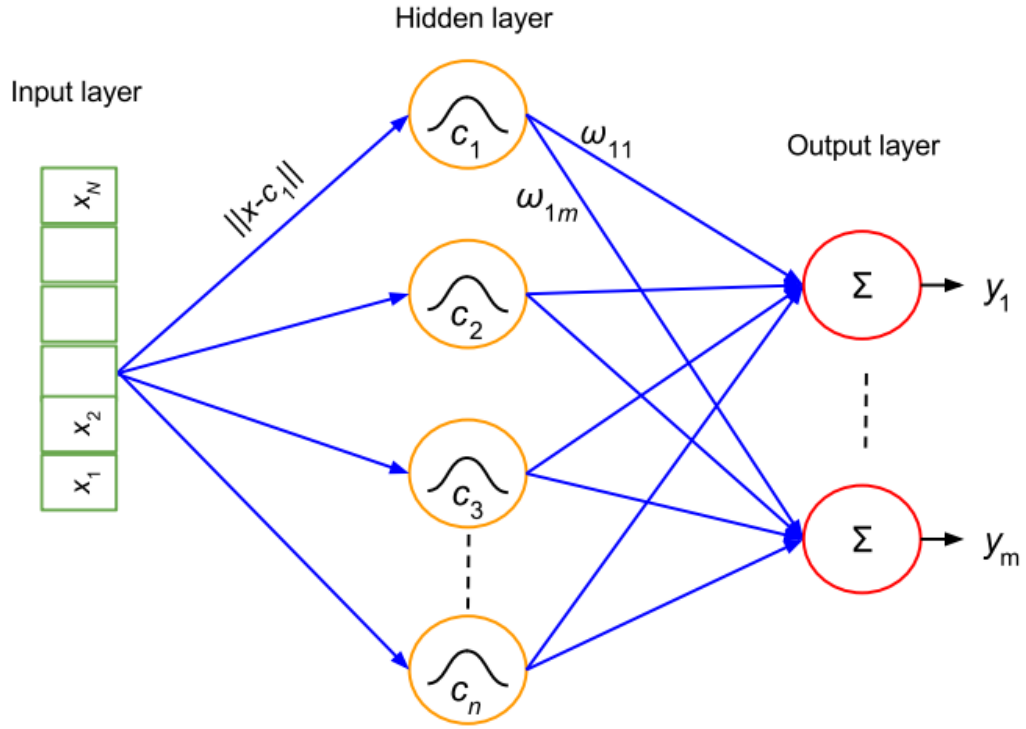


Figure 5.4. RBF neural network (Faris et al., 2017)

In the NNPC, nonlinear models such as MLP and RBF are utilized to calculate future predictions of the states. Afterwards, these predictions are utilized for the calculation of the future optimal inputs to the system in the objective function. Future predictions of the states can be calculated as,

$$y^p(k+m|k) = y(k+m|k) + d(k) \quad (5.16)$$

Where  $d$  is the disturbance to the system and  $p$  superscript shows the predicted state. By utilizing the predictions in the objective function, Eq. (5.11), the NNPC algorithm turns into a dynamic nonlinear optimization problem. As discussed in Chapter 3, there are various type of modern nonlinear optimization techniques that can be applied to solve the optimization problem. The traditional techniques may stuck to a local minimum and cause the interruption of the algorithm. However, modern techniques can overcome this issue and run the algorithm smoothly.

## 6. NEURAL NETWORK PREDICTIVE CONTROL OF A VAPOR COMPRESSION CYCLE

### 6.1. Fundamentals of Vapor Compression Cycle Control

As discussed in the other chapters, a basic Vapor Compression Cycle (VCC) consists of four components. These are the compressor, expansion valve, evaporator and condenser. Schematic representation and pressure-enthalpy diagram of a vapor compression cycle is depicted in Figure 6.1.

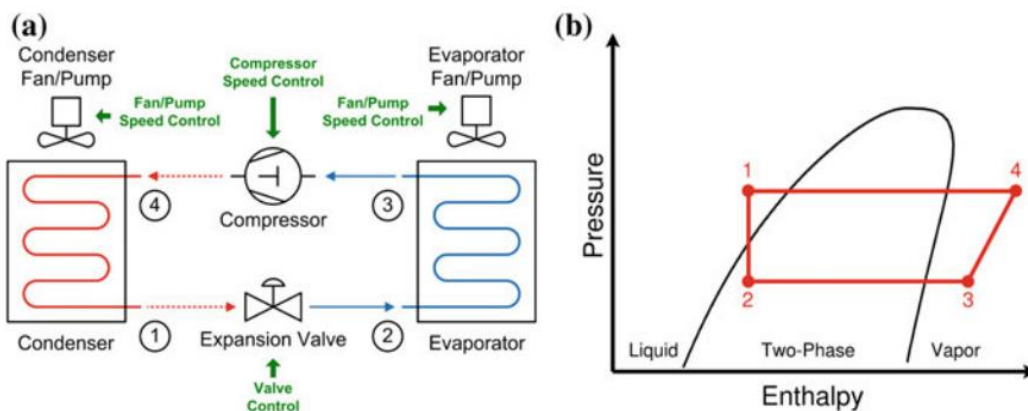


Figure 6.1. a) Schematic representation of a VCC b) Pressure-enthalpy diagram of the VCC (Wen and Mishra, 2018)

Basically, four different processes occur in a VCC. These are, isentropic compression process in the compressor, isobaric condensation process in the condenser, isentropic expansion process in the expansion valve and isobaric evaporation process in the evaporator (Wen and Mishra, 2018). To ensure the stability and optimal operation of the VCC systems, effective control systems can be developed. The control strategies should be effective particularly during start-up of the system and changing of the operating conditions. Variation of the compressor motor speed and openness of the expansion valve can directly affect the mass flow rate of the refrigerant and change the performance and load of the system immediately. On the other hand, change of the external temperature can affect the system more slowly.

Many of the industrial and household HVAC systems have long start-up times (Rasmussen and Alleyne, 2006). For this reason, single-input single-output (SISO) or bang-bang type of controllers had been developed for the HVAC systems primarily. However, it has been later realized that bang-bang controllers limit the system's effectivity due to requiring

unnecessarily large amount of power during the start-up transients. Also, SISO controllers do not perform well due to not considering cross-coupled nature of the VCC system dynamics. Applying multivariable control algorithms can be a good alternative to the bang-bang or SISO algorithms. The multivariable control algorithm can control more than one inputs while optimizing more than one objective simultaneously.

To optimally operate a VCC system, two-phase flow portion in the evaporator must be maximized. The two-phase region in the evaporator is where the most of the heat transfer between the refrigerant and the secondary fluid occurs. Thus, it can be concluded that the cooling load of a VCC is heavily dependant on the length of the two-phase region in the evaporator. However, to ensure the stability of the cycle and the compressor, the refrigerant entering the compressor must be in vapor phase. Therefore, most of the time, the superheat temperature is arranged as 5°C above the saturation temperature for the systems without a receiver.

Generally, implementing various control objectives at the same time is considered impractical for the HVAC systems. This kind of complex algorithms are only applied to large industrial processes where the economic benefits of implementing these algorithms are significant. As discussed above, applying multivariable control strategies to the VCC or HVAC systems can be a great alternative to other complex control strategies since they require extensive parameter tuning. Multivariable control strategies can be easily applied to lumped models and can effectively optimize different control objectives simultaneously such as maximizing COP, minimizing compressor work, maximizing second law efficiency, etc..

## **6.2. Dynamic Modeling of the Heat Exchangers**

Heat exchangers can be of many different types by their tube design, size and direction of the fluid flow inside the tubes (Figure 6.2). It is intended to optimize the work of the heat exchangers in the VCC where various phenomenons that happen in the components lead to different performance outcomes. For this reason, various modeling approaches have been applied to the heat exchangers.

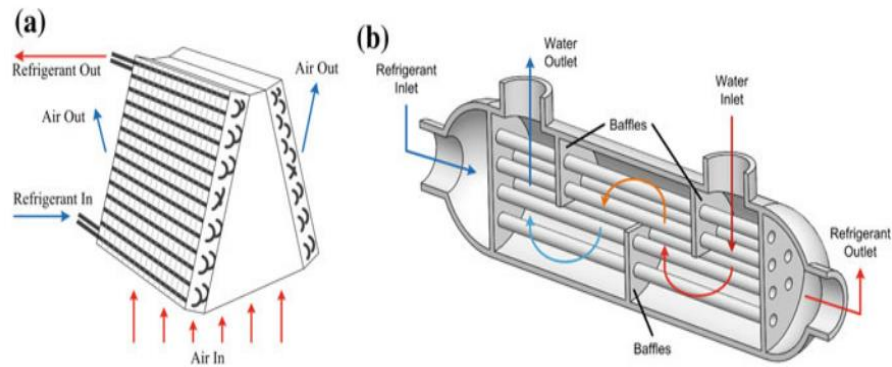


Figure 6.2. Different designs of heat exchangers (Wen and Mishra, 2018)

### 6.2.1. Multi-phase Flows in the Heat Exchangers

Evaporation and condensation processes that occur in the heat exchangers are the main source of the heat transfer in the VCC. For this reason, this processes must be modeled exactly and carefully with taking into account of heat exchanger geometry, size and some other properties. Demonstrations of some types of multi-phase flows are given in Figure 6.3. Some commercial packages can model the multi-phase flow in a heat exchanger accurately. However, control of a VCC system can not be carried out with these kind of approaches.

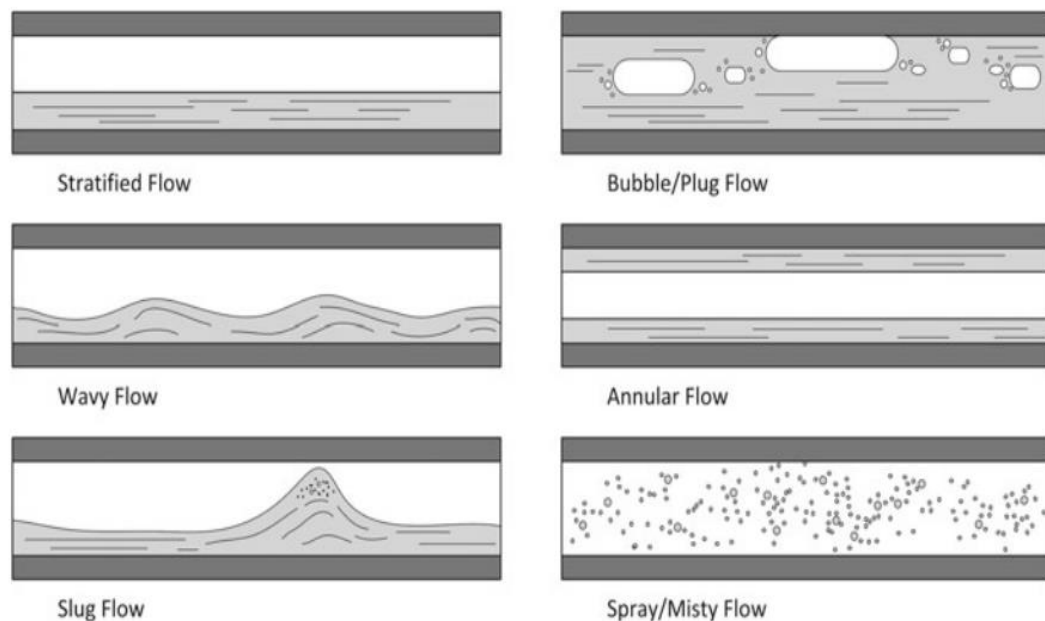


Figure 6.3. Different types of multi-phase flows in the heat exchangers (Wen and Mishra, 2018)

For the reasons described above, more simple one-dimensional uniform flow models

are considered for the modeling of the heat exchangers. Earlier models utilized the lumped parameter approach for the modeling of the whole heat exchanger. However, this approach did not result in favorable outcomes. Modern approaches relies on discretizing the heat exchanger into smaller pieces. The modern approaches result in more favorable outcomes while having the burden of extensive computational load. The two modern approaches that are widely used in the literature are Moving Boundary (MB) and Finite Control Volume (FCV). These two approaches are briefly described in the Chapter 2. More detailed descriptions of these approaches have been given place in the following sub-sections.

### 6.2.2. Fixed Control Volume Approaches

FCV approaches can be accomplished by two ways, one is dividing the heat exchanger into pieces and taking the average values of the each divided part and the second is directly discretizing the differential equation. This kind of approaches can model the heat transfer taking place in the heat exchanger precisely. The downside of the FCV approach is, it may require high computational power to calculate the outcome. A demonstration of a discretized condenser with the FCV method is given in Figure 6.4.

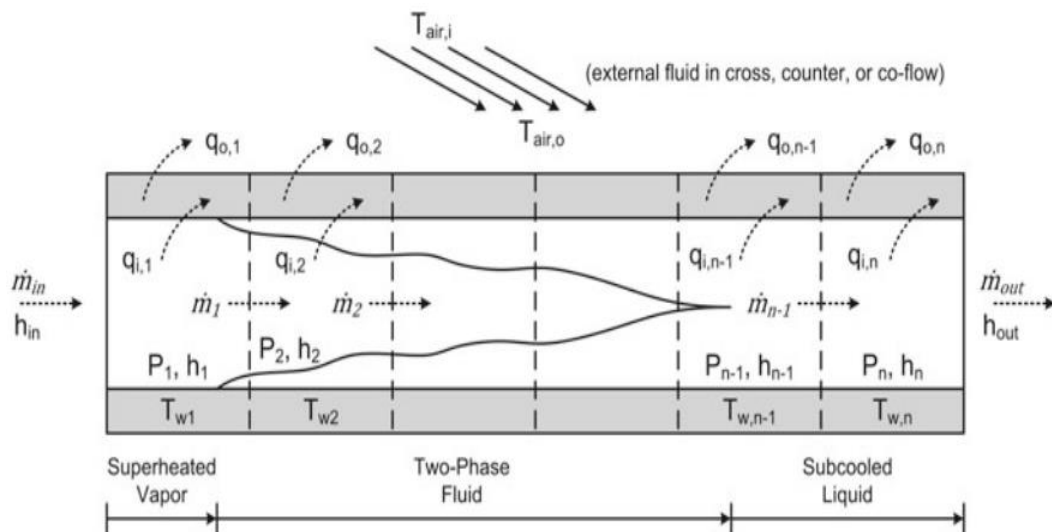


Figure 6.4. Discretized heat exchanger (Wen and Mishra, 2018)

Following steps have been followed for the modeling of the condenser,

- Conservation of the mass along the heat exchanger tube is determined by using the Eq. (6.1).
- Conservation of the energy along the heat exchanger tube is extended in terms of enthalpy and pressure.
- Conservation of the wall energy is given in Eq. (6.4).

Following formulas can be utilized for the modeling of the condenser,

$$\dot{m}_{cond,i} = \dot{m}_{i-1} - \dot{m}_i \quad (6.1)$$

$$\dot{m}_i = C_d A \sqrt{\rho(P_i - P_{i+1})} \quad (6.2)$$

$$\dot{Q}_i = \dot{m}_{i-1} h_{i-1} + \dot{m}_i h_i + q_i = \dot{m}_i u_i + \dot{m}_i \left( \frac{du_i}{dP_c} \dot{P}_i + \frac{du_i}{dh_i} \dot{h}_i \right) \quad (6.3)$$

$$q_i = \alpha A (T_{w,i} - T_{r,i}) \quad (6.4)$$

$$q_o = \alpha A (T_{air,i} - T_{w,i}) \quad (6.5)$$

$$\dot{E}_{w,i} = q_o - q_i \quad (6.6)$$

The above given equations can be transformed into the following form,

$$\begin{bmatrix} A_{11} & A_{12} & 0 \\ A_{12} & A_{12} & 0 \\ 0 & 0 & A_{33} \end{bmatrix} \begin{bmatrix} \dot{P} \\ \dot{h}_1 \\ \vdots \\ \dot{h}_n \\ \dot{T}_{w,1} \\ \vdots \\ \dot{T}_{w,n} \end{bmatrix} = \begin{bmatrix} \dot{m}_i (\dot{h}_i - \dot{h}_1) + q_i \\ \vdots \\ \dot{m}_i (\dot{h}_{k-i} - \dot{h}_1) + q_i \\ \dot{m}_i - \dot{m}_o \\ q_{o,1} - q_{i,1} \\ \vdots \\ q_{o,k} - q_{i,k} \end{bmatrix} \quad (6.7)$$

Where  $k$  is the number of discretized volumes. Using more than twenty control volumes gives acceptable results according to the literature. Also, utilizing more control volumes results in more computational load.

### 6.2.3. Moving Boundary Model

The Moving Boundary (MB) method utilizes lumped parameter for the each phase in the heat exchanger instead of the FCV method which divides the heat exchanger into small control volumes and accomplish the calculations for the each volume. The boundaries that are dividing the each phase are assumed to time-variant in the MB method. MB representation of a condenser is given in the Figure 6.5. The main idea of the MB method is capturing the dynamics of the boundaries between the phases at the same time having as low as equations as possible.

To achieve the formalization of the MB model of a condenser, analyzing the behavior of a single-phase heat exchanger is a sensible approach. Demonstration of a simple single-phase exchanger is given in Figure 6.6. Following assumptions have been made during the MB model development (Rasmussen and Alleyne, 2006),

- The heat exchanger is double pipe type and the tubes are horizontal and long enough.
- The flow in the heat exchanger is one-dimensional.
- Axial conduction phenomenon in the heat exchangers is insignificant.

- Pressure drop across the heat exchanger that occurs due to friction is neglected.

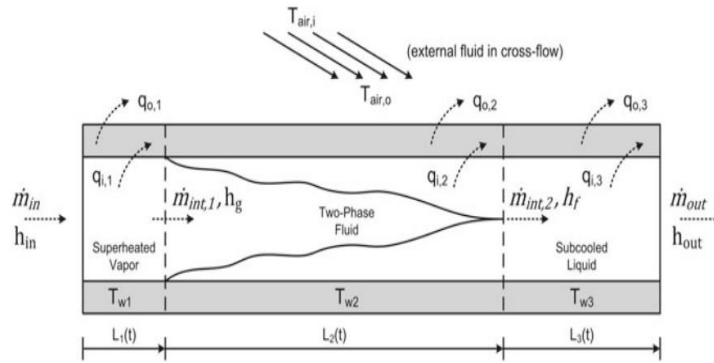


Figure 6.5. MB depiction of a heat exchanger (Wen and Mishra, 2018)

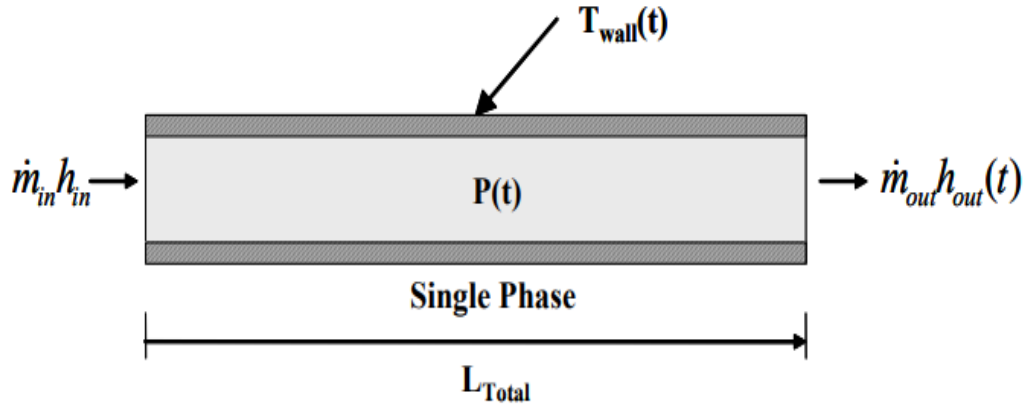


Figure 6.6. Single-phase heat exchanger (Rasmussen and Alleyne, 2006)

The general partial differential equations (PDE) that represent the conservation of energy and mass can be reduced into one-dimensional equations by taking above described assumptions into account. Following equations describe the general behavior of the refrigerant energy and mass conservation and the tube wall energy conservation,

$$\frac{\partial \rho}{\partial t} + \nabla(\rho \mathbf{u}) = \mathbf{0} \quad (6.8)$$

$$\frac{\partial(\rho \mathbf{u})}{\partial t} + \nabla(\rho \mathbf{u} \mathbf{u}) = \rho \mathbf{f} + \nabla \beta \quad (6.9)$$

$$\frac{\partial(\rho A_{cr})}{\partial t} + \frac{\partial(\dot{m})}{\partial x} = \mathbf{0} \quad (6.10)$$

$$\frac{\partial(\rho A_{cr} h - A_{cr} P)}{\partial t} + \frac{\partial(\dot{m} h)}{\partial x} = \mathbf{d}_i \alpha_i (T_{wall} - T_{ref}) \quad (6.11)$$

$$(C_p \rho A)_{wall} \frac{\partial(T_{wall})}{\partial t} = \mathbf{d}_i \alpha_i (T_{ref} - T_{wall}) + \mathbf{d}_o \alpha_o (T_{air} - T_{wall}) \quad (6.12)$$

By employing Leibniz's equation on these equations, they can be transformed into

ordinary differential equations or grouped into the matrix (state-space) form. The main conservation of refrigerant mass equation for a single-phase heat exchanger can be formalized as in Eq. (6.13). By applying integration to the formula along the tube, the equation transforms into Eq. (6.14). Then the equation transforms into Eq. (6.15) by utilizing the Leibniz's equation. Finally, dividing the calculation into separate thermodynamic variables and taking the conservation of mass results in Eq. (6.20).

$$\frac{\partial(\rho A_{cr})}{\partial t} + \frac{\partial(\dot{m})}{\partial x} = \mathbf{0} \quad (6.13)$$

$$\int_0^{L_{tot}} \frac{\partial(\rho A_{cr})}{\partial t} dx = A_{cr} \left[ \int_0^{L_{tot}} \frac{\partial \rho}{\partial t} dx \right] \quad (6.14)$$

$$\int_0^{L_{tot}} \frac{\partial(\rho A_{cr})}{\partial t} dx = A_{cr} \left[ \int_0^{L_{tot}} \rho dx \right] \quad (6.15)$$

$$\int_0^{L_{tot}} \frac{\partial(\rho A_{cr})}{\partial t} dx = A_{cr} [\rho_{co} L_{tot}] \quad (6.16)$$

$$\int_0^{L_{tot}} \frac{\partial(\rho A_{cr})}{\partial t} dx = A_{cr} [\dot{\rho}_{co} L_{tot}] \quad (6.17)$$

$$\int_0^{L_{tot}} \frac{\partial(\rho A_{cr})}{\partial t} dx = A_{cr} L_{tot} \left[ \left( \frac{\partial \rho}{\partial P_{co}} \Big|_{h_{co}} \right) P_{co} + \left( \frac{\partial \rho}{\partial h_{co}} \Big|_{P_{co}} \right) h_{co} \right] \quad (6.18)$$

$$\int_0^{L_{tot}} \frac{\partial(\dot{m})}{\partial x} dz = \dot{m}_o - \dot{m}_i \quad (6.19)$$

$$\left[ \left( \frac{\partial \rho}{\partial P_{co}} \Big|_{h_{co}} \right) A_{cr} L_{tot} P_{co} \right] + \left[ \left( \frac{\partial \rho}{\partial h_{co}} \Big|_{P_{co}} \right) A_{cr} L_{tot} h_{co} \right] + \dot{m}_o - \dot{m}_i = \mathbf{0} \quad (6.20)$$

The main conservation of refrigerant equation for a single-phase heat exchanger is given in Eq. (6.21). The equation is integrated along the tube and Eq. (6.22) is obtained. Afterwards, the Leibniz's equation is applied and Eq. (6.23) is obtained. Finally, after dividing the thermodynamic properties into sub-properties and rearranging the equations, Eq. (6.31) is found.

$$\frac{\partial(\rho A_{cr} h - A_{cr} P)}{\partial t} + \frac{\partial \dot{m} h}{\partial x} = d_i \alpha_i (T_{wall} - T_{ref}) \quad (6.21)$$

$$\int_0^{L_{tot}} \frac{\partial(\rho A_{cr} h)}{\partial t} dx = A_{cr} \left[ \int_0^{L_{tot}} \frac{\partial \rho h}{\partial t} dx \right] \quad (6.22)$$

$$\int_0^{L_{tot}} \frac{\partial(\rho A_{cr} h)}{\partial t} dx = A_{cr} \left[ \frac{d}{dt} \int_0^{L_{tot}} \rho h dx \right] \quad (6.23)$$

$$\int_0^{L_{tot}} \frac{\partial(\rho A_{cr} h)}{\partial t} dx = A_{cr} L_{tot} [\dot{\rho} h + \rho \dot{h}] \quad (6.24)$$

$$\int_0^{L_{tot}} \frac{\partial(\rho A_{cr} h)}{\partial t} dx = A_{cr} L_{tot} \left[ \left[ \left( \frac{\partial \rho}{\partial P_{co}} \Big|_{h_{co}} \right) \dot{P}_{co} + \left( \frac{\partial \rho}{\partial h_{co}} \Big|_{P_{co}} \right) \dot{h}_{co} \right] + \rho \dot{h} \right] \quad (6.25)$$

$$\int_0^{L_{tot}} \frac{\partial(\rho A_{cr} h)}{\partial t} dx = \left( \frac{\partial \rho}{\partial P_{co}} \Big|_{h_{co}} h_{co} \right) A_{cr} L_{tot} \dot{P}_{co} + \left( \frac{\partial \rho}{\partial P_{co}} \Big|_{h_{co}} h_{co} + \rho \right) A_{cr} L_{tot} \dot{h}_{co} \quad (6.26)$$

$$\int_0^{L_{tot}} \frac{\partial(PA_{cr})}{\partial t} dx = A_{cr} \int_0^{L_{tot}} \frac{\partial P}{\partial t} dx \quad (6.27)$$

$$\int_0^{L_{tot}} \frac{\partial(PA_{cr})}{\partial t} dx = A_{cr} P L_{tot} \quad (6.28)$$

$$\int_0^{L_{tot}} \frac{\partial(\dot{m}h)}{\partial x} dx = \dot{m}_o h_o - \dot{m}_i h_i \quad (6.29)$$

$$\int_0^{L_{tot}} d_i \alpha_i (T_{wall} - T_{ref}) dx = L_{tot} d_i \alpha_i (T_{wall} - T_{ref}) \quad (6.30)$$

$$\left( \frac{\partial \rho}{\partial P_{co}} \Big|_{h_{co}} h_{co} + 1 \right) A_{cr} L_{tot} \dot{P}_{co} + \left( \frac{\partial \rho}{\partial P_{co}} \Big|_{h_{co}} h_{co} + \rho \right) A_{cr} L_{tot} \dot{h}_{co} + \dot{m}_o h_o - \dot{m}_i h_i = d_i \alpha_i (T_{wall} - T_{ref}) \quad (6.31)$$

Conservation of wall energy can be formulated with the Eq. (6.32). By integrating the equation along the heat exchanger tube and rearranging the equation leads to Eq. (6.34)

$$(C_p \rho A)_{wall} \frac{\partial(T_{wall})}{\partial t} = d_i \alpha_i (T_{ref} - T_{wall}) + d_o \alpha_o (T_{air} - T_{wall}) \quad (6.32)$$

$$(C_p \rho A)_{wall} L_{tot} \frac{\partial(T_{wall})}{\partial t} = d_i \alpha_i L_{tot} (T_{ref} - T_{wall}) + d_o \alpha_o L_{tot} (T_{air} - T_{wall}) \quad (6.33)$$

$$(C_p \rho V)_{wall} \frac{\partial(T_{wall})}{\partial t} = d_i \alpha_i (T_{ref} - T_{wall}) + d_o \alpha_o (T_{air} - T_{wall}) \quad (6.34)$$

Collecting all equations into one matrix equation form results in a  $\mathbf{Ax} = \mathbf{b}$  type of equation. The equation is as follows,

$$\begin{bmatrix} \mathbf{Z}_{11} & \mathbf{Z}_{12} & \mathbf{0} \\ \mathbf{Z}_{12} & \mathbf{Z}_{22} & \mathbf{0} \\ \mathbf{0} & \mathbf{0} & \mathbf{Z}_{33} \end{bmatrix} \begin{bmatrix} \dot{P}_{cond} \\ \dot{h}_{cond} \\ \dot{T}_{wall} \end{bmatrix} = \begin{bmatrix} \dot{m}_i h_i - \dot{m}_o h_o - d_i \alpha_i (T_{wall} - T_{ref}) \\ \dot{m}_i h_i - \dot{m}_o h_o \\ d_i \alpha_i (T_{ref} - T_{wall}) - d_o \alpha_o (T_{air} - T_{wall}) \end{bmatrix} \quad (6.35)$$

The Z coefficients can be calculated by using the equations depicted in Figure 6.7.

$z_{11}$	$\left[ \left( \frac{\partial \rho_c}{\partial P_c} \Big _{h_c} \right) h_c - 1 \right] A_{cs} L_{total}$
$z_{12}$	$\left[ \left( \frac{\partial \rho_c}{\partial h_c} \Big _{P_c} \right) h_c + \rho_c \right] A_{cs} L_{total}$
$z_{21}$	$\left( \frac{\partial \rho_c}{\partial P_c} \Big _{h_c} \right) A_{cs} L_{total}$
$z_{22}$	$\left( \frac{\partial \rho_c}{\partial h_c} \Big _{P_c} \right) A_{cs} L_{total}$
$z_{33}$	$(C_p \rho V)_w$

Figure 6.7. The Z coefficients (Rasmussen and Alleyne, 2006)

Afterwards, the MB model of a condenser can be accomplished by referencing Figure 6.5 with the equations given below,

$$\begin{aligned}
 (6.36) \quad AL_{co1} \left( \frac{d\rho_{co1}}{dP_{co}} \dot{P}_{co} + \frac{d\rho_{co1}}{dh_{co1}} \dot{h}_{co1} \right) + AL_{co1} (\rho_{co1} - \rho_{vap}) &= \dot{m}_i - \dot{m}_{inte,1} \\
 AL_{co2} \left( \frac{d\rho_{co2}}{dP_{co}} \dot{P}_{co} + A(\rho_{vap} - \rho_{liq})(\dot{L}_{co1} + \gamma \dot{L}_{co2}) \right) &= \dot{m}_{inte,1} - \dot{m}_{inte,2} \quad (6.37)
 \end{aligned}$$

$$AL_{co3} \left( \frac{d\rho_{co3}}{dP_{co}} \dot{P}_{co} + \frac{d\rho_{co3}}{dh_{co3}} \dot{h}_{co3} \right) + AL_{co3} (\rho_{co3} - \rho_{liq}) = \dot{m}_{inte,3} - \dot{m}_{liq} \quad (6.38)$$

$$\begin{aligned}
 (6.39) \quad AL_{co1} \left[ \left( \frac{d\rho_{co1} h_{co1}}{dP_{co}} - 1 \right) \dot{P}_{co} + \frac{d\rho_{co1} h_{co1}}{dP_{co}} \dot{h}_{co1} \right] + AL_{co1} (\rho_{co1} h_{co1} - \rho_{vap} h_{vap}) &= \\
 \dot{m}_i h_i - \dot{m}_{inte,1} h_{inte,1} + q_{in1} &
 \end{aligned}$$

$$\begin{aligned}
 AL_{co2} \left( \frac{d\rho_{co2} h_{co2}}{dP_{co}} - 1 \right) \dot{P}_{co} + A(\rho_{vap} h_{vap} - \rho_{liq} h_{liq})(\dot{L}_{co1} + \gamma \dot{L}_{co2}) &= \\
 \dot{m}_{inte,1} h_{inte,1} - \dot{m}_{inte,2} h_{inte,2} + q_{in2} & \quad (6.40)
 \end{aligned}$$

$$\begin{aligned}
 AL_{co3} \left[ \left( \frac{d\rho_{co3} h_{co3}}{dP_{co}} - 1 \right) \dot{P}_{co} + \frac{d\rho_{co3} h_{co3}}{dP_{co}} \dot{h}_{co3} \right] + AL_{co3} (\rho_{co3} h_{co3} - \rho_{liq} h_{liq}) &= \\
 \dot{m}_{inte,2} h_{inte,2} - \dot{m}_{liq} h_{liq} + q_{in3} & \quad (6.41)
 \end{aligned}$$

$$(Mc_p)_{wall} \left[ \left( \frac{T_{wall,1} - T_{inte,1}}{L_{tot}} \right) \dot{L}_{co1} + \delta_{co1} \dot{T}_{wall,1} \right] = q_{out1} - q_{in1} \quad (6.42)$$

$$(Mc_p)_{wall} \dot{T}_{wall,2} = q_{out2} - q_{in2} \quad (6.43)$$

$$(Mc_p)_{wall} \left[ \left( \frac{T_{wall,3} - T_{inte,3}}{L_{tot}} \right) \dot{L}_{co3} + \delta_{co3} \dot{T}_{wall,3} \right] = q_{out3} - q_{in3} \quad (6.44)$$

Some of the parameters that are utilized in the equations above can be calculated as follows,

$$\delta_{co1} = \frac{L_{co1}}{L_{tot}} \quad (6.45)$$

$$q_{in1} = \alpha_{co1} A_{co1} \delta_{co1} (T_{wall,1} - T_{ref}) \quad (6.46)$$

$$q_{out2} = \alpha_{co2} A_{co2} \delta_{co2} (T_{air} - T_{wall,2}) \quad (6.47)$$

The above given equations can be grouped into matrices and form a  $A\mathbf{x} = \mathbf{b}$  type equation. The equation is given as,

$$(6.48) \quad \begin{bmatrix} A_{11} & 0 & A_{13} & 0 & 0 & 0 & 0 \\ A_{21} & A_{22} & A_{23} & A_{24} & 0 & 0 & 0 \\ A_{31} & A_{32} & A_{33} & A_{34} & 0 & 0 & 0 \\ A_{41} & A_{42} & A_{43} & A_{44} & 0 & 0 & 0 \\ A_{51} & 0 & 0 & 0 & A_{55} & 0 & 0 \\ 0 & 0 & 0 & 0 & 0 & A_{66} & 0 \\ A_{71} & A_{72} & 0 & 0 & 0 & 0 & A_{77} \end{bmatrix} \begin{bmatrix} \dot{L}_{co1} \\ \dot{L}_{co2} \\ \dot{P}_{co} \\ \dot{h}_{out} \\ \dot{T}_{wall,1} \\ \dot{T}_{wall,2} \\ \dot{T}_{wall,3} \end{bmatrix} = \begin{bmatrix} \dot{m}_{in}(h_{in} - h_{val}) + q_{in1} \\ \dot{m}_{in}h_{val} - \dot{m}_{out}h_{liq} + q_{in2} \\ \dot{m}_{out}(h_{liq} - h_{out}) + q_{in3} \\ \dot{m}_{in} - \dot{m}_{out} \\ q_{out1} - q_{in1} \\ q_{out2} - q_{in2} \\ q_{out3} - q_{in3} \end{bmatrix}$$

For the solution of the equation, the  $A$  must be inverted. The inversion process can be achievable as long as all phase regions exist, so that values of  $\delta_{co1}$  and  $\delta_{co2}$  are greater than zero. Generally, for the single-phases the average lumped parameters are considered while calculating the thermodynamic and thermophysical properties for the region. However, for the two-phase region this consideration does not hold. A void fraction is calculated and utilized during the analyze of the two-phase region. The void fraction can be described as ratio of the vapor volume in the region to the total volume of the region. Average lumped properties of the two-phase region can be calculated with the following equation,

$$\rho_{co2} h_{co2} = \rho_{liq} h_{liq} (1 - \gamma) + \rho_{vap} h_{vap} \gamma \quad (6.49)$$

Various type of experimental correlations are given in the literature to calculate the mean void fraction (Wen and Mishra, 2018). Generally, there are small differences between the FCV and MB methods due to lumped parameter employment strategy of the MB method. The FCV method comes up with more accurate results. However, modifications can be made with lumped parameter calculating strategy of the MB method to find more accurate results.

### 6.3. Case Study of Designing a Neural Network Predictive Controller for a Vapor Compression Cycle

A basic vapor compression cycle (VCC) consists of four different components:

evaporator, condenser, expansion valve and compressor. Static relationships are often utilized for the modeling of the compressor and expansion valves due to capturing much faster evolving dynamics compared to the heat exchangers. And the modeling of the heat exchangers in a VCC is most often done with two different approaches that are also described before in this thesis. They are the Finite Control Volume (FCV) and Moving Boundary (MB) approaches. The FCV method employs finite-sized control volumes that divides the heat exchanger into small pieces. The thermodynamic and thermophysical properties of the fluid in each piece are considered and calculated separately. Many commercial software packages relies on the FCV method and its ability to precisely calculate the outcome of the heat exchanger. On the other hand, in the MB method, each phase of the refrigerant in the heat exchanger is evaluated as a separate control volume. The thermodynamic and thermophysical properties of the refrigerant in these regions are calculated as an average lumped parameter. The boundaries that separate the each phase are considered as time-varying. Many studies in the literature compared the FCV method and the MB method and they found out that the FCV method comes up with more accurate results but has much more computational load compared to the MB method. The studies concluded that the MB method is a favorable alternative to the FCV method (Rasmussen, 2005; Rasmussen and Shenoy, 2008). The MB method is utilized for the modeling of the evaporator and condenser in this case study. A sample demonstration of a VCC modeled with the MB method is given in Figure 6.8. For simplifying the system, components such as accumulator and receiver are not included to the system.

The cycle employs R134a as the primary fluid and the water as the secondary fluid in the heat exchangers. Furthermore, the temperatures of the high-temperature and low-temperature reservoirs are taken as 27°C and 7°C, respectively. The CoolProp library (Bell et al., 2014) are utilized for the determination of the thermodynamic and thermophysical properties of the fluids. The temperature of the high-temperature reservoir is taken as the environmental temperature during the exergetic calculations.

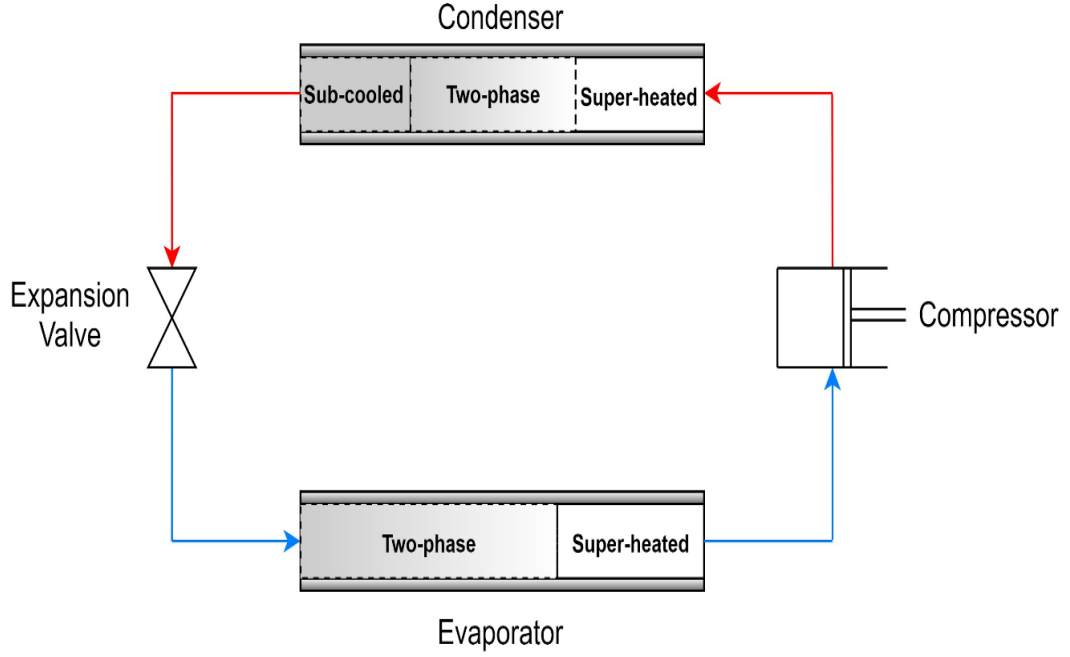


Figure 6.8. A demonstration of a VCC modeled with the MB method

The compressor is considered as a positive-displacement compressor and the expansion valve is considered as an electronic expansion valve (EEV) in this case study. Static relationships are utilized for the modeling of the EEV and compressor in this case study due to having much faster evolving dynamics compared to the that of heat exchangers. As discussed before, the compressor is considered as adiabatic and non-isentropic while the EEV is considered as isentropic and isenthalpic. The mass flow rate of the refrigerant in the compressor is calculated as follows,

$$\dot{m}_{comp} = \rho_{comp,in} V_{comp} \omega_{comp} \eta_{comp} \quad (6.50)$$

The volumetric efficiency of the compressor is calculated with the following correlation (Jain, 2013),

$$\begin{aligned} \eta_{comp} = & (0.65127) + (0.00027681)x\omega_{comp} + (-0.031338)x\frac{P_{out}}{P_{in}} + \\ & (3.0221x10^{-5})x\omega_{comp}x\frac{P_{out}}{P_{in}} + (-1.1905x10^{-7})\omega_{comp}^2 + \\ & (-0.0081256)x\left(\frac{P_{out}}{P_{in}}\right)^2 \end{aligned} \quad (6.51)$$

The output temperature of the refrigerant from the compressor is calculated with the following formula,

$$\frac{T_{comp,out}}{T_{comp,in}} = \left(\frac{P_{cond}}{P_{evap}}\right)^{\frac{\gamma-1}{\gamma}} \quad (6.52)$$

The isentropic efficiency of the compressor is calculated with the following equation,

$$\eta_{is} = 1.0 - 0.004 \frac{P_{cond}}{P_{evap}} \quad (6.53)$$

Electrical and mechanical efficiencies of the compressor are respectively taken as 0.95 and 0.9. Work consumption of the compressor is calculated as,

$$W_{comp} = \dot{m}_{comp}(h_{comp,out} - h_{comp,in}) \quad (6.54)$$

Finally exergy destruction of the compressor is calculated as follows,

$$\dot{X}_{dest,comp} = -T_H \dot{m}_{comp}(s_{comp,in} - s_{comp,out}) \quad (6.55)$$

The photo of a compressor is given in Figure 6.9.



Figure 6.9. Photo of a compressor (Rasmussen and Alleyne, 2006)

The refrigerant mass flow rate in the EEV side of the cycle is determined as follows,

$$\dot{m}_{valv} = A_{valv} C_{valv} \sqrt{(P_{valv,in} - P_{valv,out})} \quad (6.66)$$

Discharge coefficient of the EEV is calculated as follows (Jain, 2013),

$$C_{valv} = (-9.5984 \times 10^{-6}) + (2.0481 \times 10^{-6}) \alpha + (5.4106 \times 10^{-6}) \alpha (P_{out} - P_{in}) + (-7.4909 \times 10^{-10}) \alpha \alpha (P_{out} - P_{in}) + (-3.7775 \times 10^{-8}) \alpha \alpha^2 \quad (6.67)$$

The rate of exergy destruction in the EEV is determined as follows,

$$\dot{X}_{dest,valv} = -T_H \dot{m}_{valv}(s_{valv,in} - s_{valv,out}) \quad (6.68)$$

Finally, photo of an EEV is depicted in Figure 6.10. The MB model of the evaporator

consists of three separate regions: the super-heated region, two-phase region and sub-cooled region. The evaporator and condenser models are given in Figure 6.11.



Figure 6.10. Photo of an EEV (Rasmussen and Alleyne, 2006)

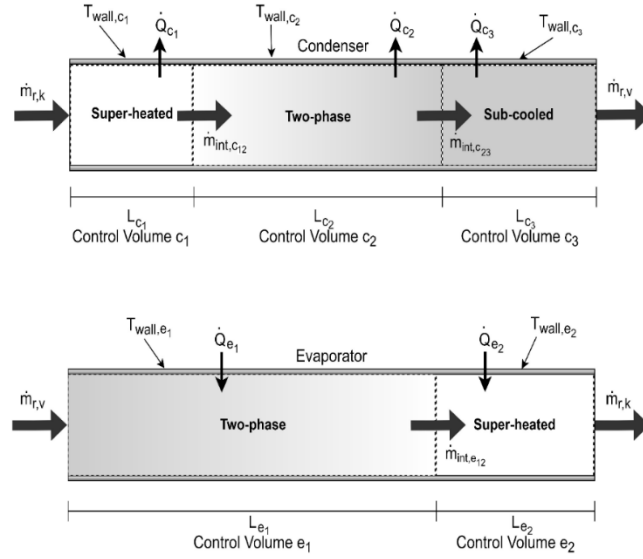


Figure 6.11. The MB models of the evaporator and condenser

The design properties of the condenser is taken as follows, the tube length is 19 m, the outer and inner tube diameters are taken respectively as 18 mm and 12 mm and wall thickness of the tube is 2 mm. The walls of the condenser is considered to be made of steel and Shah (1984) correlation is utilized for the modeling of the condensation process and Fauske (1964) correlation is used for the calculation of the mean void fraction. The equations that model the conservation of mass for the each region in the evaporator as follows,

$$(\rho_{cond,1} - \rho_{va})A\dot{L}_{cond,1} + \left[ \frac{\delta\rho_{cond,1}}{\delta P_{cond}} \Big|_{h_{cond,1}} + \frac{1}{2} \left( \frac{\delta\rho_{cond,1}}{\delta h_{cond,1}} \Big|_{P_c} \left( \frac{dh_{vap}}{dP_{cond}} \right) \right) \right] AL_{cond,1}\dot{P}_{cond} + \frac{1}{2} \left( \frac{\delta\rho_{cond,1}}{\delta h_{cond,1}} \Big|_{P_c} \right) AL_1\dot{h}_{cond} = \dot{m}_{comp} - \dot{m}_{inte,cond12} \quad (6.69)$$

$$(\rho_{vap} - \rho_{liq})A\dot{L}_{cond,1} + (\rho_{vap} - \rho_{liq})\gamma A\dot{L}_{cond,2} + \left( \frac{d\rho_{liq}}{dP_{cond}} (1 - \gamma) + \frac{d\rho_{vap}}{dP_{cond}} \gamma \right) AL_{cond,2}\dot{P}_{cond} = \dot{m}_{inte,cond12} - \dot{m}_{inte,cond23} \quad (6.70)$$

$$(\rho_{liq} - \rho_{cond,3})A(\dot{L}_{cond,1} + \dot{L}_{cond,2}) + \left[ \frac{\delta\rho_{cond,3}}{\delta P_{cond}} \Big|_{h_{cond,3}} + \frac{1}{2} \left( \frac{\delta\rho_{cond,3}}{\delta h_{cond,3}} \Big|_{P_c} \left( \frac{dh_{liq}}{dP_{cond}} \right) \right) \right] AL_{cond,3}\dot{P}_{cond} + \frac{1}{2} \left( \frac{\delta\rho_{cond,3}}{\delta h_{cond,3}} \Big|_{P_c} \right) AL_3\dot{h}_{cond} = \dot{m}_{inte,cond23} - \dot{m}_{valv} \quad (6.71)$$

Energy conservation equations for the each region are as follows,

$$\left[ \frac{\delta\rho_{cond,1}}{\delta P_{cond}} \Big|_{h_{cond,1}} + \frac{1}{2} \left( \frac{\delta\rho_{cond,1}}{\delta h_{cond,1}} \Big|_{P_c} \left( \frac{dh_{vap}}{dP_{cond}} \right) \right) \right] h_{cond,1} + \frac{1}{2} \frac{dh_{vap}}{dP_{cond}} \rho_{cond,1} - \left[ AL_{cond,1}\dot{P}_{cond} + \left[ \frac{1}{2} \left( \frac{\delta\rho_{cond,1}}{\delta h_{cond,1}} \Big|_{P_c} \right) h_{cond,1} + \frac{1}{2} \rho_{cond,1} \right] AL_{cond,1}\dot{h}_{cond} + (\rho_{cond,1}h_{cond,1} - \rho_{vap}h_{vap})A\dot{L}_{cond,1} = \dot{m}_{comp}h_{comp} - \dot{m}_{inte,cond12}h_{vap} + \right.$$

$$\alpha_{cond} A_{cond,1} \frac{L_{cond,1}}{L_{tot}} (T_{wall,cond1} - T_{ref,cond1}) \quad (6.72)$$

$$\begin{aligned} & (\rho_{vap} h_{vap} - \rho_{liq} h_{liq}) A \dot{L}_{cond,1} + (\rho_{vap} - \rho_{liq}) \gamma A \dot{L}_{cond,2} + \left( \frac{d(\rho_{liq} h_{liq})}{dP_{cond}} (1 - \gamma) + \right. \\ & \left. \frac{d(\rho_{vap} h_{vap})}{dP_{cond}} \gamma - 1 \right) A L_{cond,2} \dot{P}_{cond} = \dot{m}_{inte,cond12} h_{vap} - \dot{m}_{inte,cond12} h_{liq} + \\ & \alpha_{cond} A_{cond,2} \frac{L_{cond,2}}{L_{tot}} (T_{wall,cond2} - T_{ref,cond2}) \end{aligned} \quad (6.73)$$

$$\begin{aligned} & \left[ \frac{\delta \rho_{cond,3}}{\delta P_{cond}} \right]_{h_{cond,3}} + \frac{1}{2} \left( \frac{\delta \rho_{cond,3}}{\delta h_{cond,3}} \right)_{P_c} \left( \frac{dh_{liq}}{dP_{cond}} \right) h_{cond,3} + \frac{1}{2} \frac{dh_{liq}}{dP_{cond}} \rho_{cond,3} - \\ & 1 \left[ A L_{cond,3} \dot{P}_{cond} + \left[ \frac{1}{2} \left( \frac{\delta \rho_{cond,3}}{\delta h_{cond,3}} \right)_{P_c} \right] h_{cond,3} + \frac{1}{2} \rho_{cond,3} \right] A L_{cond,3} \dot{h}_{cond} + \\ & (\rho_{liq} h_{liq} - \rho_{cond,3} h_{cond,3}) A (\dot{L}_{cond,1} + \dot{L}_{cond,2}) = \dot{m}_{inte,cond23} h_{liq} - \\ & \dot{m}_{valv} h_{valv} + \alpha_{cond} A_{cond,3} \frac{L_{cond,3}}{L_{tot}} (T_{wall,cond3} - T_{ref,cond3}) \end{aligned} \quad (6.74)$$

Conservation of energy equations for the wall that contains with the each refrigerant phase are as follows,

$$\dot{m}_w C_{p,w} \dot{T}_{w,cond1} + \dot{m}_w C_{p,w} \left( \frac{T_{w,cond1} - T_{w,cond2}}{L_{cond1}} \right) = \alpha_{cond} A_{cond,1} (T_{ref,cond1} - T_{w,cond1}) + \alpha_{out} A_{out} (T_H - T_{w,cond1}) \quad (6.75)$$

$$\dot{m}_w C_{p,w} \dot{T}_{w,cond2} = \alpha_{cond} A_{cond,2} (T_{ref,cond2} - T_{w,cond2}) + \alpha_{out} A_{out} (T_H - T_{w,cond2}) \quad (6.76)$$

$$\begin{aligned} & \dot{m}_w C_{p,w} \dot{T}_{w,cond3} + \dot{m}_w C_{p,w} \left( \frac{T_{w,cond2} - T_{w,cond3}}{L_{cond3}} \right) (\dot{L}_{cond,1} + \dot{L}_{cond,2}) = \\ & \alpha_{cond} A_{cond,3} (T_{ref,cond3} - T_{w,cond3}) + \alpha_{out} A_{out} (T_H - T_{w,cond3}) \end{aligned} \quad (6.77)$$

Total exergy destruction of the condenser is calculated as,

$$\dot{X}_{dest,cond} = \dot{m}_{valv} (h_{cond} - T_H s_{cond,valv}) - \dot{m}_{comp} (h_{cond} - T_H s_{cond,comp}) + \dot{m}_{cond,sec} (h_{cond,sec} - T_H s_{cond,sec,valv}) \quad (6.78)$$

The above given equations can be grouped and solved as the following matrix equation form,

$$\begin{bmatrix} Z_{11} & 0 & Z_{13} & 0 & 0 & 0 & 0 \\ Z_{21} & Z_{22} & Z_{23} & Z_{24} & 0 & 0 & 0 \\ Z_{31} & Z_{32} & Z_{33} & Z_{34} & 0 & 0 & 0 \\ Z_{41} & Z_{42} & Z_{43} & Z_{44} & 0 & 0 & 0 \\ Z_{51} & 0 & 0 & 0 & Z_{55} & 0 & 0 \\ 0 & 0 & 0 & 0 & 0 & Z_{66} & 0 \\ Z_{71} & Z_{72} & 0 & 0 & 0 & 0 & Z_{77} \end{bmatrix} \begin{bmatrix} \dot{L}_{cond1} \\ \dot{L}_{cond2} \\ \dot{P}_{cond} \\ \dot{h}_{out} \\ \dot{T}_{wall,1} \\ \dot{T}_{wall,2} \\ \dot{T}_{wall,3} \end{bmatrix} =$$

$$\begin{bmatrix} \dot{m}_{in}(h_{in} - h_{val}) + q_{in1} \\ \dot{m}_{in}h_{val} - \dot{m}_{out}h_{liq} + q_{in2} \\ \dot{m}_{out}(h_{liq} - h_{out}) + q_{in3} \\ \dot{m}_{in} - \dot{m}_{out} \\ q_{out1} - q_{in1} \\ q_{out2} - q_{in2} \\ q_{out3} - q_{in3} \end{bmatrix}$$

(6.79)

The Z matrix elements are depicted in Figure 6.12 and Figure 6.13.

$z_{11}$	$\rho_1(h_1 - h_g)A_{cs}$
$z_{13}$	$\left[ \left( \left( \frac{\partial \rho_1}{\partial P_c} \right)_{h_1} \right) + \frac{1}{2} \left( \frac{\partial \rho_1}{\partial h_1} \right)_{P_c} \right] \left( \frac{dh_g}{dP_c} \right) (h_1 - h_g) + \frac{1}{2} \left( \frac{dh_g}{dP_c} \right) \rho_1 - 1 \right] A_{cs} L_1$
$z_{21}$	$(\rho_1 h_g - \rho_3 h_f) A_{cs}$
$z_{22}$	$[(\rho_g h_g - \rho_f h_f) \bar{\gamma} + (\rho_f - \rho_3) h_f] A_{cs}$
$z_{23}$	$\left[ \left( \left( \frac{\partial \rho_1}{\partial P_c} \right)_{h_1} \right) + \frac{1}{2} \left( \frac{\partial \rho_1}{\partial h_1} \right)_{P_c} \right] \left( \frac{dh_g}{dP_c} \right) h_g L_1 + \left( \frac{d(\rho_f h_f)}{dP} (1 - \bar{\gamma}) + \frac{d(\rho_g h_g)}{dP} (\bar{\gamma}) - 1 \right) L_2 + \left[ \left( \frac{\partial \rho_3}{\partial P_c} \right)_{h_3} \right] + \frac{1}{2} \left( \frac{\partial \rho_3}{\partial h_3} \right)_{P_c} \right] \left( \frac{dh_f}{dP_c} \right) h_f L_3 \right] A_{cs}$
$z_{24}$	$\frac{1}{2} \left( \frac{\partial \rho_3}{\partial h_3} \right)_{P_c} A_{cs} L_3 h_f$
$z_{31}$	$\rho_3(h_f - h_3)A_{cs}$
$z_{32}$	$\rho_3(h_f - h_3)A_{cs}$
$z_{33}$	$\left[ \left( \left( \frac{\partial \rho_3}{\partial P_c} \right)_{h_3} \right) + \frac{1}{2} \left( \frac{\partial \rho_3}{\partial h_3} \right)_{P_c} \right] \left( \frac{dh_f}{dP_c} \right) (h_3 - h_f) + \frac{1}{2} \left( \frac{dh_f}{dP_c} \right) \rho_3 - 1 \right] A_{cs} L_3$
$z_{34}$	$\left[ \frac{1}{2} \left( \frac{\partial \rho_3}{\partial h_3} \right)_{P_c} \right] (h_3 - h_f) + \frac{1}{2} \rho_3 \right] A_{cs} L_3$
$z_{41}$	$(\rho_1 - \rho_3)A_{cs}$
$z_{42}$	$[(\rho_g - \rho_f) \bar{\gamma} + (\rho_f - \rho_3)] A_{cs}$
$z_{43}$	$\left[ \left( \left( \frac{\partial \rho_1}{\partial P_c} \right)_{h_1} \right) + \frac{1}{2} \left( \frac{\partial \rho_1}{\partial h_1} \right)_{P_c} \right] \left( \frac{dh_g}{dP_c} \right) L_1 + \left( \frac{d\rho_f}{dP} (1 - \bar{\gamma}) + \frac{d\rho_g}{dP} \bar{\gamma} \right) L_2 + \left[ \left( \frac{\partial \rho_3}{\partial P_c} \right)_{h_3} \right] + \frac{1}{2} \left( \frac{\partial \rho_3}{\partial h_3} \right)_{P_c} \right] \left( \frac{dh_f}{dP_c} \right) L_3 \right] A_{cs}$

Figure 6.12. Z matrix elements (Rasmussen and Alleyne, 2006)

$z_{44}$	$\frac{1}{2} \left( \frac{\partial \rho_3}{\partial h_3} \Big _{P_e} \right) A_{cs} L_3$
$z_{51}$	$m_w C_{p,w} \left( \frac{T_{w1} - T_{w2}}{L_1} \right)$
$z_{55}$	$m_w C_{p,w}$
$z_{66}$	$m_w C_{p,w}$
$z_{71}$	$m_w C_{p,w} \left( \frac{T_{w2} - T_{w3}}{L_3} \right)$
$z_{72}$	$m_w C_{p,w} \left( \frac{T_{w2} - T_{w3}}{L_3} \right)$
$z_{77}$	$m_w C_{p,w}$

Figure 6.13. Z matrix elements (Rasmussen and Alleyne, 2006)

The evaporator has two refrigerant phases: two-phase and super-heated regions. The design properties of the evaporator are considered as follows, the tube length is 13 m, the outer and inner tube diameters are taken respectively as 18 mm and 12 mm and wall thickness of the tube is 2 mm. The wall of the evaporator is considered to be made of steel. The evaporation process is modeled with Gungor and Winterton (1986) correlation and the mean void fraction is modeled with Fauske (1964) correlation. The conservation of mass equations of the refrigerant are as follows,

$$(\rho_{liq} - \rho_{vap}) A \dot{L}_{evap1} (1 - \gamma) + \left( \frac{d\rho_{liq}}{dP_{evap}} (1 - \gamma) + \frac{d\rho_{vap}}{dP_{evap}} \gamma \right) A L_{evap1} \dot{P}_{evap} = \dot{m}_{valv} - \dot{m}_{inte, evap12} \quad (6.80)$$

$$\begin{aligned} & (\rho_{vap} - \rho_{evap,2}) A \dot{L}_{evap1} + \left[ \frac{\delta \rho_{evap2}}{\delta P_{evap}} \Big|_{h_{evap,2}} + \right. \\ & \left. \frac{1}{2} \left( \frac{\delta \rho_{evap2}}{\delta h_{evap}} \Big|_{P_{evap}} \left( \frac{dh_{vap}}{dP_{evap}} \right) \right) \right] A L_{evap2} \dot{P}_{evap} + \frac{1}{2} \left( \frac{\delta \rho_{evap2}}{\delta h_{evap2}} \Big|_{P_{evap}} \right) A L_2 \dot{h}_{evap} = \\ & \dot{m}_{inte, evap12} - \dot{m}_{comp} \end{aligned} \quad (6.81)$$

The conservation of energy equations of the each refrigerant phase in the evaporator are,

$$\begin{aligned} & (\rho_{liq} h_{liq} - \rho_{vap} h_{vap}) A \dot{L}_{evap1} (1 - \gamma) + \left( \frac{d(\rho_{liq} h_{liq})}{dP_{evap}} (1 - \gamma) + \frac{d(\rho_{vap} h_{vap})}{dP_{evap}} \gamma - \right. \\ & \left. 1 \right) A L_{evap2} \dot{P}_{evap2} = \dot{m}_{valv} h_{valv} - \dot{m}_{inte, evap12} h_{int, evap12} + \end{aligned}$$

$$\alpha_{evap} A_{evap2} \frac{L_{evap1}}{L_{tot}} (T_{wall,evap1} - T_{ref,evap1}) \quad (6.82)$$

$$\left[ \frac{\delta \rho_{evap2}}{\delta P_{evap}} \Big|_{h_{evap1}} + \frac{1}{2} \left( \frac{\delta \rho_{evap2}}{\delta h_{evap2}} \Big|_{P_{evap}} \left( \frac{dh_{vap}}{dP_{evap}} \right) \right) h_{evap2} + \frac{1}{2} \frac{dh_{vap}}{dP_{evap}} \rho_{evap2} - \right. \\ \left. 1 \right] AL_{evap2} \dot{P}_{evap} + \left[ \frac{1}{2} \left( \frac{\delta \rho_{evap2}}{\delta h_{evap2}} \Big|_{P_{evap}} \right) h_{evap2} + \frac{1}{2} \rho_{evap2} \right] AL_{evap2} \dot{h}_{evap} + \\ (\rho_{vap} h_{vap} - \rho_{evap2} h_{evap2}) AL_{evap1} = \dot{m}_{int,evap12} h_{int,evap12} - \\ \dot{m}_{comp} h_{comp} + \alpha_{evap} A_{evap2} \frac{L_{evap2}}{L_{tot}} (T_{wall,evap2} - T_{ref,evap2}) \quad (6.83)$$

The conversation of the tube wall energy formulas are,

$$\dot{m}_w C_{p,w} \dot{T}_{w,evap1} = \alpha_{evap} A_{evap1} (T_{ref,evap1} - T_{w,evap1}) + \alpha_{out} A_{out} (T_L - T_{w,evap1}) \quad (6.84)$$

$$\dot{m}_w C_{p,w} \dot{T}_{w,evap2} - \dot{m}_w C_{p,w} \dot{L}_{evap1} \left( \frac{T_{w,evap2} - T_{w,evap1}}{L_{evap2}} \right) = \\ \alpha_{evap} A_{evap2} (T_{ref,evap2} - T_{w,evap2}) + \alpha_{out} A_{out} (T_L - T_{w,evap2}) \quad (6.85)$$

The rate of exergy destruction in the evaporator is calculated as,

$$\dot{X}_{dest,evap} = \dot{m}_{comp} (h_{evap} - T_H S_{evap,comp}) - \dot{m}_{comp} (h_{evap} - T_H S_{evap,valv}) + \\ \dot{m}_{evap,sec} (h_{evap,sec} - T_H S_{evap,sec,comp}) \quad (6.86)$$

The above given equations can be grouped into the matrix form as follows,

$$\begin{bmatrix} Z_{11} & 0 & Z_{13} & 0 & 0 & 0 & 0 \\ Z_{21} & Z_{22} & Z_{23} & Z_{24} & 0 & 0 & 0 \\ Z_{31} & Z_{32} & Z_{33} & Z_{34} & 0 & 0 & 0 \\ Z_{41} & Z_{42} & Z_{43} & Z_{44} & 0 & 0 & 0 \\ Z_{51} & 0 & 0 & 0 & Z_{55} & 0 & 0 \end{bmatrix} \begin{bmatrix} \dot{L}_{evap1} \\ \dot{P}_{evap} \\ \dot{h}_{out} \\ \dot{T}_{wall,1} \\ \dot{T}_{wall,2} \end{bmatrix} = \begin{bmatrix} \dot{m}_{in} (h_{in} - h_{val}) + q_{in1} \\ \dot{m}_{out} (h_{liq} - h_{out}) + q_{in3} \\ \dot{m}_{in} - \dot{m}_{out} \\ q_{out1} - q_{in1} \\ q_{out2} - q_{in2} \end{bmatrix} \quad (6.87)$$

The elements of the matrix  $Z$  are given in Figure 6.14. The cycle cooling load is determined as,

$$\dot{Q}_{cool} = \dot{m}_{comp} h_{evap,comp} - \dot{m}_{valv} h_{evap,valv} \quad (6.88)$$

The total exergy destruction rate of the cycle is calculated as follows,

$$\dot{X}_{dest,total} = \dot{X}_{dest,comp} + \dot{X}_{dest,valv} + \dot{X}_{dest,evap} + \dot{X}_{dest,cond} \quad (6.89)$$

$z_{11}$	$[\rho_f(h_f - h_g)](1 - \bar{\gamma})A_{cs}$
$z_{12}$	$\left[ \left( \frac{d(\rho_f h_f)}{dP_e} - \frac{d\rho_f}{dP_e} h_g \right) (1 - \bar{\gamma}) + \left( \frac{d(\rho_g h_g)}{dP_e} - \frac{d\rho_g}{dP_e} h_g \right) (\bar{\gamma}) - 1 \right] A_{cs} L_1$
$z_{21}$	$\rho_2(h_g - h_2)A_{cs}$
$z_{22}$	$\left[ \left( \left( \frac{\partial \rho_2}{\partial P_e} \right)_{h_2} \right) + \left( \frac{1}{2} \right) \left( \frac{\partial \rho_2}{\partial h_2} \right)_{P_e} \left( \frac{dh_g}{dP_e} \right) \right] (h_2 - h_g) + \left( \frac{\rho_2}{2} \right) \left( \frac{dh_g}{dP_e} \right) - 1 \right] A_{cs} L_2$
$z_{23}$	$\left[ \left( \frac{1}{2} \right) \left( \frac{\partial \rho_2}{\partial h_2} \right)_{P_e} \right] (h_2 - h_g) + \left( \frac{\rho_2}{2} \right) \right] A_{cs} L_2$
$z_{31}$	$[(\rho_g - \rho_2) + (\rho_f - \rho_g)(1 - \bar{\gamma})]A_{cs}$
$z_{32}$	$\left[ \left[ \left( \frac{\partial \rho_2}{\partial P_e} \right)_{h_2} \right] + \frac{1}{2} \left( \frac{\partial \rho_2}{\partial h_2} \right)_{P_e} \right] \left( \frac{dh_g}{dP_e} \right) \right] L_2 + \left[ \left( \frac{d\rho_f}{dP_e} \right) (1 - \bar{\gamma}) + \left( \frac{d\rho_g}{dP_e} \right) (\bar{\gamma}) \right] L_1 \right] A_{cs}$
$z_{33}$	$\frac{1}{2} \left( \frac{\partial \rho_2}{\partial h_2} \right)_{P_e} \right] A_{cs} L_2$
$z_{44}$	$(C_p \rho V)_w$
$z_{51}$	$(C_p \rho V)_w \left( \frac{T_{w1} - T_{w2}}{L_2} \right)$
$z_{55}$	$(C_p \rho V)_w$

Figure 6.14. Z matrix elements (Rasmussen and Alleyne, 2006)

The COP and second law efficiency of the cycle are calculated as,

$$COP = \frac{\dot{Q}_{cool}}{\dot{W}_{comp}} \quad (6.90)$$

$$\eta_{II} = 1 - \frac{\dot{X}_{dest,total}}{\dot{W}_{comp}} \quad (6.91)$$

Aspen software (Aspen, 2013) is utilized for the verification of the cycle model described above. The time-varying data of the state variables with respect to the randomly-generated inputs are compared with that of the Aspen Plus Dynamics. Aspen Plus is a market-leading software package utilized in the industry and chemical plants that model the thermodynamic processes. Same as the MB model, R134a is used for the primary fluid and water is utilized as the secondary fluid. The desing properties of the components that are used in the VCC for the model verification is as follows, the condenser tube length is 15 m, the outer and inner tube diameters are taken respectively as 18 mm and 12 mm and wall thickness of the tube is 2 mm. The evaporator tube length is 9 m, the outer and inner tube diameters are taken respectively as 18 mm and 12 mm and wall thickness of the tube is 2 mm. Both of the heat exchangers are considered to be made of steel. And the high-temperature and low-

temperature reservoirs are respectively taken as 27°C and 7°C. Both the MB model system and Aspen system are perturbed with randomly-generated signals over a period of time. The MB system is simulated in the Python environment. Randomly-generated perturbation signals are shown in Figure 6.15. And the comparison of the three selected state variables as a result of the perturbation signals are given in Figure 6.16. The selected state variables are the evaporator pressure, evaporator outlet enthalpy and compressor outlet entropy. Figure 6.16 shows that the results are fairly similar. The highest variance between the two models occur in the evaporator pressure by 1.7%.

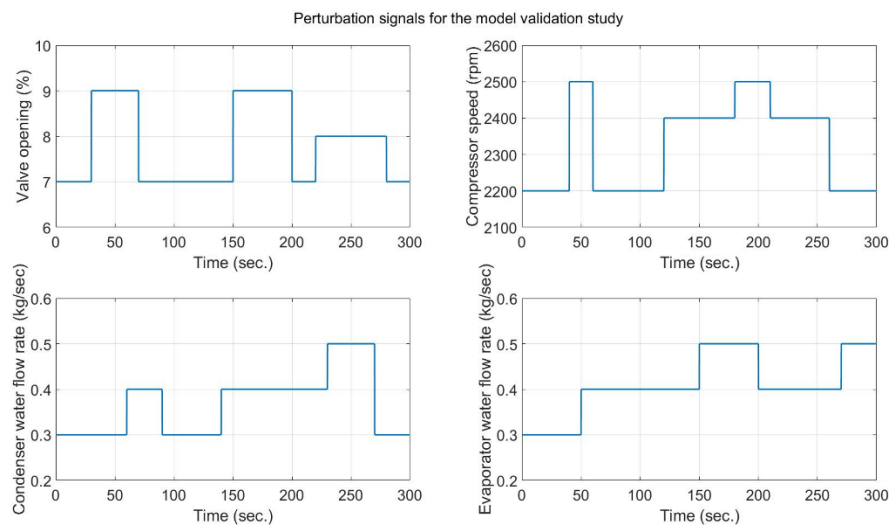


Figure 6.15. Perturbation signals to the systems

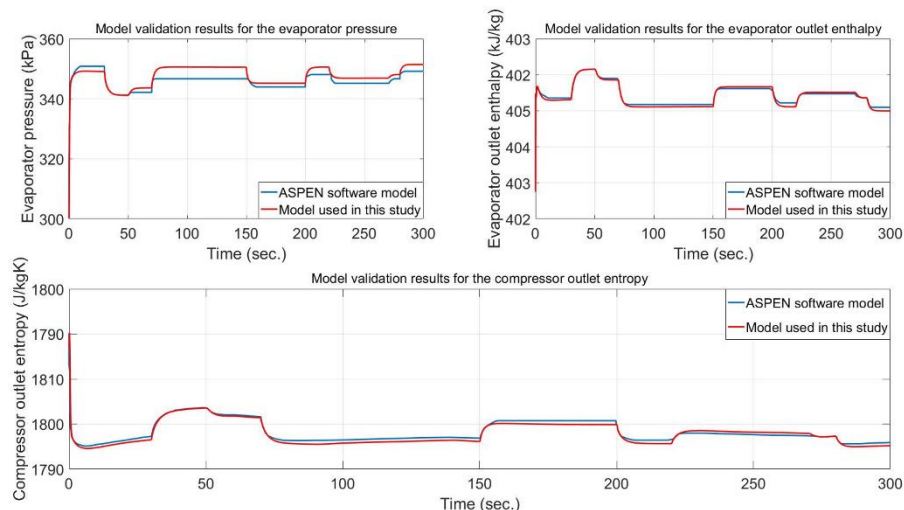


Figure 6.16. Model verification results of the state variables

A Model Predictive Controller (MPC) type of controller is utilized to control the system. As described and discussed in Chapter 5, MPC is a class of optimization-based control

algorithms that are widely used in the industry, especially in the chemical processes. MPC algorithms are applicable to both linear and non-linear systems. It has been realized that if the MPC algorithm is applied to a non-linear system, the performance and accuracy of the controller is improved compared to that of linear systems. Selection of the model type is a crucial part of the MPC algorithm. As discussed in Chapter 5, different kind of models can be utilized as the model in the MPC algorithm. The artificial neural network is used as the model in this case study. The neural networks has some advantages compared to other non-linear models. Some of the advantages of the neural networks are: they have less parameters to be tuned compared to the other models, they form a direct relationship between the inputs and outputs, they are universal approximators. The Neural Network Predictive Controller (NNPC) is utilized in many works in the literature and performed well in all control scenarios.

The neural network model is utilized for the prediction of the future states in the NNPC. An objective function is formed and solved with an optimization algorithm for the each time step to determine the future control signals. The future control signals optimally satisfy the performance criterion while ensuring the trajectory tracking of the system. The objective function can be formulated as follows,

$$J(\mathbf{k}) = \sum_{\mathbf{a}=N_{minimum}}^{N_{maximum}} [\tau \mathbf{y}_{ref}(\mathbf{k} + \mathbf{a}) - \mathbf{y}(\mathbf{k} + \mathbf{a})]^2 + \varphi \sum_{\mathbf{a}=1}^{N_u} [\Delta \mathbf{u}(\mathbf{k} + \mathbf{a} - 1)]^2 \quad (6.92)$$

The objective function given above is subject to following constraints,

$$\mathbf{u}_{minimum} \leq \mathbf{u} \leq \mathbf{u}_{maximum} \quad (6.93)$$

$$\Delta \mathbf{u}_{minimum} \leq \Delta \mathbf{u} \leq \Delta \mathbf{u}_{maximum} \quad (6.94)$$

$$\mathbf{y}_{minimum} \leq \mathbf{y} \leq \mathbf{y}_{maximum} \quad (6.95)$$

$$\Delta \mathbf{y}_{minimum} \leq \Delta \mathbf{y} \leq \Delta \mathbf{y}_{maximum} \quad (6.96)$$

There are four different controllers that are considered for the testing of the overall controller performance. They are the cooling load case, first law efficiency, entropy generation and second law efficiency controllers. The objective of the cooling load controller is to only track the desired cooling load trajectory which also is used as the main benchmark controller. The other three controllers have specific objectives other than the common main objective which is the cooling load trajectory tracking. All of the controllers have been named after their specific performance objectives. For example, the objective of the first law efficiency controller is to optimize the work consumption of the controller, thus maximizing the COP of the cycle while ensuring the stable cooling load trajectory tracking of the cycle. The four controllers can be formalized as follows,

$$J_{VCC,co} = \|\dot{Q}_{des} - \dot{Q}_{achi}\|_2 \quad (6.97)$$

$$J_{VCC,fl} = \|\dot{Q}_{des} - \dot{Q}_{achi}\|_2 + \varphi \sum_{a=1}^{N_{pred}} W_{comp}(a) \quad (6.98)$$

$$J_{VCC,eg} = \|\dot{Q}_{des} - \dot{Q}_{achi}\|_2 + \varphi \sum_{a=1}^{N_{pred}} \dot{S}_{comp}(a) \quad (6.99)$$

$$J_{VCC,sf} = \|\dot{Q}_{des} - \dot{Q}_{achi}\|_2 - \varphi \sum_{a=1}^{N_{pred}} \eta_{II}(a) \quad (6.100)$$

The Whale Optimization Algorithm (WOA) is utilized for the solution of the objective function of the MPC controller at the each time step. The WOA is described in detail in Chapter 3. The WOA is a swarm-based nature-inspired metaheuristic algorithm that mimics the hunting behavior of the humpback whales in the nature. The algorithm has favorable exploratory and exploitation characteristics and can search large search spaces effectively. The algorithm mainly consists of three phases: encircling prey, bubble-net attacking method and searching for new prey. Encircling the prey represents the exploration phase of the algorithm, bubble-net attacking method represents the exploitation phase of the algorithm and the searching for new preys represents the looking for new possible solution behavior of the algorithm.

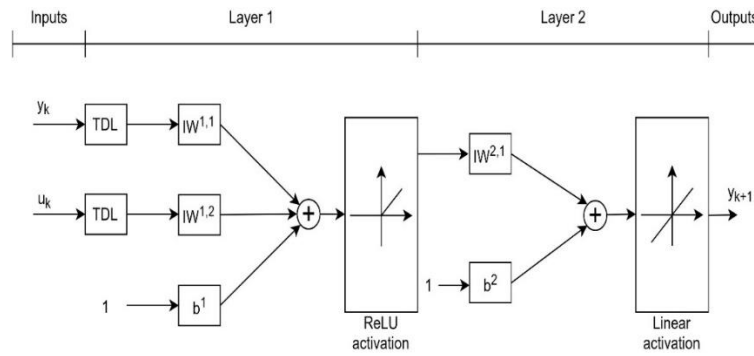


Figure 6.17. Main structure of the Artificial Neural Network used as the model

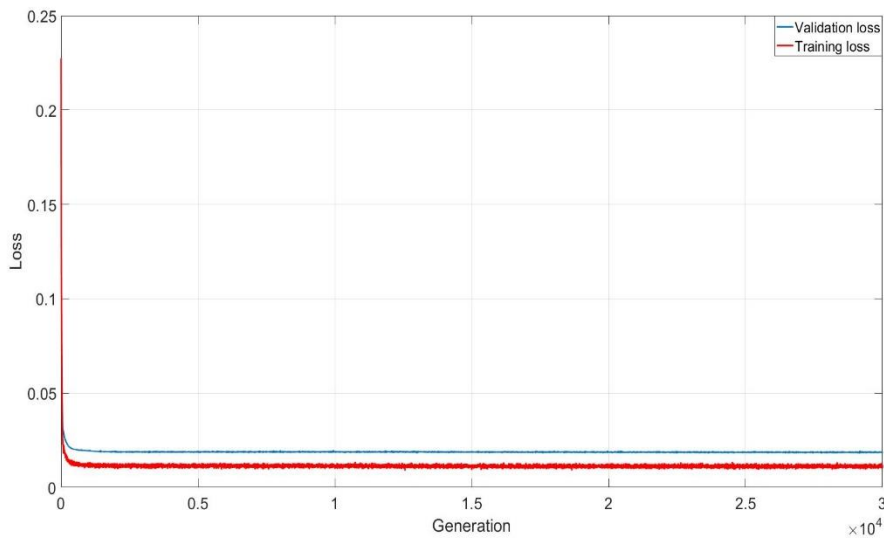


Figure 6.18. The training and validation losses of the ANN

Main structure of the ANN used in this study is given in Figure 6.17. *TDL* means the tapped delay line which stores the previous and current time information of the ANN inputs,  $IW^{l,1}$  is the matrix of weights that connects the input state variable neurons to the hidden layer neurons,  $IW^{l,2}$  is the matrix of weights that connects the input signal neurons to the hidden layer neurons,  $IW^{2,1}$  is the matrix of weights that connects the hidden layer neurons to the output layer neurons,  $b^1$  is the hidden layer biases vector and  $b^2$  is the output layer biases vector. There is one time delay at the input neurons and the overall ANN consists of three layers, which are the input, hidden and output layers. The ANN has 30 neurons in the hidden layer, all of them have ReLU (Nair and Hinton, 2010) activation function and 9 neurons in the output layer, all of them have the linear activation function. The ANN is trained with Tensorflow library (Abadi et al., 2015) in an off-line manner with the ADAM (Kingma and Ba, 2015) optimization algorithm. The learning rate of the optimization is heuristically selected as 0.001. 9000 samples have been collected from the dynamic VCC model with 0.1 second time intervals and 70% of the samples are utilized as in the training of the ANN and remaining 30% of the samples are utilized in the validation of the ANN. The batch size of the training samples are selected to be 256. The ANN is trained with nine state variables and four inputs. The state variables are the condenser and evaporator outlet enthalpy and entropy, compressor and EEV mass flow rate, compressor outlet enthalpy, compressor outlet entropy and EEV outlet entropy. The four inputs are evaporator and condenser secondary fluid mass flow rates, compressor motor speed and EEV opening rate. The ANN training and validation errors are depicted in Figure 6.18. At the end of this phase, the normalized training loss is found to be 0.012 and the normalized validation loss is found to be 0.014. Both values are assumed as acceptable. Moreover, validation of the three selected state variables, condenser outlet enthalpy, evaporator outlet enthalpy and compressor outlet enthalpy are depicted in Figure 6.19, Figure 6.20 and Figure 6.21, respectively. The highest absolute error is observed as 0.2 for the three cases. This error value is assumed to be acceptable and it has been concluded that the ANN fitted well.

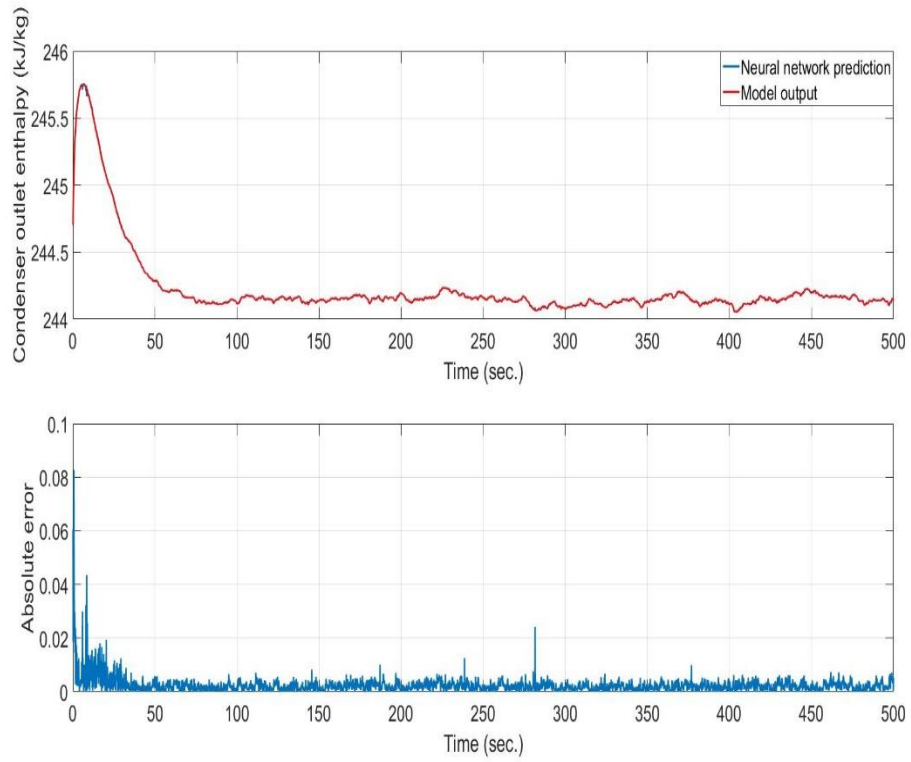


Figure 6.19. Condenser outlet enthalpy state variable validation

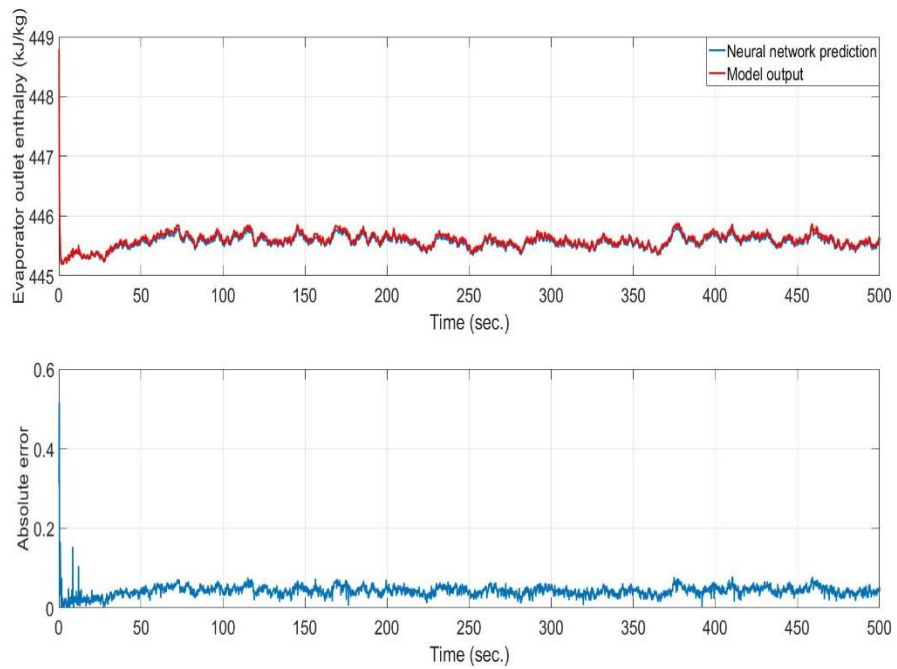


Figure 6.20. Evaporator outlet enthalpy state variable validation

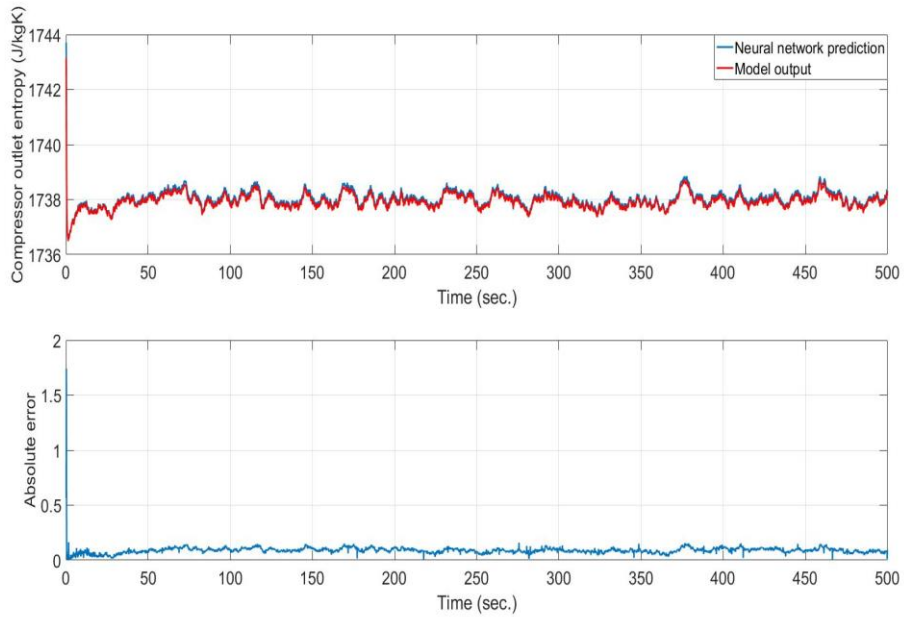


Figure 6.21. Compressor outlet entropy state variable validation

The NNPC controller has been programmed and the simulation has been accomplished in the Java programming environment. The control horizon and the prediction horizon of the controller are respectively selected as 15 and 5. The number of iterations and the population size of the WOA algorithm are respectively selected as 1000 and 40. The objective weights in the NNPC algorithm are chosen as 0,  $4 \times 10^{-3}$ , 10 and 10 for the controllers cooling load, first law efficiency, entropy generation and second law efficiency, respectively. The boundaries of the control input signals are depicted in Table 6.1. The slew rate limits of the control signals are depicted in Table 6.2. And the desired cooling load trajectory is shown in Figure 6.22.

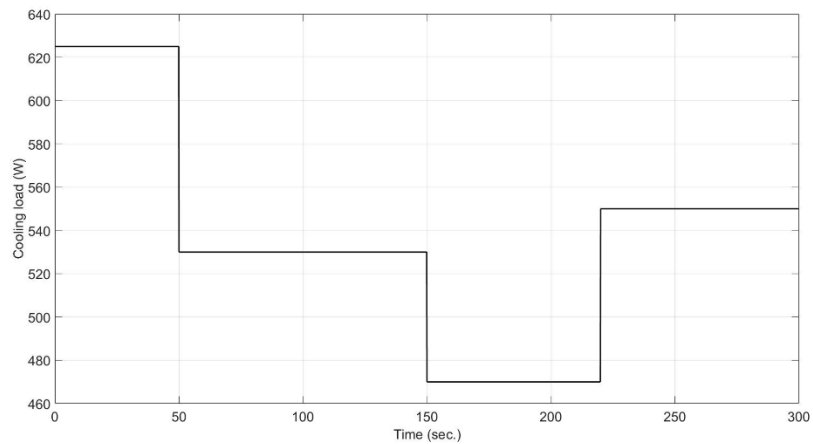


Figure 6.22. Desired cooling load trajectory

Table 6.1. Control signal boundaries

Input limits	Minimum Value	Maximum Value
EEV opening (%)	7	9.5
Compressor speed (RPM)	2000	2900
Condenser secondary fluid mass flow rate (kg/sec)	0.1	0.5
Evaporator secondary fluid mass flow rate (kg/sec)	0.1	0.5

Table 6.2. Slew rate limits of the control signals

Slew rate limits	Minimum and Maximum limits in a time step
EEV opening (%)	±0.05
Compressor speed (RPM)	±10
Condenser secondary fluid mass flow rate (kg/sec)	±0.01
Evaporator secondary fluid mass flow rate (kg/sec)	±0.01

The Gouy-Stodola theorem is a phenomenon that is worthwhile to be analyzed in this case study. The theorem states that there is no difference between the minimizing the compressor power consumption and minimizing the cycle entropy generation if the reversible power consumption remains unchanged. In most cases the theorem holds valid, however in some cases it does not. It will be shown in this case study that it does not hold valid for this case. The theorem can be mathematically represented as follows,

$$\dot{W}_{reversible} = \dot{W}_{comp} - \dot{X}_{dest,total} \quad (6.101)$$

$$\dot{W}_{reversible} = \sum_{i=1}^{N_{maximum}} (\dot{m}_{comp} h_{evap,comp} - \dot{m}_{valv} h_{evap,valv}) - \sum_{i=1}^{N_{maximum}} \dot{X}_{dest,total} \quad (6.102)$$

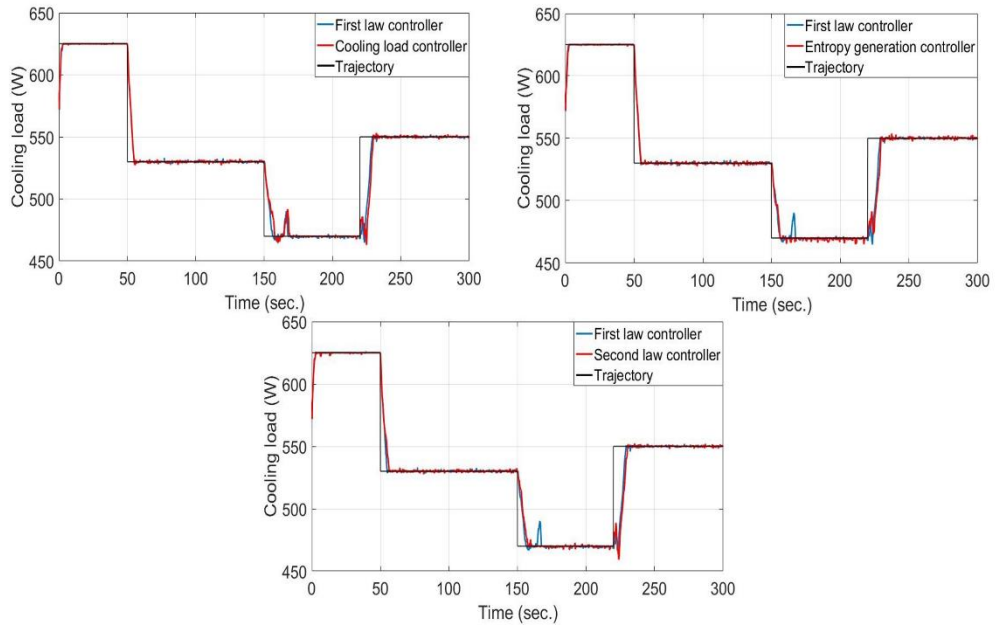


Figure 6.23. Pairwise trajectory tracking performance comparison of the controllers

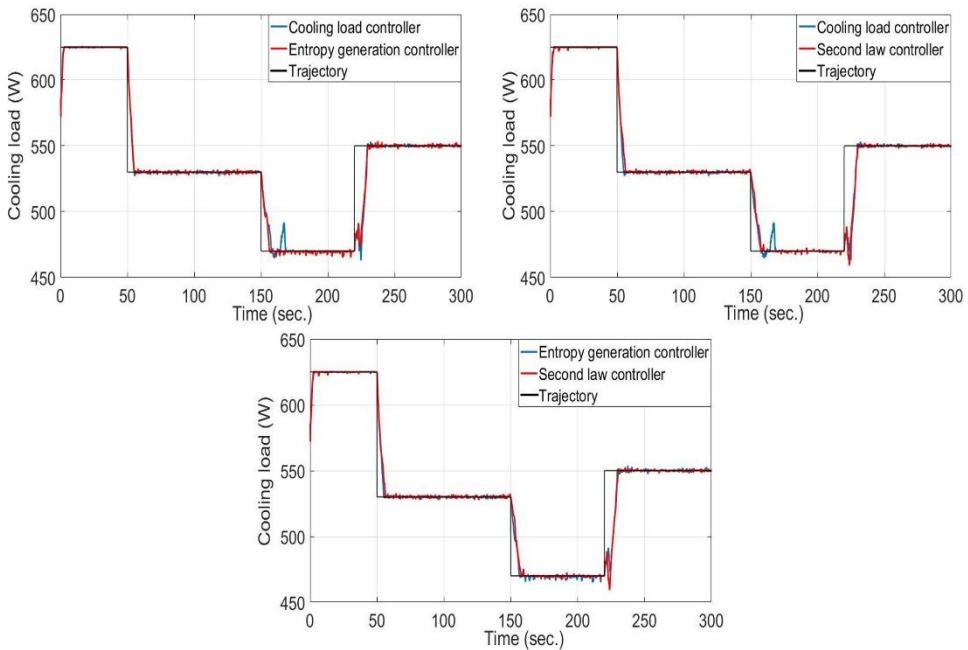


Figure 6.24. Pairwise trajectory tracking performance comparison of the controllers

Comparison of the trajectory tracking performances of the controllers are depicted in Figure 6.23 and Figure 6.24. It can be seen from the figures that most significant differences occur around 470 W stabilization point. The overshoots that occur at the beginning and end of the 470 W stabilization point have a major impact at the controller performances. The variation of the control signals over the simulation time are given in Figure 6.25 and Figure 6.26. It can be seen from the figures that the signals follow a similar trajectory to that of the cooling load and each combination of control signals produce a similar cooling load value. Moreover,

trajectory of the control signals for the each controller is unique, this phenomenon is thought to be a major cause of performance differences between the controllers.

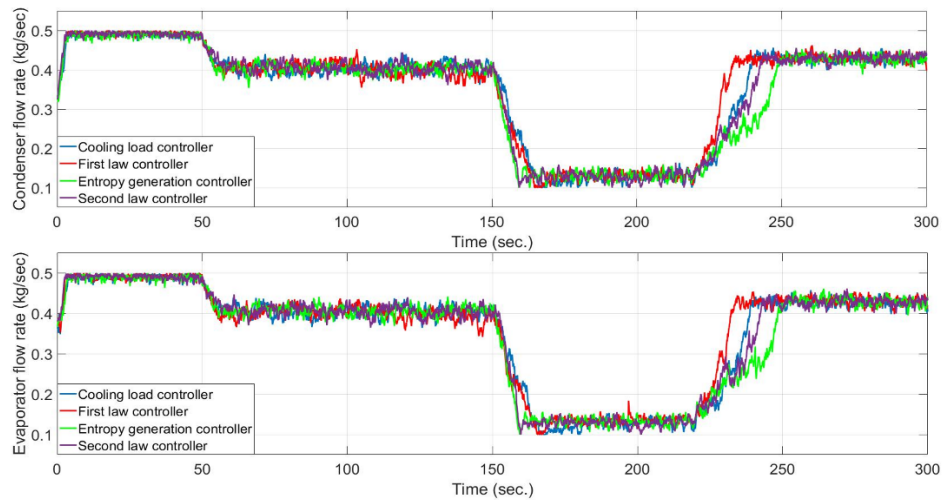


Figure 6.25. Variations of the control signals for the each controller

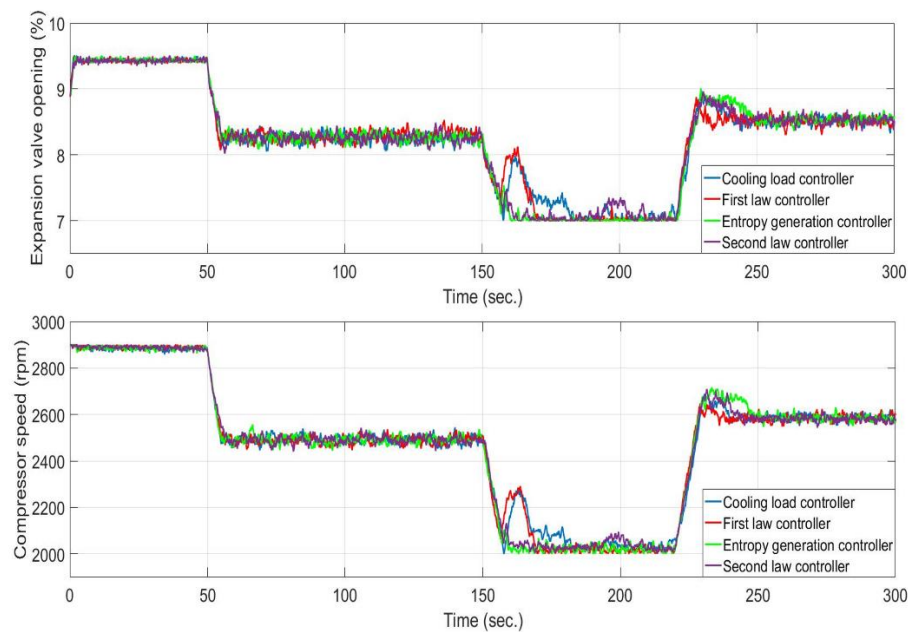


Figure 6.26. Variations of the control signals for the each controller

The exergy destruction rates of the each component of the VCC is given in Figure 6.27 and Figure 6.28. As some papers in the literature suggests, the compressor is found to be the component with the highest exergy destruction rate. However, if the working bounds of the VCC is modified the exergy destruction rates of the other components can approach to that of the compressor. Most VCC in the real world employs a pump to circuit the fluids in the cycle. However, in this case study, exergy destruction rate of the pump is neglected due to having much lower exergy destruction rate than that of the other major components. Furthermore, the

overshoot that occurs at the beginning of the 470 W stabilization point have much larger impact on the evaporator and condenser exergy destruction rates.

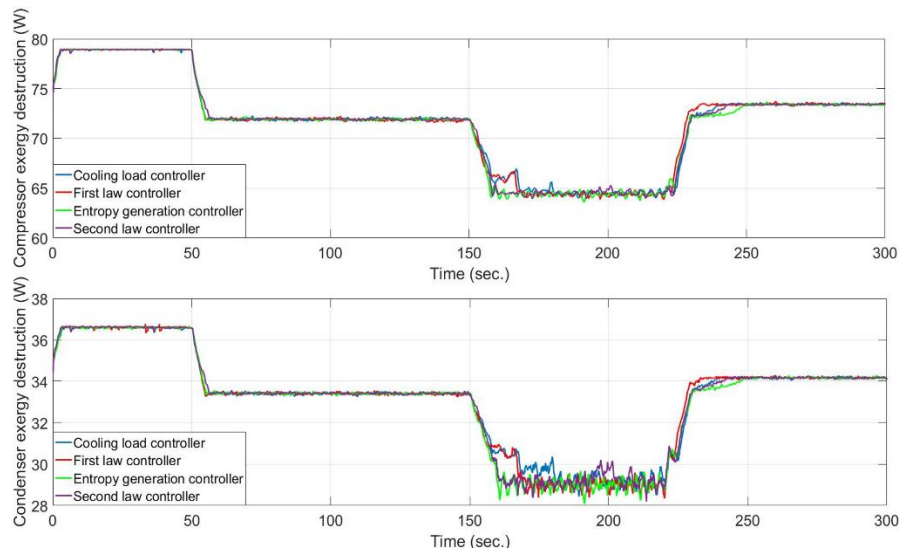


Figure 6.27. The exergy destruction rates of the components

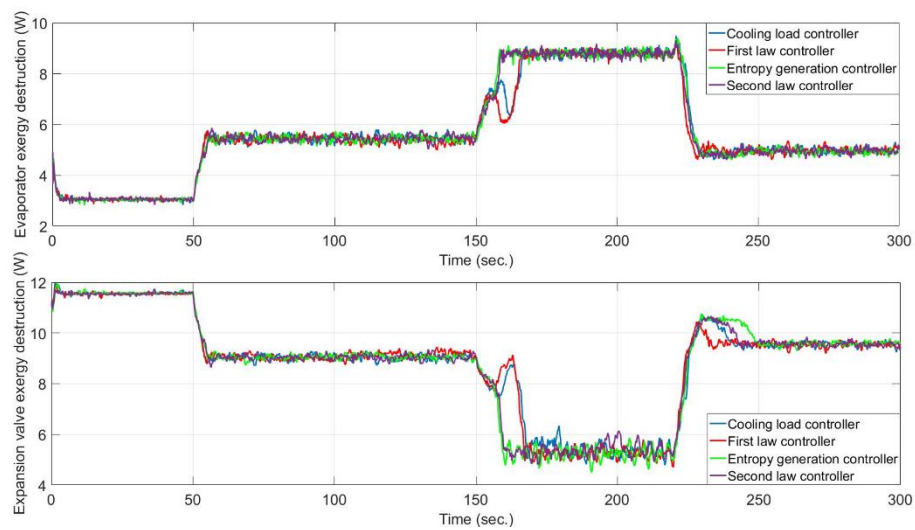


Figure 6.28. The exergy destruction rates of the components

The compressor power consumption variation through the simulation time is given in Figure 6.27. By observing Figure 6.27, Figure 6.28 and Figure 6.29, it can be realized that the reversible compressor power consumption does not stay constant. Therefore, the Gouy-Stodola theorem does not hold for this case study. Total exergy destruction rates of the each component for the each controller are given in Table 6.3. The entropy generation controller achieved the lowest exergy destruction rates of the component except the evaporator. The second law efficiency controller is the second best in terms of the total exergy destruction rate after the entropy generation controller. The first law efficiency controller gives more desirable compressor power consumption value than that of the cooling load controller, which is

expected. The exergy destruction rate of the EEV for the entropy generation controller is 0.8% lower than that of the cooling load controller. Furthermore, the exergy destruction rates of the compressor and condenser for the entropy generation controller are respectively 0.2% and 0.4% than that of the cooling load controller.

Table 6.3. Exergy destruction rates of the each component for the each controller

Exergy destruction rate by component (kJ)	Cooling load controller	First law controller	Entropy generation controller	Second law controller
EEV	26.695	26.647	26.506	26.526
Compressor	215.236	215.227	214.832	215.049
Condenser	99.603	99.524	99.261	99.463
Evaporator	16.991	16.870	17.048	17.051

Total exergy destruction and energy consumption rates for the controllers are given in Table 6.4. The best performer in the total exergy destruction rate category is the entropy generation controller with 357.649 W total exergy destruction. The second best in the same category is the second law efficiency controller with 358.090 W total exergy destruction. The entropy generation minimization controller concentrates on minimizing the total entropy generation and exergy destruction. However, the second law efficiency controller tries to find a compromise between the work consumption and the exergy destruction. For this reason, the entropy generation controller gives better results than the second law efficiency controller in terms of total exergy destruction. Also, for the bot total exergy destruction and energy consumption cases the cooling load controller is the worst performer as expected. The COP and second law variations of the cycle for the each controller are depicted in 6.30. Avarage COP values through time simulation time for the controllers, cooling load, first law, entropy generation and second law are calculated as 2.96143, 2.96405, 2.97108 and 2.96642, respectively. And the avarage second law efficiency values through time simulation time for the controllers, cooling load, first law, entropy generation and second law are calculated as 0.33976, 033962, 0.33983 and 0.34025, respectively. The second law efficiency controller performed the best in terms of avarage second law efficiency through the time as expected.

Table 6.4. Total energy consumption and exergy destruction rates for the controllers

	Cooling load controller	First law controller	Entropy generation controller	Second law controller
Total exergy destroyed (kJ)	358.526	358.269	357.649	358.090
Total energy consumed (kJ)	542.815	542.331	540.810	541.847

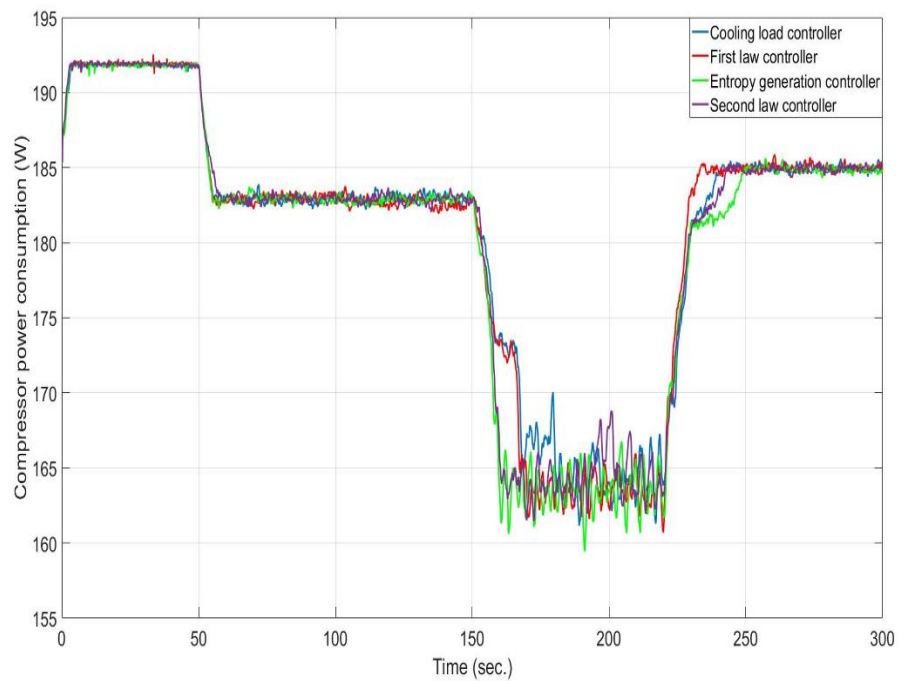


Figure 6.29. The compressor power consumption for the each controller

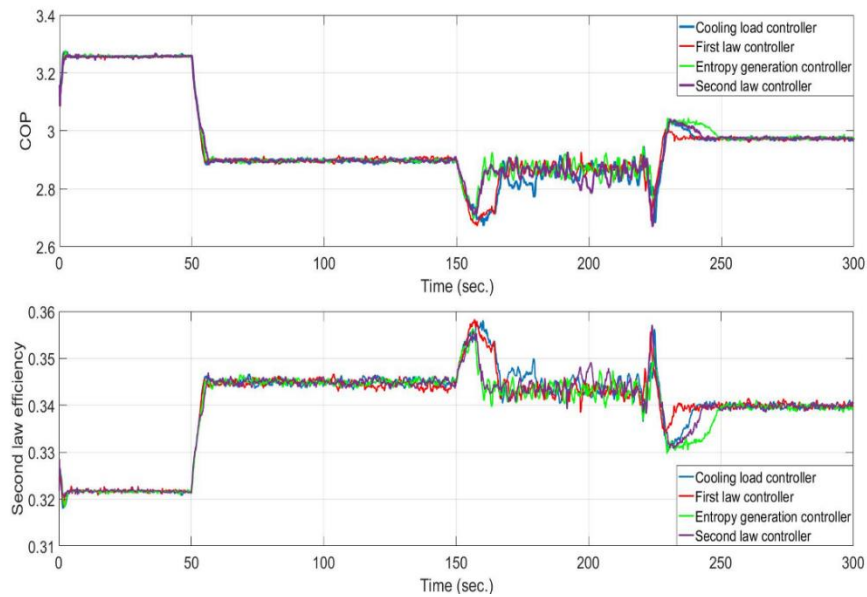


Figure 6.30. The COP and second law efficiency variations for the each controller

## 7. CONCLUSION

The HVAC systems is the primary energy consumption source of the countries nowadays. US Department of Energy found out that HVAC systems are responsible for 30% of the energy consumption of a building. Different approaches have been suggested by the researchers to reduce this large energy consumption. Dynamic analysis, design optimization and control are the main approaches that have been offered by the researchers to efficiently reduce the large energy consumption of the HVAC systems.

Dynamic analysis of a vapor compression cycle is studied as the first part of the thesis. The cycle is analyzed with two different refrigerants, namely R134a and R1234yf. R134a is a widely-used refrigerant in the HVAC systems, however it has high Global Warming Potential (GWP) and Ozone Depletion Potential (ODP) values. Recently, R1234yf has been suggested by the researchers as an alternative to the R134a. R1234yf has low GWP and ODP values. Finite Difference Method has been utilized for the modeling of the evaporator and condenser. Orifice equation is utilized for the modeling of the expansion valve. Modeling of the compressor has been accomplished in two parts. First, the refrigerant leaving the evaporator enters the compressor and interacts with the shell and other parts of the compressor. Thus heat exchange occurs between the refrigerant and parts of the compressor. Thereafter, the

refrigerant reaches the compression room and isentropic compression occurs. The results showed that R134a performs better than R1234yf in terms of the required compression power and overall cycle COP. Also, it has been observed that, after some time has been elapsed, the condenser and the evaporator output temperatures heats up and cools down, respectively and gets into the saturation curve and the COP of the cycle quickly drops to zero. Therefore, the cycle stops working.

Control of the HVAC systems is a more recent field for the energy efficiency of the HVAC systems. More and more research papers about the control of the HVAC systems are finding their place in the literature day by day. The control study of a vapor compression has been demonstrated in the sixth chapter of the thesis. Non-linear dynamic modeling of the vapor compression cycle (VCC) has been modeled as follows, the electronic expansion valve and the compressor is modeled with the static relationships because they have much faster evolving dynamics compared to that of the heat exchangers. The evaporator and condenser has been modeled with the lumped parameter Moving Boundary (MB) approach. The MB approach has some advantages and disadvantages compared to other modeling approaches in the literature. The MB approach requires less computational power, however, the results it has found may not be very accurate. The non-linear systems also have some advantages compared to their linear counterparts. Linearization process may eliminate some complex behaviors of the non-linear systems. The non-linearity of a system model is most of the time desired since almost all systems in the real world display non-linear behavior. The model verification of the system is accomplished with comparing the established model with a model developed in Aspen Plus Dynamics software with the same design specifications. Thereafter, an artificial neural network is trained with the data obtained from the model. The outcomes of the model and the artificial neural network has been compared with each other and the highest absolute error between the outcomes is observed as 0.2. It has been concluded that 0.2 is an acceptable error value and the neural network is fitted well.

A Neural Network Predictive Controller (NNPC) has been developed for the control of the VCC. The Whale Optimization Algorithm (WOA) is utilized for the solution of the objective function to determine the next control signal for the each time step in the NNPC. The WOA is a swarm-based nature-inspired metaheuristic algorithm that mimics the hunting behavior of the humpback whales in the nature. The WOA has favorable exploration and exploitation characteristics and can discover large search-spaces effectively. Four different controllers have been considered for this case study. The name of the controllers are the cooling load, first law efficiency, entropy generation and second law efficiency. Each controller take its name from the unique performance objective that it has to achieve except the

cooling load controller which has only the common objective of the all four controllers, cooling load trajectory tracking. The results showed that the second law efficiency performed the best overall second law efficiency through the simulation time with 0.34025 efficiency value. And the entropy generation controller achieved the lowest total exergy destruction rate through the time with 0.2% lower than that of the cooling load controller.

The case studies analyzed in this thesis are theoretical studies. As a future work, controlling and dynamically analyzing an experimental VCC systems is expected. Furthermore, different types of non-linear control algorithms are expected to be applied to the VCC systems.

## LIST OF REFERENCES

- Abadi, M., Agarwal, A., Barham, P., Brevdo, E., Chen, Z., Citro, C., Corrado, G.S., Davis, A., Dean, J., Devin, M., Ghemawat, S., Goodfellow, I., Harp, A., Irving, G., Isard, M., Jozefowicz, R., Jia, Y., Kaiser, L., Kudlur, M., Levenberg, J., Mane, D., Schuster, M., Monga, R., Moore, S., Murray, D., Olah, C., Shlens, J., Steiner, B., Sutskever, I., Talwar, K., Tucker, P., Vanhoucke, V., Vasudevan, V., Viegas, F., Vinyals, O., Warden, P., Wattenberg, P., Wicke, M., Yu, Y. and Zheng, X., 2015,** Tensorflow: Large-scale machine learning on heterogeneous systems, Software available from tensorflow.org.
- Afram, A. and Janabi-Sharifi, F., 2014,** Theory and applications of HVAC control systems- A review of model predictive control (MPC), *Building and Environment*, 72:343-355p.
- Aggarwal, C.C., 2018,** *Neural Networks and Deep Learning*, 1<sup>st</sup> edition, Springer, New Jersey, USA.
- Ahamed, J.U., Saidur, R. and Masjuki, H.H., 2010,** Thermodynamic performance analysis of R-600 and R-600a as refrigerant, *Energy e-Transactions*, 5:11-18p.
- Allgöwer, F. and Zheng, A., 2000,** *Nonlinear Model Predictive Control*, 1<sup>st</sup> edition, Springer, Berlin, Germany.

- Arora, A. and Kaushik, S.C.**, 2008, Theoretical analysis of a vapour compression refrigeration system with R502, R404A and R507A, *International Journal of Refrigeration*, 31:998-1005p.
- Aspen Plus**, 2013, Aspen Technology, USA.
- Bayrakci, H.C. and Ozgur, A.E.**, 2009, Energy and exergy analysis of vapor compression refrigeration system using hydrocarbon refrigerants, *International Journal of Energy Research*, 33:1070-1075p.
- Bell, I.H., Wronski, J., Quoilin, S. and Lemort, V.**, 2014, Pure and Pseudo-pure Fluid Thermophysical Property Evaluation and the Open-Source Thermophysical Property Library CoolProp, *Industrial & Engineering Chemistry Research*, 2498-2508p.
- Bendapudi, S. and Braun, J.E.**, 2002, A review of Literature on Dynamic Models of Vapor Compression Equipment, ASHRAE Report #4036-5.
- Bonne, U., Patani, A., Jacobson, R. and Muller, D.**, 1980, Electric-driven heat pump system: simulation and controls, ASHRAE Transactions LA-80-5 Los Angeles, California.
- Boussaada, Z., Curea, O., Remaci, A., Camblong, H. and Bellaaj, N.M.**, 2018, A Nonlinear Autoregressive Exogenous (NARX) Neural Network Model for the Prediction of the Daily Direct Solar Radiation, *Energies*, 11:620p.

#### **LIST OF REFERENCES (continued)**

- Bozorg-Haddad, O., Solgi, M. and Loaiciga, H.A.**, 2017, *Meta-Heuristic and Evolutionary Algorithms for Engineering Optimization*, Wiley, Hoboken, USA.
- Bright Hub Engineering**, "*How Thermostatic Expansion Valve Works?*", <https://www.brighthouseengineering.com/hvac/59422-working-of-the-thermostatic-expansion-valve> (Received: 1 December 2018)
- Chen, Z.J. and Lin, W.**, 1991, Dynamic simulation and optimal matching of a small-scale refrigeration system, *International Journal of Refrigeration*, 14:329-335.
- Chi, J.**, 1976, Computer simulation of fossil-fuel-fired hydronic boilers, Second ASHRAE HVAC equipment.
- Chi, J.**, 1979, DEPAC- a computer model for design and performance analysis of central chillers, ASME Paper No 77-HT-11.
- Chi, J. and Didion, D.**, 1982, A simulation model of the transient performance of a heat pump, *International Journal of Refrigeration*, 5:176-184p.

- Chowdhury, J.I., Nguyen, B.K. and Thornhill, D.**, 2015, Modelling of Evaporator in Waste Heat Recovery System using Finite Volume Method and Fuzzy Technique, *Energies*, 8:14078-14097.
- Dyakowski, T. and Brodowicz, K.**, 1993, *Heat Pumps*, 1<sup>st</sup> edition, Butterworth-Heinemann, Oxford, UK.
- Faris, H., Aljarah, I. and Mirjalili, S.**, 2017, Evolving Radial Basis Function Networks Using Moth-Flame Optimizer, *Handbook of Neural Computation*, 537-550p.
- Fauske, H.K.**, 1964, Some ideas about the mechanism causing two-phase critical flow, *Applied Scientific Research*, 149-160p.
- Findelsen, R., Allgöwer, F. and Biegler, L.T.**, 2007, *Assesment and Future Directions of Nonlinear Model Predictive Control*, 1<sup>st</sup> edition, Springer, Berlin, Germany.
- Fong K.F., Hanby, V.I. and Chow, T.T.**, 2009, System optimization for HVAC energy management using the robust evolutionary algorithm, *Applied Thermal Engineering*, 29:2327-2334.
- Fu, L., Ding, G. and Zhang, C.**, 2003, Dynamic simulation of air-to-water dual-mode heat pump with screw compressor, *Applied Thermal Engineering*, 23:1629-1645p.
- Glover, F.**, 1989, Tabu Search: Part I, *ORSA Journal on Computing*, 1:190-206.
- Gnielinski, V.**, 1976, New equations for heat and mass transfer in turbulent pipe and channel flow, *International Journal of Chemical Engineering*, 16:359-368.
- Goetzler, W., Shandross, R., Young, J., Petritchenko, O., Ringo, D. and McClive, S.**, 2017, *Energy Savings Potential and RD&D Opportunities for Commercial Building HVAC Systems*, US Department of Energy, Massachusetts, USA.

#### **LIST OF REFERENCES (continued)**

- Goldberg, D.E.**, 2008, *Genetic Algorithms*, 1<sup>st</sup> edition, Dorling Kindersley, New York, USA.
- Grüne, L. and Pannek, J.**, 2011, *Nonlinear Model Predictive Control*, 1<sup>st</sup> edition, Springer, London, UK.
- Gungor, K.E. and Winterton, R.H.S.**, 1986, A general correlation for flow boiling in tubes and annuli, *International Journal of Heat and Mass Transfer*, 29: 351-358p.
- Hagan, M.T., Demuth, H.B., Beale, M.H. and Jesus, O.D.**, 2014, *Neural Network Design*, 2<sup>nd</sup> edition, Martin Hagan, Oklahoma, USA.
- Haykin, S.**, 2009, *Neural Networks and Learning Machines*, Pearson, 3<sup>rd</sup> edition, Hoboken, USA.
- Hepbasli, A.**, 2005, Thermodynamic analysis of a ground-source heat pump system for district heating, *International Journal of Energy Research*, 29:671-687p.
- Herold, K.E., Radermacher, R. and Klein, S.A.**, 2016, *Absorption and Chiller Heat Pumps*, 2<sup>nd</sup> edition, CRC Press, Boca Raton, Florida, USA.

- Hundy, G.F., Trott, A.R. and Welch, T.C.**, 2016, Refrigeration, Air Conditioning and Heat Pumps, 5<sup>th</sup> edition, Elsevier, Oxford, UK.
- Jain, N.**, 2013, Thermodynamics-based Optimization and Control of Integrated Energy Systems, University of Illinois Urbana-Champaign, PhD Thesis.
- Jain, N. and Alleyne, A.G.**, 2014, Transient exergy destruction analysis for a vapor compression system, In: International refrigeration and air conditioning conference, West Lafayette, USA.
- Jain, N. and Alleyne, A.**, 2015, Exergy-based optimal control of a vapor compression system, Energy Conversion and Management, 92:353-365p.
- Jain, V., Sachdeva, G., Kavhhwaha, S.S. and Patel, B.**, 2016, Thermo-economic and environmental analyses based multi-objective optimization of vapor compression-absorption cascaded refrigeration system using NSGA-II technique, Energy Conversion and Management, 113:230-242p.
- James, K.A. and James, R.W.**, 1987, Transient analysis of thermostatic expansion valves for refrigeration system evaporators using mathematical models, Transactions of the Institute of Measurement and Control 9:350-355.
- Karaboga, D.**, 2005, An idea based on honey bee swarm for numerical optimization, Technical Report TR06, Kayseri Erciyes University.
- Karaboga, D.**, 2010, Artificial Bee Colony, Scholarpedia, 5:6915.
- Kennedy, J. and Eberhart, R.**, 1995, Particle Swarm Optimization, Proceedings of ICNN'95- International Conference on Neural Networks.

### **LIST OF REFERENCES (continued)**

- Kingma, D.P. and Ba. L.J.**, 2015, Adam: A method for stochastic optimization, International Conference on Learning Representations (ICLR 2015), San Diego, USA.
- Korzen, A. and Taler, D.**, 2015, Modeling of transient response of a plate fin and tube heat exchanger, International Journal of Thermal Sciences, 92:188-198p.
- Lebrun, J. and Bourdouxhe, J.-P.**, 1998, Reference Guide for Dynamic Models of HVAC Equipment, ASHRAE, Atlanta, GA, Project 738-TRP.
- Li, B. and Alleyne, A.G.**, 2010, A dynamic model of a vapor compression cycle with shut-down and start-up operations, International Journal of Refrigeration, 33:538-552p.
- MacArthur, J.W.**, 1984, Transient heat pump behavior: a theoretical investigation, International Journal of Refrigeration, 7: 123-132p.
- McKinley, T.L. and Alleyne, A.G.**, 2008, An advanced nonlinear switched heat exchanger model for vapor compression cycles using the moving-boundary method, International Journal of Refrigeration 31:1253-1264p.

- Mirjalili, S. and Lewis, A.**, 2016, The Whale Optimization Algorithm, *Advances in Engineering Software*, 95:51-67p.
- Nair, V. and Hinton, G.E.**, 2010, Rectified linear units improve restricted boltzmann machines, in: *Proceedings of the 27<sup>th</sup> International Conference on Machine Learning*, Haifa, Israel.
- Nguyen, N.T. and Szczerbicki, E.**, 2009, *Intelligent Systems for Knowledge Management*, 1<sup>st</sup> edition, Springer, Berlin, Germany.
- Prindle, B., Eldridge, M., Eckhardt, M. and Frederick, A.**, 2007, *The Twin Pillars of Sustainable Energy: Synergies between Energy Efficiency and Renewable Energy Technology and Policy*, American Council for an Energy-Efficient Economy (ACEEE), ACEEE Report Number E074.
- Reay, D.A. and Macmichael, D.B.A.**, 1988, *Heat Pumps*, 2<sup>nd</sup> edition, Pergamon, Oxford, UK.
- Rasmussen, B.P. and Alleyne, A.G.**, 2006, *Dynamic Modeling and Advanced Control of Air Conditioning and Refrigeration Systems*, University of Illinois Urbana-Champaign Technical Report Code: ACRC-TR 244.
- Rasmussen, B.P. and Shenoy, B.**, 2008, Dynamic modeling for vapor compression systems-Part II: Simulation tutorial, *HVAC&R Research*, 18:956-973p.
- Rasmussen, B.P.**, 2015, Dynamic modeling for vapor compression systems-Part I: Literature review, *HVAC&R Research*, 18:934-955p.
- Renewable Energy World**, “*A guide for effective energy saving*”, <http://www.renewableenergyworld.com/ugc/blogs/2015/04/a-guide-for-effective-energy-saving.html> (Received: 1 December 2018)

#### **LIST OF REFERENCES (continued)**

- Rojas, R.**, 1996, *Neural Networks: A Systematic Introduction*, Springer-Verlag, California, USA.
- Sayyadi, H. and Nejatolahi, M.**, 2011, Multi-objective optimization of a cooling tower assisted vapor compression refrigeration system, *International Journal of Refrigeration*, 34:243-256.
- Silva, I.N.d., Spatti, D.H., Flauzino, R.A., Liboni, L.H.B. and Alves, S.F.d.**, 2017, *Artificial Neural Networks*, 1<sup>st</sup> edition, Springer, Switzerland.
- Singer, S. and Nelder, J.**, 2009, Nelder-Mead algorithm, *Scholarpedia*, 4:2928.
- Storn, R. and Price, K.**, 1997, Differential Evolution – A Simple and Efficient Heuristic for Global Optimization over Continuous Spaces, *Journal of Global Optimization*, 11:341-359p.
- Travis, D.P., Baron, A.G. and Rohsenow, W.M.**, 1971 Forced-convection condensation inside tubes, *MIT Heat Transfer Laboratory*, 74, 1971.

- Towards Data Science**, “*Gradient Descent in a Nutshell*”,  
<https://towardsdatascience.com/gradient-descent-in-a-nutshell-eaf8c18212f0>,  
 (Received: 1 December 2018)
- Turgut, M.S. and Coban, M.T.**, 2018, Dynamic Performance Comparison of R134a and R1234yf Refrigerants for a Vapor Compression Refrigeration Cycle, *Hittite Journal of Science & Engineering*, 5:9-14p.
- Van Laarhoven, P.J.M. and Aarts, E.H.L.**, 1987, *Simulated Annealing: Theory and Applications*, Springer, Dordrecht, Netherlands.
- Vanderplaats, R.**, 2007, *Multidiscipline Design Optimization*, Colorado Springs, Vanderplaats Research and Development Inc.
- Vasickaninova, A., Bakosova, M., Meszaros, A. and Klemes, J.J.**, 2011, Neural network predictive control of a heat exchanger, *Applied Thermal Engineering*, 31:2094-2100p.
- Venter, G.**, 2010, Review of Optimization Techniques, *Encyclopedia of Aerospace Engineering*, Wiley&Sons, London, UK.
- Wen, J.T. and Mishra, S.**, 2018, *Intelligent Building Control Systems*, 1<sup>st</sup> edition, Springer, Cham, Switzerland.
- Wright, J.A. and Hanby, V.I.**, 1987, The formulation, characteristics and solution of HVAC system optimized design problems, *ASHRAE Transactions*, 93:2133-2145p.
- Wright, J.A.**, 1996, HVAC optimisation studies: sizing by genetic algorithm, *Building Services Engineering Research and Technology*, 17:7-14.
- Yakub, F.**, 2013, Model Predictive Control for Car Vehicle Dynamic System-Comparative Study, in: *IEEE International Conference on Information Science and Technology*, Yangzhou, China.

#### **LIST OF REFERENCES (continued)**

- Yang, X.S.**, 2010, A new metaheuristic bat-inspired algorithm, *Nature-Inspired Cooperative Strategies for Optimization (NICSO 2010)*, 284:65-74p.
- Yang, X.S.**, 2010, Firefly Algorithm, *Stochastic Test Functions and Design Optimization*, *International Journal of Bio-Inspired Computation*, 2:77-84p.
- Yang, X.S. and Deb, S.**, 2010, Engineering Optimisation by Cuckoo Search, *International Journal of Mathematical Modelling and Numerical Optimisation*, 1:330-343p.
- Yang, X.S.**, 2018, *Nature-inspired Algorithms and Applied Optimization*, Springer-Verlag, London.
- Yin, X., Wang, X., Li, S. and Cai, W.**, 2016, Energy-efficiency-oriented cascade control for vapor compression refrigeration cycle systems, *Energy*, 116:1006-1019p.
- Zhu, Y., Jin, X., Du, Z., Fan, B. and Fu, S.**, 2013, Generic simulation model of multi-evaporator variable refrigerant flow air conditioning system for control analysis, *International Journal of Refrigeration*, 36:1602-1615p.

## **ACKNOWLEDGEMENTS**

I would like to thank my family for their support during my graduate education. I would also like to thank my supervisor Assoc. Prof. Dr. Mustafa Turhan ÇOBAN for his advice and mentorship throughout my doctorate education.

.... / .... / 20..

### **AUTHOR BIOGRAPHY**

Mert Sinan TURGUT was born in Izmir, Turkey in 1989. He attended the primary, secondary and high school in Izmir. He received the B.E. degree in mechanical engineering from the Dokuz Eylul University in 2010. Then, he received the M.S. degree in mechatronics engineering from the Dokuz Eylul University in 2015. He is currently pursuing his Ph.D. degree in mechanical engineering with energy specialization from the Ege University. His research interests include optimization algorithms, modeling and optimization of energy systems, control theory and control of energy systems.

